THESIS

SEDIMENTOLOGY, FACIES ARCHITECTURE AND SEQUENCE STRATIGRAPHY OF A MISSISSIPPIAN-AGE, BLACK MUDSTONE SUCCESSION — THE UPPER MEMBER OF THE BAKKEN FORMATION, NORTH DAKOTA, U.S.A.

Submitted by

Damien A. Borcovsky

Department of Geoscience

In partial fulfillment of the requirements

For the Degree of Master of Science

Colorado State University

Fort Collins, Colorado

Fall 2013

Master's Committee:

Advisor: Sven Egenhoff

Dennis Harry
Joseph von Fischer
Neil Fishman

ABSTRACT

SEDIMENTOLOGY, FACIES ARCHITECTURE AND SEQUENCE STRATIGRAPHY OF A MISSISSIPPIAN-AGE, BLACK MUDSTONE SUCCESSION — THE UPPER MEMBER OF THE BAKKEN FORMATION, NORTH DAKOTA, U.S.A.

The early Mississippian age, upper member of the Bakken Formation in the North Dakota portion of the Williston Basin consists of a succession of organic-rich, black siliciclastic mudstones deposited offshore on a low-gradient ramp or shelf. Based on ichnological and sedimentological characteristics twelve fine-grained facies are recognized within the succession and these are grouped into five reoccurring facies associations. Very fine-grained, massive to faintly laminated mudstone (FA1) records deposition in the deepest, calmest parts of the offshore environment, whereas well laminated mudstones (FA2a), well laminated clay clast-bearing mudstones (FA2b), burrow-mottled mudstone with shells (FA3), and interlaminated siltstone and mudstone (FA4) contain sedimentological evidence that argues for deposition in the shallower, less calm, and generally more proximal parts of the offshore environment. These proximal-offshore mudstones (FA2a, FA2b, FA3, and FA4) reflect (1) variation in overall bottom water oxygen levels from dysoxic to possibly as high as oxic, and (2) lateral variation in the input of silt and clay clasts along the basin margin. Ubiquitous *Phycosiphon incertum* fecal strings throughout the succession along with patches of small shells and centimeter-scale burrows, and rare agglutinated foraminifera indicate that the upper Bakken member was likely deposited primarily in dysoxic to suboxic basinal conditions, and not within a persistently stratified, anoxic environment.

In all facies associations, storm event laminae deposited by bedload processes range from sparse to ubiquitous. Repeated stacking of facies associations, which reflect different offshore energy regimes define up to ten coarsening-upward parasequences mostly 0.15-0.60 m thick. These are bounded by flooding surfaces that can be correlated laterally for at least 300 km through the basin, delimiting individual parasequences. Distinct formation-scale facies changes indicate that the lower half of the succession, herein termed Interval 1, represents the distal expression of a transgressive systems tract and was characterized by high radiolaria productivity with minor silt input during higher order sea level lowstands. The upper half of the succession, herein termed Interval 2 represents the distal expression of the base of a highstand systems tract. In contrast to Interval 1, the Interval 2 mudstones are generally characterized by high clay content, low radiolaria productivity, and intermittent colonization of the sea floor by bivalves and millimeter to centimeter-scale burrowing organisms during higher order sea level lowstands.

Core descriptions, radiolaria distribution patterns, x-ray diffraction data and comparisons to other shale plays in the United States of America suggest that thermally mature mudstones in the Interval 1 part of the succession outside of the depocenter, and in isolated silt-rich sub-basins, might be sufficiently brittle and permeable to exploit for hydrocarbons utilizing horizontal drilling and hydraulic fracturing technologies.

ACKNOWLEDGMENTS

I would like to thank Hess Corporation for providing the financial support to undertake the research for this master's thesis. I am especially grateful to my advisor Dr. Sven Egenhoff for the discussions, the enthusiasm and for the countless hours of time and effort that went into the many detailed revisions of the text. I would also like to thank Dr. Sven Egenhoff, Neil Fishman and Dr. Jörg Maletz for hand logging many of the cores and for the help given out during the period of this research. In addition, I would like to thank the members of my thesis committee Dr. Sven Egenhoff, Dr. Denis Harry, Dr. Joe von Fischer and Neil Fishman for their helpful suggestions and comments that improved the quality of the thesis. I am thankful to Heather Lowers and Adam Boehlke at the USGS for helping me with the SEM and XRD data, respectively, and to Julie LeFever at the NDGS for providing me with the ArcGIS isopach map that I used extensively in this project. Many thanks go to the Colorado State Sedimentology working group, including Stacie Albert, Matt Petrowsky, Ketki Kolte, Jamie Mackie, Lauren Droege, Eric Curtis Gaver, Ali Çigri and Will Horner for the technical help and discussions, and for making our office such a great place to work. I would also like to give a special thanks to my wife Elyse Cadogan for all of the support and encouragement over the last two years.

TABLE OF CONTENTS

1.0 INTRODUCTION

Research into the temporal and lithological variability of mudstone facies and sequence stratigraphy of fine-grained successions has been relatively sparse until recently (e.g. Bohacs, 1993; Bohacs and Schwalbach, 1992; Creaney and Passey, 1993; Herbin et al., 1995; Macquaker et al., 1998, 2007; Macquaker and Howell, 1999; Macquaker and Taylor, 1996; Schieber, 1998b; Wignall and Newton, 2001). This is in part because the very fine-grained fabric and the small-scale heterogeneity of these sediments make them difficult to characterize visually and petrographically, especially on a succession-scale, without a large number of costly thin sections. Furthermore, application of stratigraphic methods to distal mudstone successions has probably been minimal also because of the enduring notion that deposition of clay in basinal settings can only occur by suspension settling (e.g. Potter et al., 2005, p. 23-24; Dalrymple, 2005, 2006) and thus occurs independently of and disconnected from the advective depositional processes that characterize coarser sediments in proximal sedimentary systems. However, recent research into wave- and current-induced gravity-driven fluid mud flows (see review by Wright and Friedrichs, 2006; Macquaker et al., 2010a) has identified physical processes that may have transported large volumes of fluid mud offshore across low-gradient shelves as bed-load and near-bed suspensions. Furthermore, recent flume experiments by Schieber et al. (2007) indicate that mud can be transported by bedload processes in the form of floccules. In addition, microtextural analyses of ancient mudrocks have identified physical evidence that silt-bearing, clay-rich laminae (<10 mm thick) can be deposited in the offshore environment by traction currents (Ghadeer and Macquaker, 2011; Ghadeer and Macquaker, 2012; Macquaker et al., 2010b; Schieber, 1999). These findings connect distal mudstone successions with proximal coarse-grained clastic marine successions by common processes and genetically related strata. This

suggests that sequence stratigraphy, even though developed for more proximal sedimentary systems (e.g. Posamentier and Vail 1988; Sarg, 1988; Vail et al., 1977; Van Wagoner et al., 1990), may be equally applicable to mudstone successions.

This paradigm shift in mudstone research comes at a time when black shales are becoming increasingly important as unconventional reservoirs. The upper and lower members of the Bakken Formation are both classic black shales, and combined are estimated to have generated 32 to 300 billion barrels of oil based on recent calculations (Flannery and Kraus, 2006; Meissner and Banks, 2000; see also review by LeFever and Helms, 2006). Surprisingly, in spite of the extensive Bakken core catalogue at the North Dakota Geological Survey and the recent explosion of shale plays in the United States which rely heavily on lithological and geomechanical facies mapping there is no published research that investigates either of the Bakken black shales in terms of internal facies architecture.

This study aims at using the upper Bakken member black shale to develop a parasequence-scale facies architecture for this world-class source rock and potential unconventional reservoir. Distinct mudstone facies changes are here used to define sequence stratigraphic key surfaces within this homogenous-appearing fine-grained siliciclastic mudstone unit. This approach allows for the upper Bakken member to be subdivided into time-equivalent packages that can be correlated through the eastern North Dakota and western Montana portion of the Williston Basin. This study shows that black shales have a basin-wide correlatable fine-scale internal architecture, and that sequence stratigraphic principles developed for coarse-grained proximal sedimentary rocks can be readily applied to mudstone systems.

2.0 GEOLOGICAL SETTING

The Williston Basin represents an elliptical-shaped intracratonic basin covering an area of approximately 250,000 km^2 with a diameter of 450 to 600 km (Kent and Christopher, 1994). The depocenter for the upper Bakken member is located in eastern North Dakota within Williams County. The basin includes large parts of Montana and southern Saskatchewan, with marginal areas of the basin also extending into South Dakota and Manitoba (Fig. 1). In Alberta the upper Bakken member grades laterally into coeval black shales in the basal part of the Banff Formation (Smith and Bustin, 2000) that were deposited in the Prophet Trough (Fig. 2) (Richards, 1989; Johnston et al., 2010).

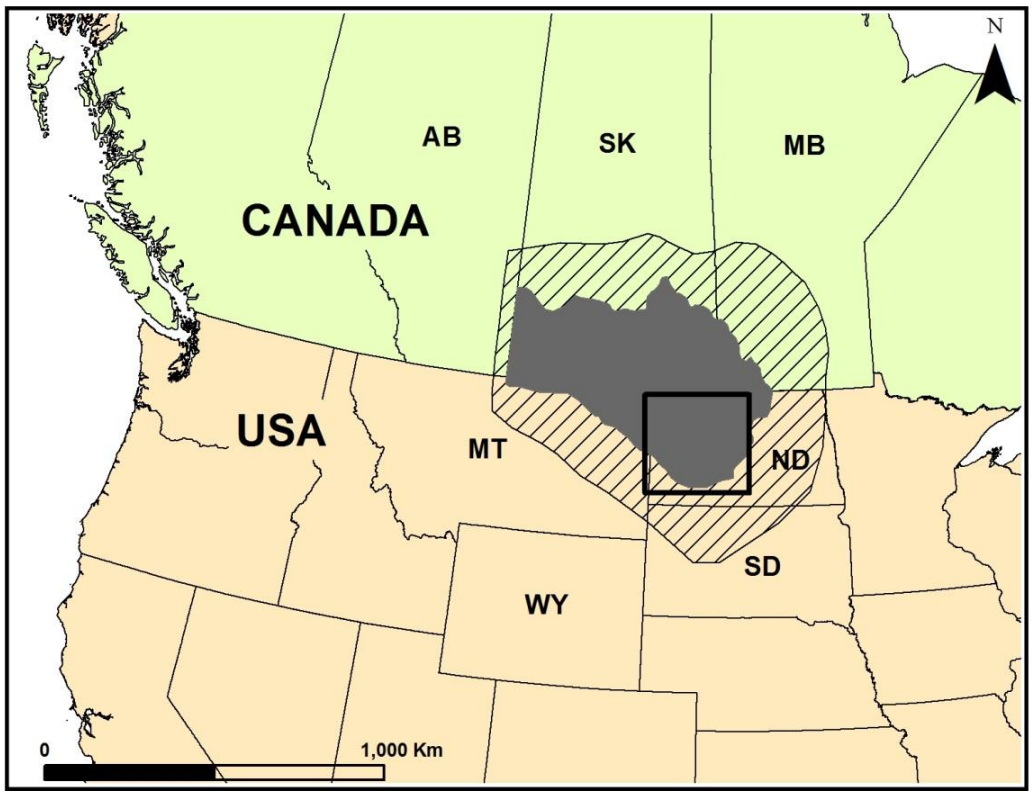

Figure 1. Location map of the Williston Basin (hatched) and depositional area of the upper Bakken member (shaded). Black square outlines the project study area located in western North Dakota. Basin outline and depositional area created from geological data provided online by the TGI Williston Basin Project, and from maps by Kent and Christopher (1994) and Link (1958).

The basin is bounded to the west by the Sweetgrass and North Battleford Arches, to the north by the Punnichy Arch, and to the south and east by the Black Hill Uplift and Sioux Uplift, respectively (Hatch, 1988; Kent and Christopher, 1994) (Fig. 2). Paleogeographic reconstructions indicate that during the Early Mississippian (Tournasian) the Williston Basin was located near the equator, within or near the Southern Hemisphere high pressure cell, resulting in a relatively dry tropical climate (Cecil et al., 1994; Scotese, 1994) (Fig. 2). This interpretation is supported by the presence of Early Mississippian evaporites, carbonates, paleo-Verticols and paleo-Aridosols (Cecil et al., 1994).

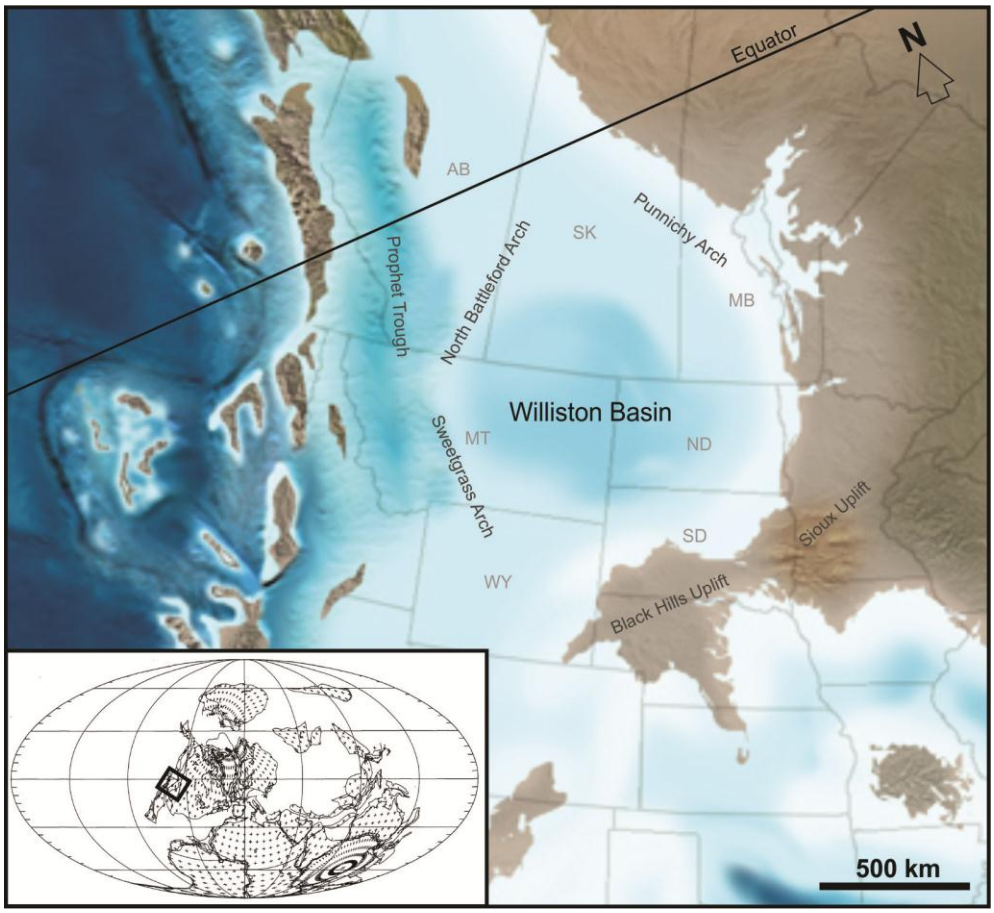

Figure 2. Paleogeography of the Williston Basin and surrounding region during the Early Mississippian (modified from Professor Blakey's website http://jan.ucc.nau.edu/~rcb7/namM345.jpg). Inset showing Early Mississippian (Tournasian) paleogeographic plate reconstruction from Scotese (1994).

Sedimentary rocks preserved within the Williston Basin overlie crystalline basement and record a Phanerozoic succession that starts in the Cambrian and attains a maximum thickness of 5,400 m in the Watford Deep, southeast of Williston, ND (Gerhard et al., 1990) (Fig. 3). Paleozoic rocks within the Williston Basin are dominated by carbonates with intercalated evaporites and siliciclastic units, which host most of the hydrocarbon reservoirs and source rocks (Zhuoheng et al., 2009) and include the Bakken-Three Forks petroleum system.

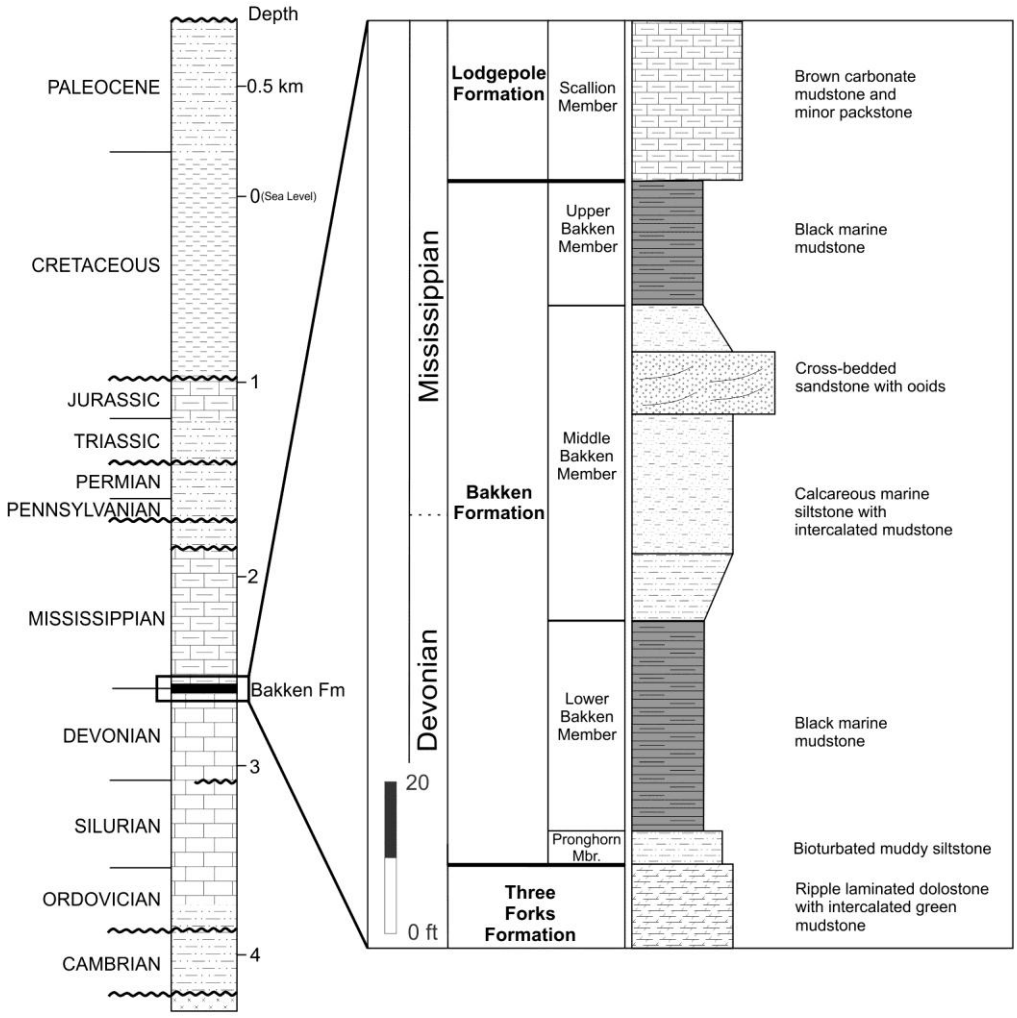

Figure 3: Generalized stratigraphic column of the Phanerozoic succession in the central Williston Basin (left) modified from Burrus et al. (1996), and of the Bakken Formation (right) modified from Egenhoff et al. (2011b) and Sonnenberg et al. (2011).

The Bakken Formation straddles the Upper Devonian - Lower Mississippian boundary, while the upper Bakken member falls entirely within the Lower Mississippian (Fig. 3). On the basis of conodont biostratigraphy, deposition of the upper member may have commenced as early as the Upper *Siphonodella duplicata* Biozone but probably started during the Lower *Siphonodella crenulata* Biozone (Holland et al., 1987). Deposition continued into the Lower *S. crenulata* Biozone, which includes the lower part of the overlying Lodgepole Formation (Holland et al., 1987; Johnston et al., 2010).

The Three Forks Formation, which underlies the Bakken Formation, was deposited primarily within peritidal and sabka environments and is characterized by argillaceous and dolomitic siltstones (Egenhoff et al., 2011b; Mitchell, 2013). The Scallion member, which represents the lower 5-10 m of the Lodgepole Formation, overlies the Bakken Formation and consists of nodular skeletal wackestones and packstones with intercalated carbonate mudstones (Mackie, 2013). Due to uplifts associated with the latter part of the Antler Orogeny and Cordilleran tectonics, Pennsylvanian to Holocene strata in the Williston Basin is composed primarily of siliciclastic sediment with only minor carbonate and evaporites during the Pennsylvanian to Jurassic.

The Bakken Formation occurs solely in the subsurface and reaches a maximum thickness of approximately 45 m in western Mountrail County (Meissner, 1978; Webster, 1984). It is subdivided into four members, which from base to top are: (1) the Pronghorn member (see LeFever et al., 2011), also referred to as the Sanish Sand or the Grassy Butte member, (2) the lower Bakken member, (3) the middle Bakken member, and (4) the upper Bakken member (Fig. 3). Each member occupies a smaller depositional area than the overlying member. The Pronghorn member generally consists of burrowed and bioturbated muddy siltstone and minor

fine sandstone (Berwick & Hendricks, 2011), and the middle Bakken member consists primarily of mixed carbonate-siliciclastic siltstones with minor oolites (Egenhoff et al., 2011b). The lower and upper Bakken members are both black shales with an average TOC of 8% and 10%, respectively, in the U.S. portion (Smith and Bustin, 2000); and 11.7% and 17.6%, respectively, in Canada (Chen et al., 2009).

The upper Bakken member is mostly 2-7 m in thickness and is described as a fairly monotonous unit that consists of slightly calcareous, fissile black shale with disseminated pyrite, and laminae of pyrite and silt (e.g. LeFever et al., 2011; Smith and Bustin, 1998, 2000; Sonnenberg and Pramudito, 2009; Webster, 1984). On the basis of planar laminae, high pyrite content, and the paucity of bioturbation and fossils it is commonly interpreted to have been deposited in stagnant, anoxic offshore bottom waters at the base of a stratified water column (e.g. LeFever, 1991; Smith and Bustin, 1998; Sonnenberg and Pramudito, 2009; Webster, 1984). Based on the absence of distinct storm deposits, Smith and Bustin (1998) postulate that the upper Bakken member was deposited in water >200 m deep. However, Egenhoff and Fishman (2013) have recently proposed a more dynamic model that includes dysoxic bottom-water conditions and bed-load transport processes to account for observations of small *Phycosiphon incertum* fecal strings, small *Planolites* trace fossils, and millimeter-scale lags and downlapping silt laminae.

2.1 History of Upper Bakken Petroleum Exploration

From 1970 to 2001 the Bakken play development focused on sweet spots within oil-saturated thermally mature shales of the Upper Bakken member where reservoirs formed primarily by natural fracturing (Cramer, 1991; Druyff, 1991; Hansen and Long, 1991b; LeFever, 1991;

LeFever, 2005; Monson and Lund, 1991; Sonnenberg and Pramudito, 2009). This development was centered on the Antelope structure and Nesson Anticline, and within a 50 km wide, NW-SE oriented belt termed the Bakken Fairway which parallels 320 km of the upper Bakken member depositional edge along the southwest margin of the basin (Hansen and Long, 1991a; LeFever, 1991). Horizontal drilling of the upper Bakken member shales, which targeted fracture systems within the Bakken Fairway, began in 1987 and continued until the early 1990s (LeFever, 2005). In 2001, advanced horizontal completion and hydraulic fracturing technologies shifted industry attention to the tight siltstone and sandstone reservoirs of the middle Bakken member (Mason, 2012).

3.0 METHODOLOGY

Detailed visual core logging was carried out on thirty-seven upper Bakken member drill cores housed at the North Dakota Geological Survey's (NDGS) Wilson M. Laird Core and Sample Library and at the United State Geological Survey (USGS) Core Research Center in Denver, Colorado (Table 1, Fig. 4). The entire upper Bakken section has been cored in all but four of the thirty-seven cores described in this study. The goal of visual core logging was to create a large dataset that covered most of the North Dakota portion of the Williston Basin and, importantly, recorded a continuous core log of the small-scale (mm-cm) textural and compositional variations within the succession. A total of 116 polished, oriented thin sections, 20 µm thick, most of them cut perpendicular to bedding with eleven cut parallel to bedding, were prepared from core samples from twenty-one different cores. Three additional thin-sections from the Conoco Karsky 35 #2 core were provided by the Wilson M. Laird Core and Sample Library. Transmitted light microscopy was carried out on thin sections to observe the composition, microtexture and small-scale sedimentary structures in order to determine the origin and distribution of biogenic and clastic constituents as well as the biologic and sedimentary processes that were active during and soon after deposition. These petrographic observations were investigated using a Nikon SMZ 1500 microscope equipped with a polarizing filter, a white (halogen) light source and a Nikon DS-Fi1 5.0 megapixel camera. Fluorescent microscopy to aid in the identification of organic constituents was carried out with an Olympic BX51 petrographic microscope equipped with an Olympus Q-Color3 3.2 megapixel camera and an Olympus U-LH100HG 100W fluorescence light source. Volume percentages for organic, clastic and biogenic components were determined by visual estimation in drill core and also by transmitted light microscopy of thin sections utilizing standard comparison charts (e.g. Matthew et al., 1991; Baccelle and Bosellini, 1965).

Table 1. List of wells with cores logged in this study. Well localities are shown in Figure 4. Well file # refers to North Dakota Geological Survey well file number, except R311, E385 and B679, which are cores stored at the USGS Core Research Center in Denver.

Map Locator #	Original Operator	Original Well Name	Well file #
1	BALCRON OIL	44-24 VAIRA	R311
2	LYCO ENERGY CORPORATION	TITAN F-WP 32-14-H	12331
3	BRIGHAM OIL & GAS, L.P.	OLSON 10-15 1-H	17513
4	NEWFIELD PRODUCTION COMPANY	SERGEANT MAJOR 1-21H	18086
5	AMERADA HESS CORPORATION	ANDERSON SMITH 1-26H	16083
6	AMERADA HESS CORPORATION	SARA G. BARSTAD 6-44H	15889
7	AMERADA HESS CORPORATION	J. HORST 1-11H	15986
8	BRIGHAM OIL & GAS, L.P.	ANDERSON 28 1-H	17351
9	WHITING OIL AND GAS CORPORATION	BRAAFLAT 11-11H	17023
10	MARATHON OIL COMPANY	JENSEN #12-44	8069
11	STANOLIND OIL & GAS CO.	WALTER & INGEBERG WASWICK #1	105
12	ANSBRO PETROLEUM COMPANY, LLC	LOUCKS 44-30	15722
13	SAMSON RESOURCES COMPANY	NORDSTOG 14-23-161-98H	16089
14	CONOCO INC.	SKARPHOL "D" #5	13167
15	NORTH PLAINS ENERGY, LLC	COMFORD 9-12H	19060
16	HESS CORPORATION	H. BAKKEN 12-07H	16565
17	HEADINGTON OIL COMPANY LLC	NESSON STATE 42X-36	17015
18	HELIS OIL & GAS COMPANY, L.L.C.	LINSETH 4-8H	16689
19	BURLINGTON RESOURCES OIL & GAS CO	PRAIRIE ROSE 24-31H	16798
20	ANSCHUTZ EXPLORATION CORPORATION	SADOWSKY 24-14H	17808
21	CONOCO INC.	KARSKY 35 #2	13789
22	MAXUS EXPLORATION CO.	RAUCH SHAPIRO FEE #13-3	12494
23	MERIDIAN OIL, INC.	MOI #44-27	12331
24	JERRY CHAMBERS	USA #1-24	8251
25	TENNECO OIL CO.	GRAHAM USA #1-15	8474
26	FLORIDA EXPLORATION COMPANY	11-4 FEDERAL	E385
27	FLORIDA EXPLORATION COMPANY	FEDERAL #12-1	9426
28	WHITING OIL AND GAS CORPORATION	TEDDY 44-13TFH	18502
29	FLORIDA EXPLORATION CO.	FEDERAL 34-1	10803
30	TEXACO INC.	THOMPSON UNIT #5-1	12748
31	GULF OIL CORP.	MARTIN WEBER #1-18-1C	6082
32	SHELL OIL CO.	BURBANK BIA #23-8	8709
33	QUESTAR EXPLORATION & PROD. CO.	MHA 1-18H-150-90	17434
34	EOG RESOURCES, INC.	SIDONIA 1-06H	17676
35	CIRQUE RESOURCES, LP	TRIPPELL 32-16H	17699
36	CLARION RESOURCES, INC.	1-24 SLATER	B679
37	C & K PETROLEUM, INC.	KOCH #2-28	8824

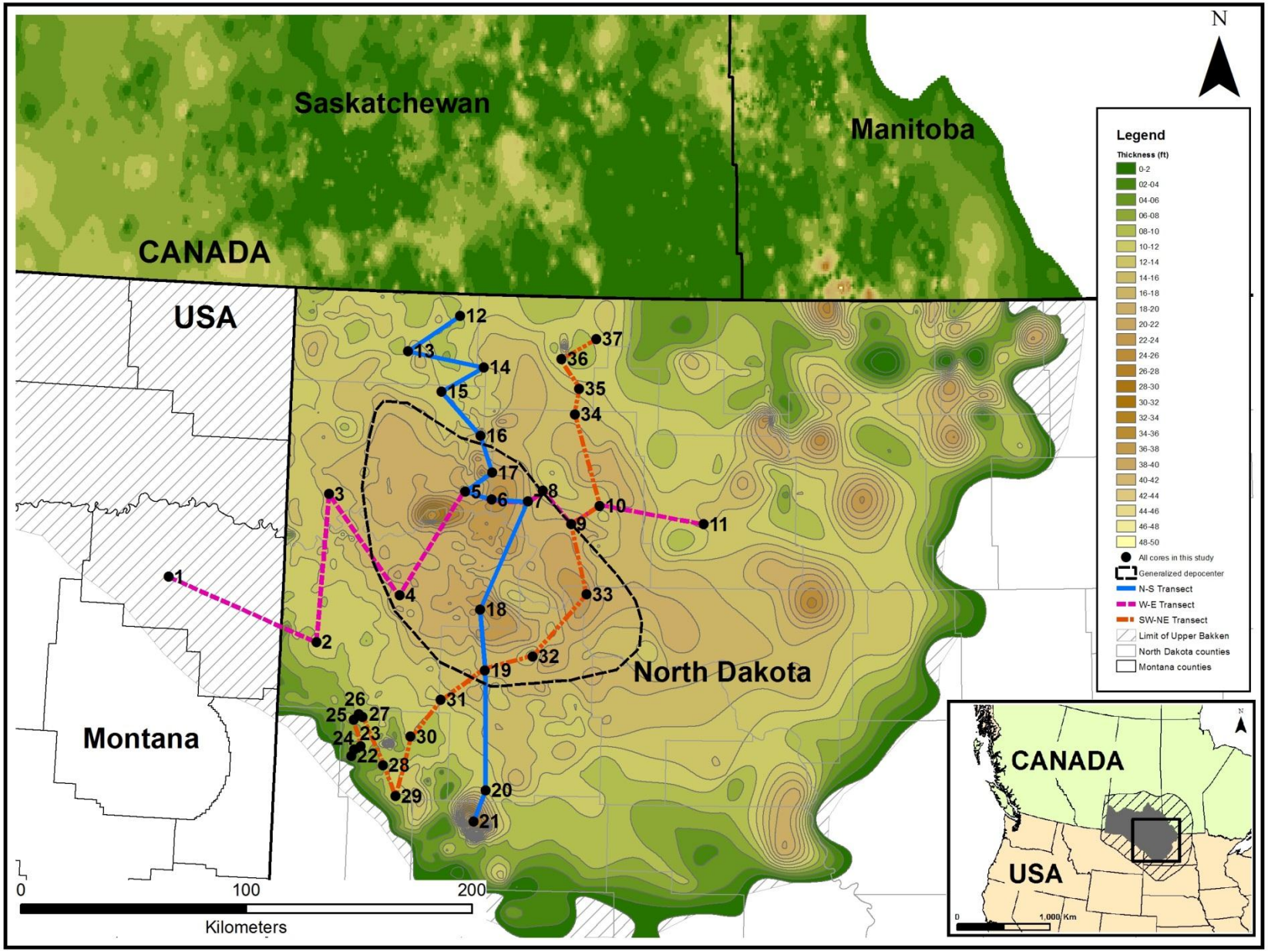
Saskatchewan
Manitoba
CANADA
USA
Montana
North Dakota
N
Legend
Thickness (ft)
0-2
02-04
04-06
06-08
08-10
10-12
12-14
14-16
16-18
18-20
20-22
22-24
24-26
26-28
28-30
30-32
32-34
34-36
36-38
38-40
40-42
42-44
44-46
46-48
48-50
All cores in this study
Generalized depocenter
N-S Transect
W-E Transect
SW-NE Transect
Limit of Upper Bakken
North Dakota counties
Montana counties
1
2
3
4
5
6
7
8
9
10
11
12
13
14
15
16
17
18
19
20
21
22
23
24
25
26
27
28
29
30
31
32
33
34
35
36
37
0
100
200
Kilometers
CANADA
USA
0
1,000 Km

Figure 4 (Previous Page). Isopach map of the upper Bakken member showing well locations of cores used in this study (Table 1) and stratigraphic transects included in Appendices 1, 2 and 3. Generalized upper Bakken member depocenter referenced in text is shown by the dashed ellipse. North Dakota isopach map by J. LeFever (pers. comm., 2013). Canada portion isopach is a computed-contoured map created from data provided by the TGI Williston Basin Project.

Selected polished thin sections were also investigated with a JEOL 5800LV scanning electron microscope (SEM) equipped with an energy dispersive spectrometer (EDS) housed at the United States Geological Survey in Denver, Colorado. SEM observations and analyses were carried out to determine the texture and composition of clay-size material and organic matter within the matrix.

X-ray diffraction (XRD) data were collected on twenty-one mudstone samples to provide quantitative mineralogy of the inorganic constituents, including clay mineralogy. XRD data provided by Neil Fishman and Sven Egenhoff (pers. comm., 2013) of an additional forty-one mudstone samples from the Texaco Inc. Thompson Unit #5-1 and Al Aquitaine 1-23 BN cores were incorporated into the study. For all XRD analyses, organic carbon was removed from powdered samples using the techniques outlined by Soukup et al. (2008), and whole rock XRD data was determined using the automated approach outlined by Eberl (2003). Clay mineralogy was confirmed using the XRD methods described by Drever (1973) and Pollastro (1982), and diffractograms were interpreted by Adam Boehlke at the USGS in Denver using the techniques described by Brown and Brindley (1980) and Moore and Reynolds (1989).

A total of twelve TOC analyses were used in this study. Sample preparation for TOC analysis utilized an acid digestion to remove carbonate minerals and standard induction furnace techniques at Weatherford Labs. Whole rock vitrinite reflectance and Rock-Eval pyrolysis

analyses were performed on one sample from the Helis Oil & Gas Linseth 4-8H core to determine maturity and Tmax, respectively.

4.0 SEDIMENTOLOGY

Detailed logging of thirty-seven cored wells and analysis of 116 thin sections enabled the upper Bakken member to be subdivided into twelve fine-grained facies which are described in detail within Table 2. Lithologs of these cored wells are presented in three transects through the study area with available gamma ray logs in Appendices 1-3. The twelve fine grained facies are classified on the basis of microtextural observations, visual grain size estimates and compositional attributes after a modified version of the nomenclature of Macquaker and Adams (2003). Microcrystalline quartz grains were excluded from percentage estimates for detrital siliciclastic sediment. This decision was based on observations by Schieber (1996) and Schieber et al. (2000) which indicate that up to 100% of the microcrystalline quartz grains in the similar Devonian Chattanooga black shale have a biogenic or diagenetic origin.

Much of the upper Bakken member succession consists primarily of one of two facies: (1) silt-bearing mudstone, and (2) silt- and clay clast-bearing mudstone, these are facies 4a and 4b, respectively. The silt- and clay clast-bearing mudstone (facies 4b) is identical to silt-bearing mudstone (facies 4a) except in thin section where clay clasts can be observed with magnification. The other ten facies that are described in Table 2 typically occur as laminae and thin beds that are intercalated into the succession and are irregularly distributed stratigraphically.

Many of the facies described below contain horizontal *Planolites* burrows and multidirectional *Phycosiphon incertum* fecal strings. Both of these trace fossils have been subdivided into type A and type B forms by Egenhoff and Fishman (2013) primarily in terms of size, and these names are also used in this study. In summary, *Planolites* type A burrows are 0.3 to 1 mm in width whereas the type B variant is much larger and up to 10 mm in width. *Phycosiphon incertum* type A fecal strings are up to 1.5 mm in width, whereas the type B fecal string is typically only 0.2-

0.4 mm across. For a more detailed description of these trace fossils see Egenhoff and Fishman (2013). Silt-filled *Teichichnus* burrows 0.3-10 mm in diameter and 5-10 mm wide occur in places and well as highly compressed burrows resembling *Thalassinoides* in mudstones at the contact with the overlying Lodgepole Formation (Luis Buatois pers. comm., 2013).

Radiolarite and radiolaria-bearing mudstone is not easily distinguishable in hand specimen and are thus combined on the detailed core logs (Appendices 1-3).

4.1 Sedimentary Facies

Table 2. Summary of sedimentologic attributes of facies identified within the upper Bakken member. Modified from Egenhoff and Fishman (2013). Examples of each facies are illustrated in Figure 5.

	Facies	Facies Thickness	Description and sedimentary structures	Composition (by volume)	Interpretation
1	Radiolarite	5-20 mm	Massive laminae and laminasets Rare discontinuous laminae Compacted, ptygmatic mineralized fractures, typically filled with carbonate minerals, are common.	80-90% radiolaria tests 20-10% dark brown organic matter-rich matrix	Individual laminae record suspension sedimentation of radiolaria tests during blooms, with some bedload influence in places.
2	Radiolaria-bearing mudstone	1-40 mm	Planar to undulating, continuous and discontinuous laminae and laminasets, generally with sharp contacts In places consists of very thin discontinuous laminae 2-5 tests thick Fabric varies from massive to well laminated Normally-graded in places Basal scour surfaces in places Variable abundance of *Phycosiphon incertum* type B fecal strings 0.2-0.4 mm wide Rare *Planolites* type A burrows Compacted, ptygmatic mineralized fractures, typically filled with carbonate minerals, are common.	40-70% dark brown organic matter-bearing clay matrix 15-50% radiolaria tests 5-20% detrital siliciclastic and carbonate silt	Assimilation of tests with muddy sea-floor sediment by bedload processes during and after radiolaria blooms. Massive layers probably reflect bioturbation and destruction of primary laminated fabric by the organism producing *Phycosiphon incertum* type B fecal strings. Bedload transport
3	Clay-dominated mudstone	0.1-2 mm	Even thickness, continuous laminae with massive fabric. Variable abundance of *Phycosiphon incertum* type B fecal strings	90-99% dark-brown organic matter-bearing clay-rich matrix 1-10% fine-grained siliciclastic and carbonate silt	Suspension settling of clay, organic matter and minor fine-grained silt in a very calm environment.
4a	Silt-bearing mudstone	1-1000 mm	Planar laminae and relict laminae 0.5-5 mm thick. Predominantly massive in texture, normally graded in places Rare sub-mm relict laminae containing <5% clay-clasts Pyrite concretions 5-15 mm in length, and pyrite lenses and continuous laminae in places Very rare agglutinated foraminifera 0.1 - 0.25 mm in length *Phycosiphon incertum* type B fecal strings are relatively common Moderately to intensely bioturbated by minute *Phycosiphon incertum* type B Rare mud-filled *Planolites* type A burrows 0.3-10 mm in diameter *Planolites* type A burrows fairly common Very rare thick-walled *Tasmanites* cysts 100-150 µm	65-90% organic matter-bearing clay-rich matrix 10-35% detrital siliciclastic and carbonate silt (ave. 21%) 0-2% silt-size phosphate and siliceous fossil clasts	Diminutive ichnofauna and low ichnodiversity suggest stressful environment (Buatois and Mangano, 2011, p.105, 118). Depositional process in many places unclear. Normally graded laminae indicate deposition by waning flows.
4b	Silt- and clay clast-bearing, mudstone	3 to >30 mm	Planar, massive and normally-graded laminae 0.1-2 mm thick Abundant flaser-shaped clay clasts 0.01-0.2 mm in length Abundant lamellar bituminite lenses 0.1-1.0 mm in length Weakly to moderately bioturbated by minute *Phycosiphon incertum* type B	15-50% clay clasts (ave. 21%) 15-40% organic matter-bearing clay matrix 8-30% detrital siliciclastic and carbonate silt (ave. 13%) 2-20% lamellar bituminite lenses 0-5% silt-size phosphate and siliceous fossil clasts 0-2% silt-size pyrite	Clay clasts represent water-rich mud fragments derived from up-dip erosion of the sea-floor (Schieber et al., 2010). Ubiquitous clay clasts indicate sedimentation dominated by bedload transport processes. Diminutive ichnofauna and low ichnodiversity suggest stressful environment (Buatois and Mangano, 2011, p.105, 118).
5	Ripple-laminated mudstone	1-5 mm	Low-angle downlapping and converging silt-bearing, clay-rich laminae Weakly to moderately bioturbated by *Phycosiphon incertum* type B fecal strings	65-80% organic matter-bearing clay matrix 20-35% detrital siliciclastic and carbonate silt	Lateral accretion of clay-rich sediment. Mud floccule ripples during bedload transport.

	Facies	Facies Thickness	Description and sedimentary structures	Composition (by volume)	Interpretation
6a	Phosphate- and fossil-bearing mudstone	0.1-20 mm	Normally-graded to massive laminae Discontinuous lenses in places Rare basal scour surfaces Fossil clasts consist mostly of whole and fragmented conodont elements, sponge spicules, and radiolaria.	10-60% organic matter-bearing clay-rich matrix (ave. 40%) 10-40% phosphate and fossil clasts 25-30% detrital siliciclastic and carbonate silt 2-10% silt-size pyrite	Presence of sponge spicules and rare erosion surfaces indicate these mudstone laminae represent lags (distal tempestites) deposited during high energy events, e.g. storms.
6b	Clay-clast-, phosphate- and fossil-bearing mudstone	0.1-30 mm	Normally-graded to massive laminae and thin beds up to 30 mm thick Discontinuous lenses and rare basal scour surfaces in places Fossil clasts consist mostly of whole and fragmented conodont elements, sponge spicules, and radiolaria Scattered lamellar bituminite lenses 0.1-1.0 mm in length Abundant fine sand in some laminae	15-50% clay clasts (ave. 30%) 10-45% organic matter-bearing clay matrix (ave. 25%) 10-40% phosphate and fossil clasts (ave. 20%) 12-30% detrital siliciclastic and carbonate silt (ave. 20%) 5-15% silt-size pyrite 5-10% lamellar bituminite	Presence of sponge spicules, clay clasts and rare erosion surfaces indicate these mudstone laminae represent lags (distal tempestites) deposited during high energy events, e.g. storms. Clay clasts represent water-rich mud fragments (Schieber et al., 2010) and were derived from up-dip erosion of the sea-floor and redeposited by bedload processes.
7	Siltstone	0.5-30 mm	Mostly individual laminae <1 mm thick, laminasets up to 30 mm thick in places Lamina and laminasets vary from continuous to discontinuous, and contain ripple laminae in places Basal erosion surfaces and converging laminae common within laminasets. Silt-filled *Planolites* type B and *Teichichnus* burrows 0.3-10 mm in diameter and 5-10 mm wide in places (Luis Buatois pers. comm., 2013)	90-100% detrital siliciclastic and carbonate silt 0-15% siliceous fossil fragments 0-5% fine sand	Distal tempestites. Intermittent, high-energy events that transported and deposited silt and fine sand (mostly) by bed load processes.
8	Burrow-mottled siltstone	3-10 mm	Siltstone with abundant horizontal and inclined burrows mostly 3-10 mm in Diameter. The ichnospecies cannot be determined for this facies but may include *Planolites* type B (Luis Buatois pers. comm., 2013)	95-100% detrital siliciclastic and (minor) carbonate silt 0-2% fossil fragments and rare phosphate grains 0-5% fine sand	Siltstone laminae and laminasets indicate deposition (mostly) by bedload processes and represent high energy events e.g. storms. Moderately dysoxic to oxic bottom waters.
9	Burrow-mottled mudstone	10-100 mm	Intensely bioturbated fabric with relict laminae in places *Planolites* type B (burrows <10 mm wide) and other indeterminate burrows 1-10 mm in diameter filled with light-colored mudstone Planolites type B burrows are present *Phycosiphon incertum* type A and B fecal strings are common Samples at the contact with the overlying Lodgepole Formation contain highly compressed burrows resembling *Thalassinoides* (Luis Buatois pers. comm., 2013)	30-90% brown organic matter-bearing, clay-rich matrix 10-30% siliciclastic and carbonate silt	Dysoxic to oxic bottom waters. Depositional process unclear due to bioturbation.
10	Shell-bearing mudstone	10-300 mm	Articulate and disarticulate shells 0.3-30mm wide. Fabric varies from faintly laminated to burrow-mottled *Phycosiphon incertum* type A and B fecal strings are common	30-85% organic matter-bearing, clay-rich matrix 10-30% siliciclastic and carbonate silt 2-10% shells, some replaced by pyrite	Dysoxic to oxic bottom waters. Depositional process unclear due to bioturbation.

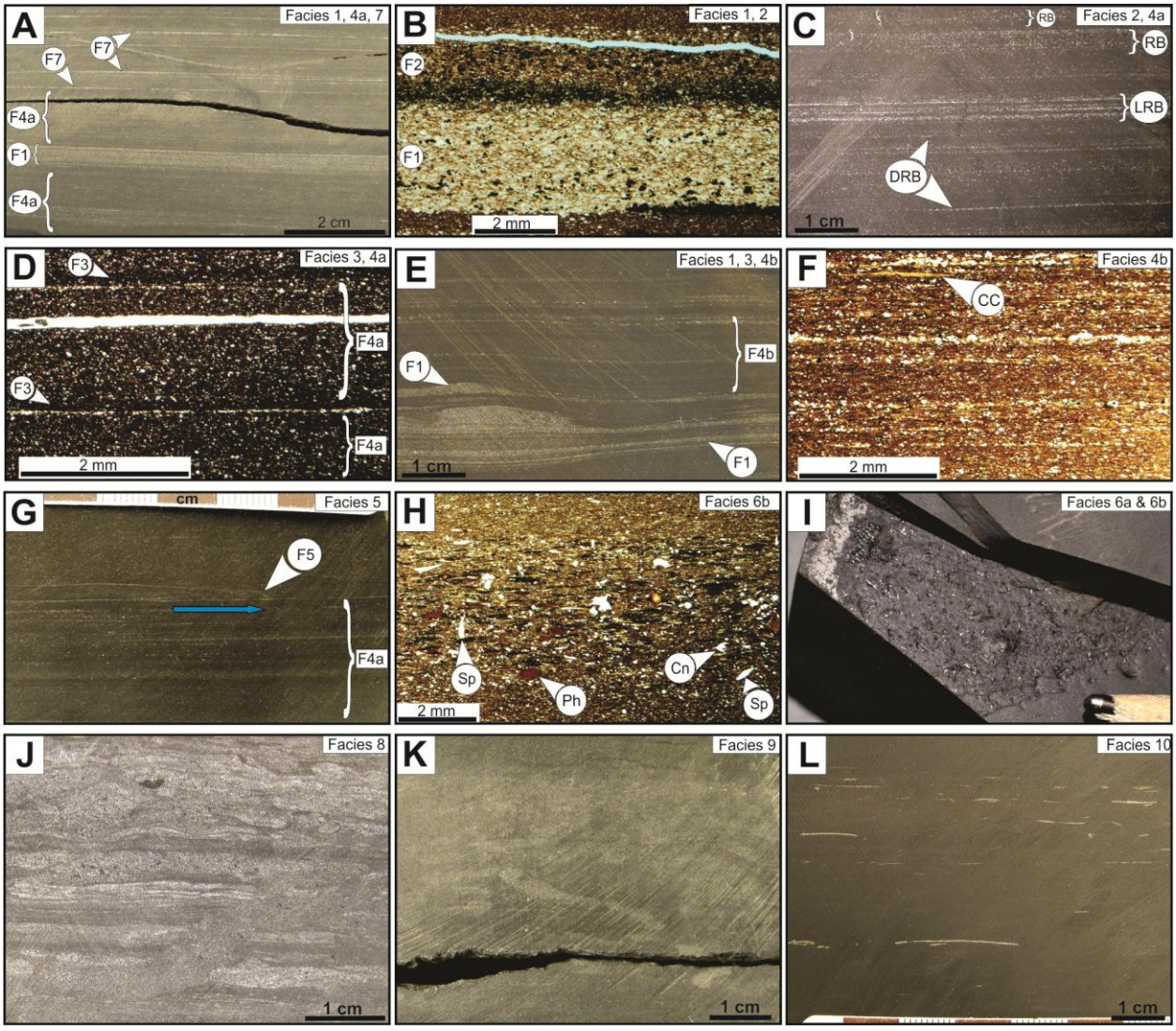

Figure 5. Fine-grained facies of the upper Bakken member. 'Facies' is abbreviated to 'F' in annotations and captions: **(A)** Core photograph illustrating silt-bearing mudstone (F4a) intercalated with radiolarite (F1), and siltstone laminae (F7) (EOG Sidonia 1-06H, 8732.8 ft). **(B)** Optical micrograph of radiolarite (F1) overlain by radiolaria-bearing mudstone (F2) (Whiting Oil & Gas Corp. Braaflat 11-11-H, 9872.9 ft). **(C)** Core photograph illustrating the textural variability of radiolaria-bearing mudstone (F2): massive layers of radiolaria-bearing mudstone (RB), laminasets of radiolaria-bearing mudstone (LRB), discontinuous ultra-thin laminae of radiolaria-bearing mudstone (DRB) (Conoco Karsky 35 #2, 10146.6 ft). **(D)** Optical micrograph showing silt-bearing mudstone (F4a) and very thin laminae of clay-dominated mudstone (F3) (Brigham Oil & Gas 10-15 1H, 10613.5 ft). **(E)** Core photograph illustrating silt- and clay clast-bearing mudstone (F4b) containing a partially reworked laminasets of radiolaria-rich mudstone (F1). Note similarity with Figure 5A of mudstone without clay clasts (Marathon Jensen #12-44, 9166.3 ft). **(F)** Optical micrograph of silt- and clay clast-bearing mudstone (F4b). Arrow

CC points to a large clay clast (Marathon Jensen #12-44, 9164.2 ft). **(G)** Core photograph showing ripple-laminated mudstone (F5) and two laminae of radiolarite (F1). Blue arrow represents apparent flow direction (Helis Oil & Gas Linseth 4-8H, 10786.7 ft). **(H)** Optical micrograph of clay clast-, phosphate- and fossil-bearing mudstone laminae (F6b). The laminae include red-brown phosphate (Ph), conodonts (Cn) and sponge spicules (Sp) (Marathon Jensen #12-44, 9163.5 ft). **(I)** Core photograph showing a bedding plane of a 2 mm thick laminae consisting of phosphate- and fossil-bearing mudstone (F6a), which in hand specimens appear identical to clay clast-, phosphate- and fossil-bearing mudstone (F6b). Pencil tip for scale (Samson Resources Nordstog 14-23-161-98H, 8602.3 ft). **(J)** Core photograph of burrow-mottled siltstone (F8) (Conoco Karsky 35 #2, 10124.1 ft). **(K)** Core photograph of burrow-mottled mudstone (F9) (Helis Oil & Gas Linseth 4-8H, 10777.8 ft). **(L)** Core photograph of shell-bearing mudstone (F10) (Newfield Production Sergeant Major1-21H, 11048.6 ft.

4.2 Facies Associations

The twelve fine-grained facies described in Table 2 are organized with the upper Bakken member into five facies associations which are summarized in Table 3 and described in detail below.

Table 3: Summary of lithologic components and average grain-size distribution of silt within four mudstone facies associations. Percentages estimated from thin section. Percentage estimates are not provided for interlaminated siltstone and mudstone (FA4) because of insufficient thin section coverage and significant mudstone heterogeneity. The silt content of thin beds of radiolaria-bearing mudstone and radiolarite is not incorporated into these measurements.

			Percent (average)					Grain size distribution of detrital silt component (ave. percent normalized to 100%)		
Facies Association		*n*	Clay clasts	Total clay +clay clasts + organic matter	Detrital quartz silt	Carbonate silt	Total silt	Fine-grained silt	Medium-grained silt	Coarse-grained silt
FA1	Massive to faintly laminated mudstone	27	4	>80%	13	4	17	47	46	7
FA2a	Well laminated mudstone	50	1	>75%	19	6	24	36	41	23
FA2b	Well laminated, clay clast-bearing mudstone	21	21	>80%	12	5	17	29	45	25
FA3	Burrow-mottled mudstone with shells	9	0	>75%	15	11	25	37	48	15
FA4	Interlaminated siltstone and mudstone	2	0	-	-	-	-	-	-	-

4.2.1 Facies association 1 | Massive to Faintly Laminated Mudstone

Massive to faintly laminated mudstone commonly forms continuous sections that range in vertical thickness from 0.2-3 m. This is the most abundant facies association and represents approximately 75% of the bulk rock volume. It consists principally of silt-bearing mudstone with a structureless to very faintly laminated fabric. The faint laminae (typically 0.2-1.0 mm thick) are highly disturbed by *Phycosiphon incertum* type B fecal strings (Fig. 6C, 6E). On average, detrital silt makes up 17% of the rock and 93% of it is fine- to medium-silt size (Table 3). In rare cases, wavy non-parallel laminae, and relict laminae that are defined by scattered clay clasts (0.1-0.5 mm long) and sand-size phosphate grains occur in thoroughly bioturbated samples. Very rarely, this facies association includes mudstone laminae containing up to 20% clay clasts. Thin beds, laminae and laminasets mostly 3-40 mm thick consisting of radiolarite and radiolaria-bearing mudstone are intercalated into the succession. These are variably distributed both laterally and vertically, and make up 1-20% of this facies association (Fig. 6A, 6B, 6C). Continuous and discontinuous intercalated laminae (typically <2 mm) of phosphate- and fossil-bearing mudstone also occur in places (Fig. 6D). Prasinophyte alginite macerals <40 μm in length make up <1% of the mudstone (Fig. 7A-C). The clay-size fraction consists of siliciclastic grains, clay minerals, pyrite, and disseminated amorphous bituminite. Patches of pyrite concretions and discontinuous pyrite lenses 5-30 mm and 2-10 mm in length, respectively, are common (Fig. 6B, 6D). The pyrite laminae consist mostly of euhedral pyrite grains and also as massive diagenetic pyrite lenses. Agglutinated foraminifera are very rare (Fig. 8A, 8B). Horizontal *Planolites* type A burrows are sparse and predominantly <1 mm in length (Fig. 8D).

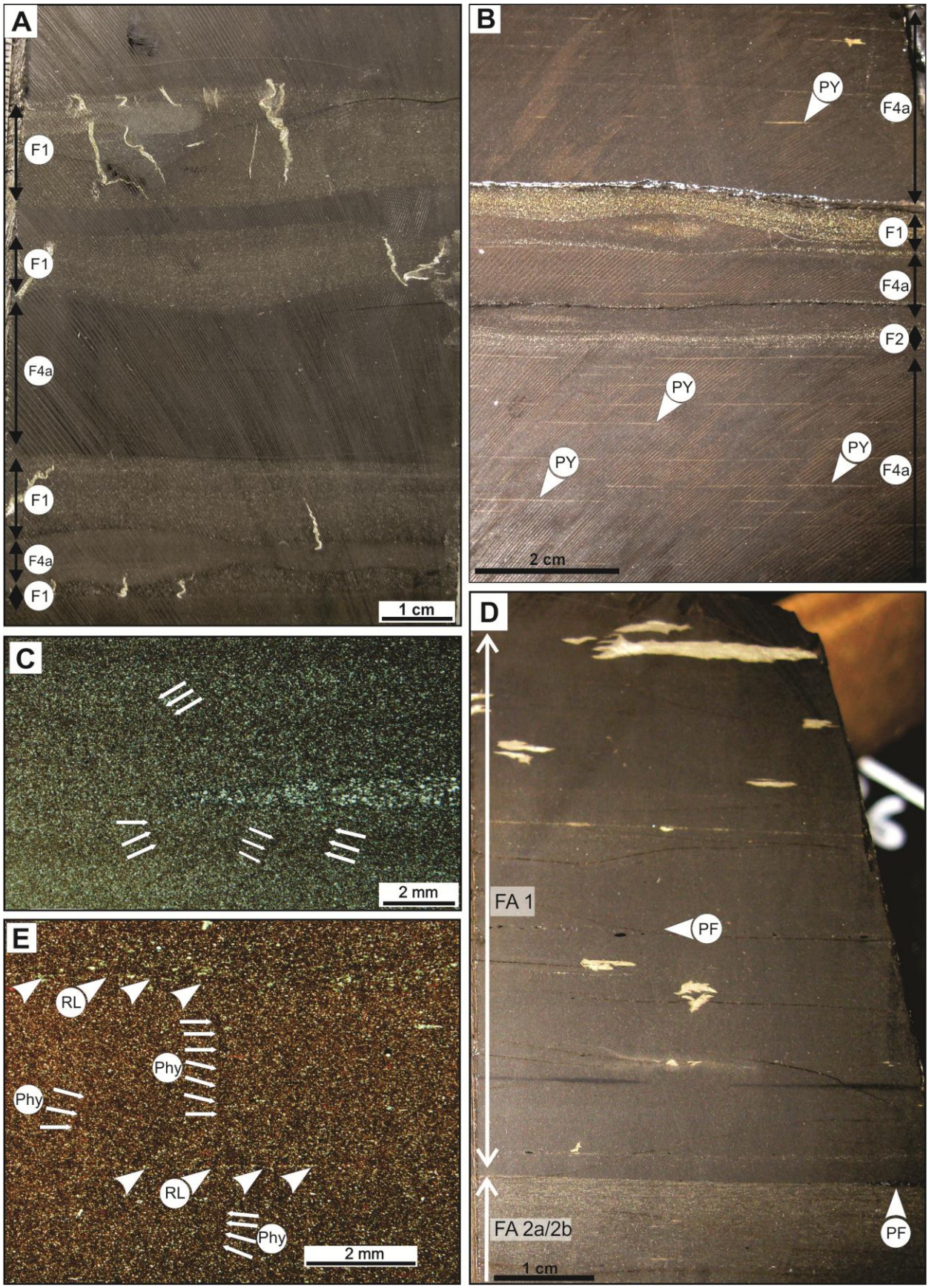
A
F1
F1
F4a
F1
F4a
F1
1 cm
B
PY
F4a
F1
F4a
F2
PY
PY
PY
F4a
2 cm
C
2 mm
D
FA 1
PF
FA 2a/2b
PF
1 cm
E
RL
Phy
Phy
RL
Phy
2 mm

Figure 6 (previous page). Examples of massive to faintly laminated mudstones (facies association 1). **(A)** Massive to faintly laminated mudstones containing thin beds of radiolarite (F1), which display mineralized compacted fractures (Shell Oil Burbank BIA 23-8, 10533.1 ft). **(B)** Core photograph showing layers of pyrite-mineralized radiolaria-bearing mudstone (F2) and radiolarite (F1), and abundant discontinuous pyrite laminae (PY) (Newfield production Sergeant Major 1-21H, 11056.0 ft). **(C)** Optical micrograph of silt-bearing mudstone mudstone containing a lens of radiolaria-bearing mudstone that was deposited by bedload processes. Note very faint silt-bearing, relict planar banding and ubiquitous, albeit vague, *Phycosiphon incertum* type B fecal strings (arrows) (Meridian Oil Inc. MOI 44-27H, 10244.4 ft). **(D)** Core photograph illustrating typical section of massive to faintly laminated mudstone with numerous pyrite concretions. Photograph also shows lenses of phosphate- and fossil-bearing mudstone (PF), and a knife-sharp, possibly erosive, contact with the underlying facies association 2 mudstone. (Headington Oil Co. Nesson State 42X-36, 10309.7 ft). **(E)** Optical micrograph of silt-bearing mudstone illustrating faint relict laminae (RL) and vague, although ubiquitous, *Phycosiphon incertum* type B fecal strings (Phy) (Amerada Hess Corp. J. Horst 1-11H, 10515.9 ft).

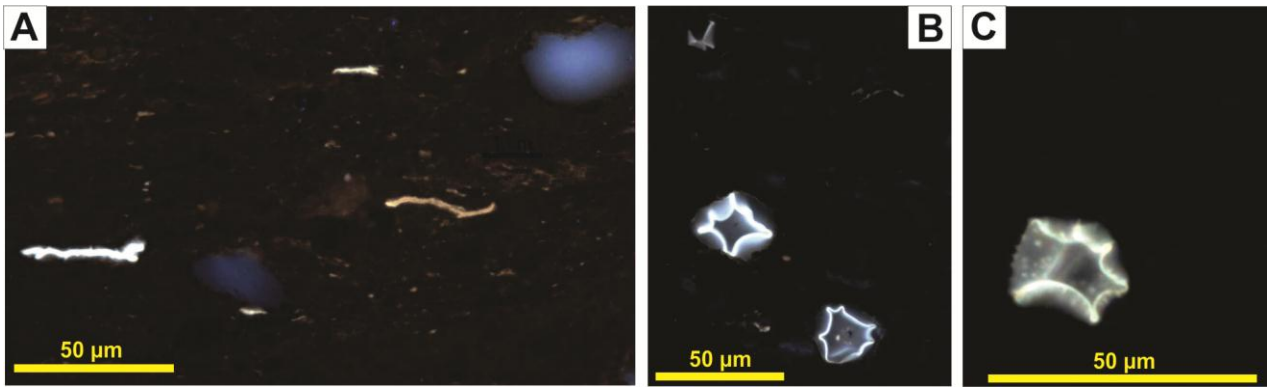

Figure 7. Incident UV light photomicrographs showing fluorescent unicellular Prasinophyte alginite macerals. **(A)** Photomicrograph of flattened Prasinophyte alginite macerals typical of most clay-rich mudstone samples within the upper Bakken member. Photomicrograph is of clay clast-bearing mudstone (EOG Resources Inc. Sidonia 1-06H, 8731.4 ft). **(B, C)** Photomicrographs of silica-filled Prasinophyte alginite macerals within radiolarite (Stanolind Oil & Gas W & I Waswick #1, 7570.1 ft).

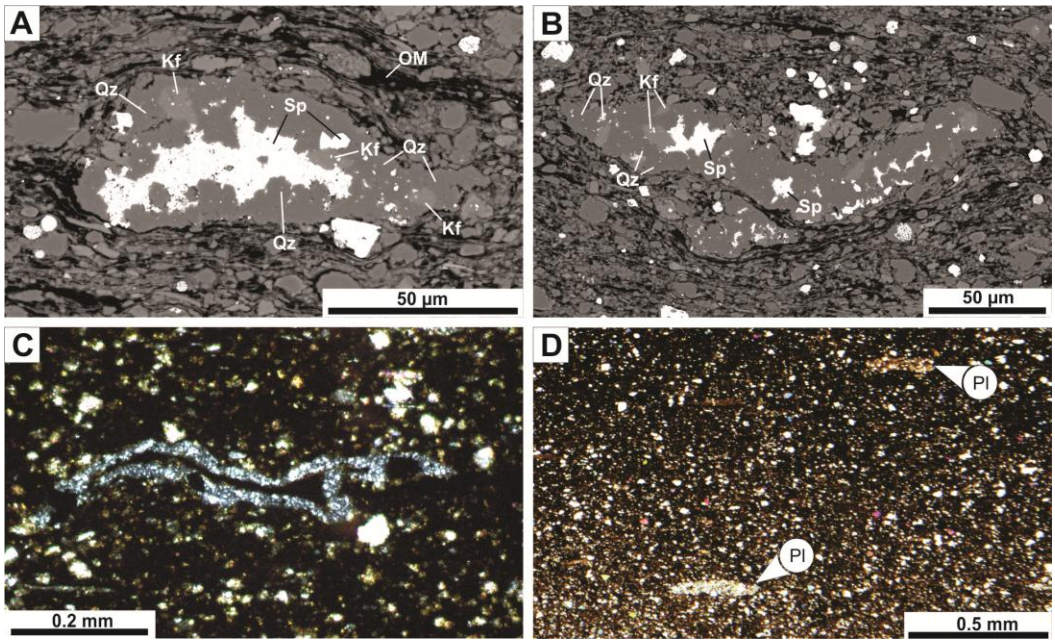

Figure 8**. (A and B)** SEM backscatter micrographs of massive to faintly laminated mudstone (FA1) within Amerada Hess Corp. J Horst 1-11H at 10515.9 ft shown in Figure 6E. Images show cemented mineral aggregates interpreted to be agglutinated foraminifera. Agglutinated tests are composed of quartz grains (Qz) and minor potassium feldspar (Kf). Voids within the tests are filled with diagenetic sphalerite (Sp). Low η (black colored) grains in matrix are organic matter (OM). **(C)** Photomicrograph in cross-polarized light showing collapsed agglutinated foraminifera test within burrow-mottled mudstone with shells (FA3) (Helis Oil & Gas Linseth 4-8H, 10777.3 ft). **(D)** Photomicrograph of massive to faintly laminated mudstone (FA1) containing *Planolites* type A burrows (Pl) (Headington Oil Co. Nesson State 42X-36, 10303.7 ft).

4.2.2 Facies association 2a | Well laminated Mudstone

Well laminated mudstone (FA2a) forms continuous vertical sections that range from 50 mm to 2.5 m in thickness. This facies association has a moderately to well laminated fabric (Fig. 9A) and consists of silt-bearing mudstone with intercalated laminae and thin beds of radiolarite (Fig. 9A, 9B) and radiolaria-bearing mudstone (Fig. 9F), which generally make up 10-25% of the rock. The clay-rich, silt-bearing mudstone laminae are mostly 1-5 mm in thickness (Fig. 9A-D) and are weakly to moderately disturbed by *Phycosiphon incertum* type B fecal strings (Fig. 9C, 9D) and rare *Planolites* type A burrows. In some places the mudstone displays downlapping

laminae (e.g. Fig. 5G). Carbonate and siliciclastic silt makes up 10-30% of the rock and on average, 77% of it is fine- to medium-grained silt size. The clay size fraction consists of clay minerals, siliciclastic and carbonate grains, pyrite and fine-grained organic matter. The organic matter is composed mainly of amorphous matrix bituminite and in places includes 10-20% lenses up to 0.1 mm in length of red-brown lamellar bituminite, and small (<50 μm) Prasinophyte alginite macerals (e.g. Fig. 7A-C). Some samples contain 1-5% clay clasts which are up to 0.4 mm in length. Continuous dark brown laminae typically <1 mm in thickness consisting of clay-dominated mudstone occur in some thin sections (Fig. 9C). Intercalated continuous and discontinuous laminae of siltstone (Fig. 9B), as well as laminae of phosphate- and fossil-bearing mudstone (Fig. 9G), are common and these are typically less than 2 mm in thickness. Radiolaria-bearing mudstone occurs in a range of morphologies and fabrics within this facies association and these include: (1) scattered discontinuous very thin laminae only 2-5 radiolaria tests thick and 5-30 mm long (Fig. 5C) that tend to be patchy in distribution, (2) laminasets typically 3-10 mm thick (Fig. 5C), and (3) massive laminae and thin beds mostly 3-15 mm in thickness which occasionally show basal scouring (Fig. 9F).

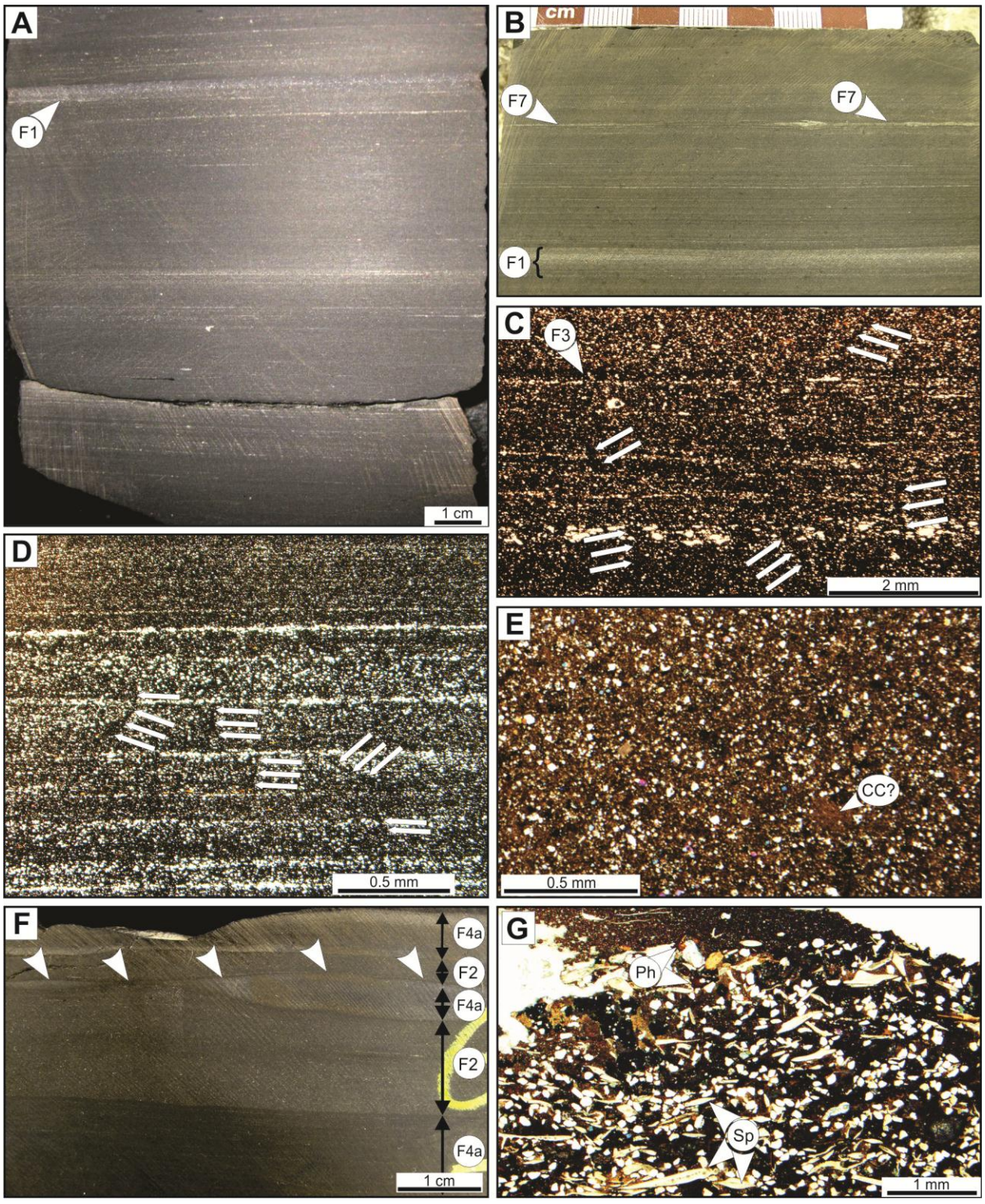

Figure 9. Examples of well laminated mudstones (facies association 2a). **(A, B)** Core photograph of well laminated mudstone (FA2a) illustrating the well laminated fabric in hand specimen. Samples contain radiolarite (F1) and siltstone (F7). Compare fabric to massive to faintly laminated mudstone (FA1) in Figures 6A, 6B, 6D. (A: Cirque

Resources Trippell 32-16H, 8332.9 ft); B: Cirque Resources Trippell 32-16H, 8332.3 ft). **(C, D)** Optical micrographs of silt-bearing mudstone. C includes thin laminae of clay-dominated mudstone (F3). Arrows point to *Phycosiphon incertum* type B fecal strings that disrupt the lamina fabric (C: Brigham Oil & Gas Olson 10-15 1H, 10615.0 ft; D: Texaco Inc. Thompson Unit #5-1, 11049.0 ft; **(E)** Optical micrograph of thin section cut parallel to bedding illustrating paucity of clay clasts within this facies association (compare to Figure 10C) (Meridian Oil Inc. MOI #44-27, 10224.4 ft). **(F)** Core photograph showing an erosion surface (arrows) at the base of a layer of radiolaria-bearing mudstone (F2). Erosion surface truncates a thin layer of silt-bearing mudstone (Oxy USA Inc. Sadowsky 24-14H, 10461.9 ft). **(G)** Optical micrograph of phosphate- and fossil-bearing mudstone containing phosphate clasts (Ph) and numerous sponge spicules (Sp) (Meridian Oil MOI #44-27, 10225.9 ft).

4.2.3 Facies association 2b | Well laminated Clay Clast-Bearing Mudstone

Well laminated, clay clast-bearing mudstone (FA2b) is identifiable only in thin section (where clay clasts can be observed) but based on numerous thin sections of this mudstone in Marathon Jensen #12-44, and Stanolind Oil & Gas W & I Waswick 1, may form continuous vertical sections potentially up to 2.5 m in thickness. Laminae are typically 1-5 mm thick and are defined primarily by variations in the abundance of silt grains and clay clasts (Fig. 10A, 10B, 10D). Clay clasts make up 5-50% of the rock and in thin sections cut parallel to bedding they are very irregular in shape and have ragged edges (Fig. 10C). Dark brown, silt-poor laminae of clay-dominated mudstone occur in places and these typically are continuous, laterally even in thickness and are devoid of clay clasts. Carbonate and siliciclastic detritus makes up 8-30% of the mudstone overall and 75% of the silt on average is fine- to medium-silt size (Table 3). The clay size fraction consists of siliciclastic and carbonate grains, clay minerals, pyrite, and organic matter. The organic matter is composed of amorphous matrix bituminite, 5-20% red-brown colored lamellar bituminite lenses (typically <1 mm but up to 3 mm in length) (Fig. 10D), and <1% small (<40μm) Prasinophyte alginite macerals (Fig. 7A). *Phycosiphon incertum* type B fecal strings vary from sparse to abundant and disrupt the fine mudstone laminae. Intercalated

continuous and discontinuous siltstone laminae typically <2 mm thick are common, and in places these contain fragments of siliceous microfossils and clay clasts (Fig. 10A). Mudstone laminae containing clay clasts, phosphate clasts, sponge spicules and conodont elements occur in places; they are typically 1-3 mm in thickness and are sometimes discontinuous (Fig. 10G). These laminae often contain abundant pyrite (up to 35%), which is precipitated preferentially around the margins of clay clasts in some samples (Fig. 10F). Laminae and thin bed of radiolaria-bearing mudstone make up 1-10% of the rock and take on a variety of morphologies identical to those within well laminated mudstones (FA2a) and these are:(1) dispersed discontinuous laminae only 2-5 tests thick, (2) laminasets typically 3-10 mm thick, and (3) massive laminae and thin beds mostly 3-15 mm in thickness. Laminae of radiolarite are also intercalated into these mudstones in places. These are generally continuous and laterally even in thickness but are also laterally variable in thickness and discontinuous in places (e.g. Fig. 5E).

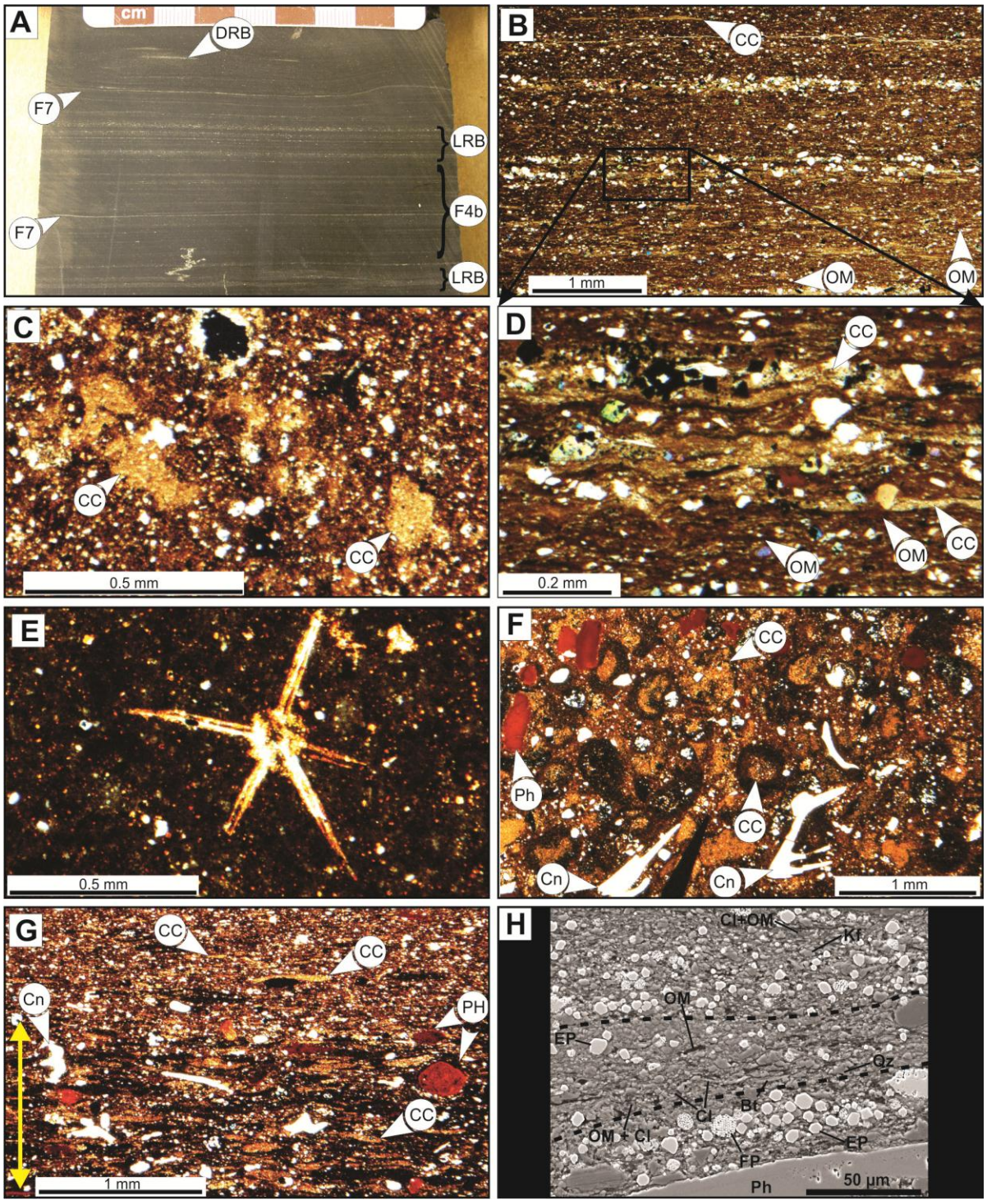

Figure 10. Examples of well laminated, clay clast-bearing mudstones (FA2b). **(A)** Core photograph illustrating the well laminated fabric typical of this facies association. Mudstone sample includes thin siltstone laminae (F7), very thin discontinuous laminae of radiolaria (DRB), and laminasets of radiolaria-bearing mudstone (LRB). Note mineralized fracture within LRB (Marathon Jensen #12-44, 9164.5 ft). **(B,)** Optical micrographs of silt- and clay clast-bearing mudstone (facies 4b) showing red-brown lenses of lamellar bituminite (OM) and large clay clast (CC)

(Marathon Jensen #12-44, 9169.0 ft). **(C)** Optical micrograph of silt- and clay clast-bearing mudstone showing irregular shape of clay clasts (CC) in thin sections cut parallel to bedding (Amerada Hess Corp. J. Horst 1-11H, 10527.0 ft). **(D)** Close-up view of a clay clast-rich lamina shown in Fig. 10B. **(E)** Photomicrograph of a well-preserved radiolaria test within silt- and clay clast-bearing mudstone. Thin section cut parallel to bedding (Marathon Jensen #12-44, 9163.5 ft). **(F)** Optical micrograph illustrating clay clast-, phosphate- and fossil-bearing mudstone (facies 6b) in a thin section cut parallel to bedding. Note dark pyrite-rich rims around clay clasts (CC). Cn: conodont elements, Ph: phosphate clast (Amerada Hess Corp. J. Horst 1-11H, 10527.0 ft). **(G)** Optical micrograph of laminae consisting of clay clast-, phosphate- and fossil-bearing mudstone (yellow arrow). Note the large size of clay clasts (CC) relative to most clay clasts in the overlying silt- and clay clast-bearing mudstone. The lamina includes phosphate clasts (Ph) and conodont elements (Cn) (Amerada Hess Corp. J. Horst 1-11H, 10527.0 ft). **(H)** SEM backscatter micrograph showing higher magnification view of a clay clast (dashed outline) from thin section shown in (G). Minerals identified within clay clast include clays (Cl), organic matter (OM), euhedral pyrite (EP), biotite (Bt) and quartz (Qz). The clay clast clearly contains less euhedral and framboidal pyrite (FP) than the surrounding matrix.

4.3.4 Facies association 3 | Burrow-Mottled Mudstone with Shells

Burrow-mottled mudstone with shells (FA3) consists of varying amounts of shell-bearing mudstone, burrow-mottled mudstone and silt-bearing mudstone (Fig. 11A, 11F). The ichnofauna typically includes highly compressed indeterminate horizontal burrows 2-10 mm in width, and inclined indeterminate burrows < 10mm diameter and <40 mm in length (Fig. 11A, 11B, 11C). In places, samples at the contact with the overlying Lodgepole Formation contain highly compressed burrows resembling *Thalassinoides* (Luis Buatois pers. comm., 2013) and *Planolites* type B (Fig. 11B). Most burrows are filled with a light-colored mud resulting in a mottled texture in highly bioturbated samples (e.g. Fig. 11A). Shells are mostly 0.3-10 mm long, but can be up to 30 mm in length (Fig. 5L, 8F). Agglutinated foraminifera are numerous in some samples (Fig. 8C). Two pyritized shells were observed on broken core ends. One of them has comarginal growth rings, is preserved in life position with the valves splayed open, and is tentatively

interpreted to be a Paleozoic relative of the *Bositra* genus (Fig. 11E). The other is a slightly disarticulated indeterminate bivalve (as indicated by its equivalves) with radial riblets (Fig. 11D).

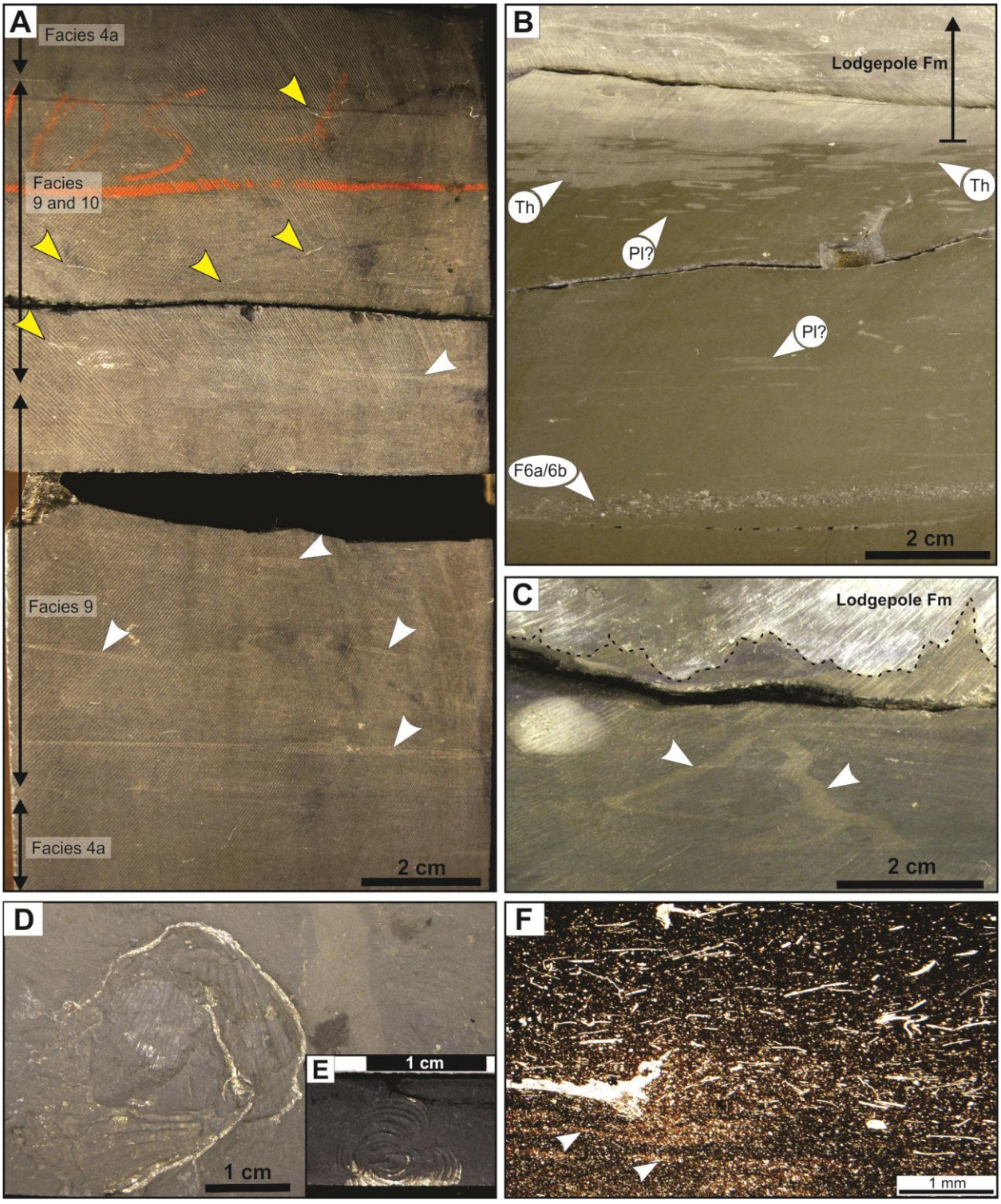

Figure 11 (previous page). Examples of burrow-mottled mudstone with shells (FA3). **(A)** Digitally contrast-enhanced core photograph illustrating typical stacking pattern of silt-bearing mudstone (facies 4a), burrow-mottled mudstone (facies 9) and shell-bearing mudstone (facies 10) within burrow-mottled mudstone with shells (FA3). White arrows point to indeterminate burrows. Yellow arrows point to shells and shell fragments (Shell Oil Burbank BIA 23-8, 10521.2 ft). **(B, C)** Core photographs of the bioturbated contact between the Lodgepole Formation and the underlying upper Bakken member. Photograph B contains highly compressed burrows (arrows) including possible *Thalassinoides* (Th), Planolites type B (Pl), and a lag of phosphate- and fossil-bearing mudstone. C contains large indeterminate inclined burrows (arrows) and illustrates a highly irregular contact with the Lodgepole Formation indicative of soft sediment deformation (B: Lyco Energy Titan FWP 32-14H, 10674.3 ft; C: Helis Oil & Gas Linseth 4-8H (10776.1 ft). **(D)** Indeterminate bivalve (Shell Oil Burbank BIA 23-8, 10525.1 ft). **(E)** Articulate bivalve preserved in life position (*Bositra*?) (Samson Resources Nordstog 14-23-161-98H, 8606.6 ft). **(F)** Optical micrograph of burrow-mottled mudstone with shells (FA3) showing lighter-colored burrows (white arrows) and numerous small shells <1 mm (Headington Oil Co. Nesson State 42X-36, 10296.4 ft).

4.3.5 Facies association 4 | Interlaminated Siltstone and Mudstone

Interlaminated siltstone and mudstone (FA4) was observed primarily in the Conoco Karsky 35 #2 well where it dominates a 5 m thick section of core (Appendix 2). In other wells, interlaminated siltstone and mudstone (FA4) occurs only rarely in horizons typically <10 cm thick. This facies association is characterized by continuous and discontinuous lenses, laminae and laminasets of siltstone 1-10 mm thick intercalated with silt-bearing, clay-rich mudstone. (Fig. 12). Ripple-laminae and erosion surfaces at the base of siltstone laminasets are common. Ichnofauna consist primarily of *Planolites* type B burrows 1-2 mm in length (Luis Buatois pers. comm., 2013) and *Phycosiphon incertum* type B fecal strings, which are abundant within the intercalated silt-bearing mudstone layers. Sparse *Teichichnus* burrows also occur in places (Luis Buatois pers. comm., 2013) (Fig. 12). Agglutinated foraminifera are rare. From 10124.0 to 10125.3 ft within the Conoco Karsky 35 #2 core, much of the siltstone is burrow-mottled (Fig. 5J), which is otherwise uncommon.

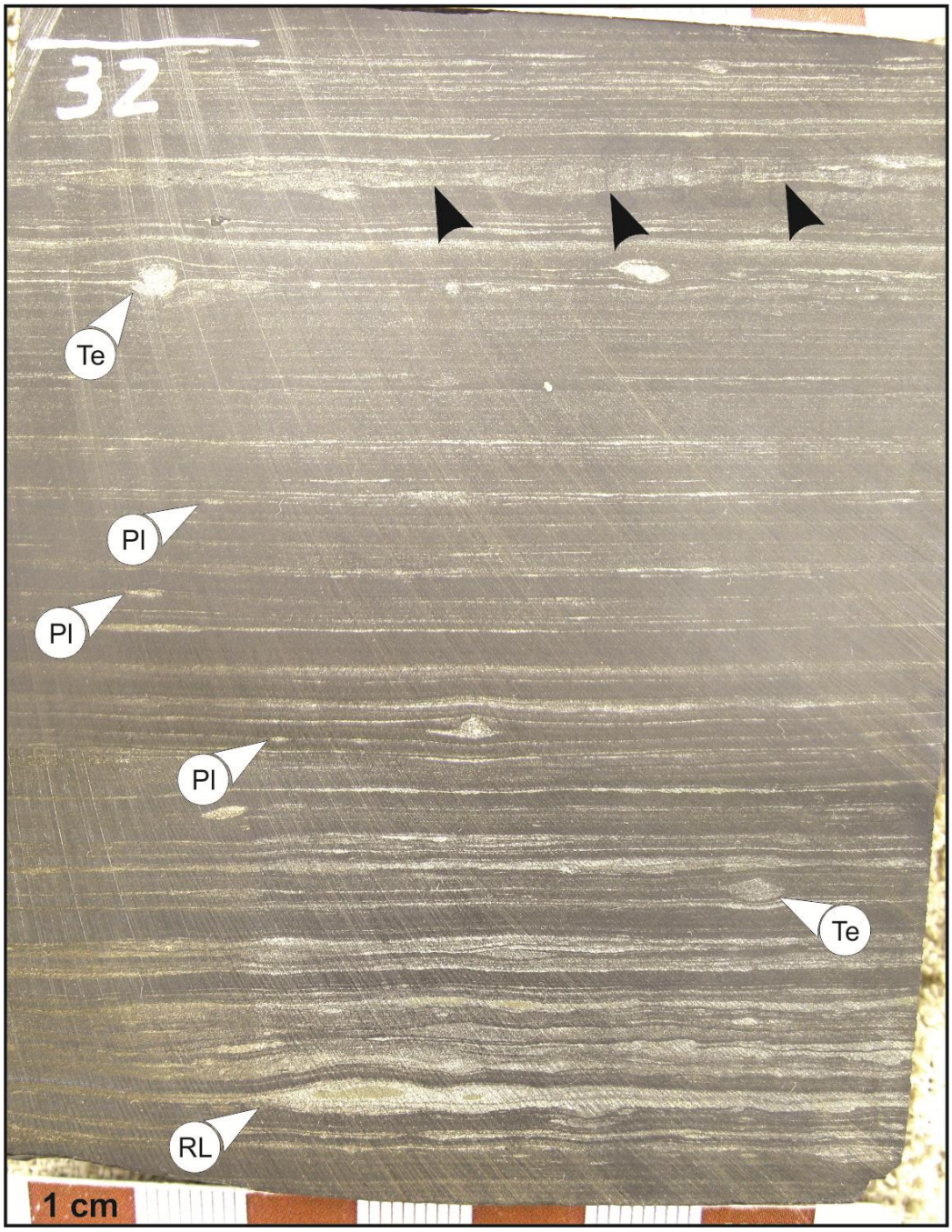

Figure 12. Core photograph of interlaminated siltstone and mudstone (FA4) containing small *Planolites* type B (Pl), *Teichichnus* (Te) (Luis Buatois pers. comm., 2013) and silt ripple laminae (RL). Black arrows delineate an erosion surface along the base of a siltstone laminaset (Conoco Karsky 35 #2, 10132.2 ft).

4.4 Interpretation of Facies Associations

The presence of predominantly clay-size particles as well as suspension-derived planktic radiolaria, conodont elements and small Prasinophyte alginite macerals within this finely-laminated mudstone succession suggests that the upper Bakken member was deposited below storm wave base in a distal shelf environment (Egenhoff and Fishman, 2013; Ormiston, 1993; Stasiuk, 1994; Stasiuk and Fowler, 2004; Sweet and Donoghue, 2001). Nevertheless, the laminae of siltstone, phosphate- and fossil-bearing mudstone, and clay clast-, phosphate- and fossil-bearing mudstone are all interpreted to represent distal storm-induced deposits, not produced by storm waves, but by storm-induced currents that can influence deposition also below storm wave base (Einsele, 2000, p.101; Macquaker et al., 2010; Friedrichs and Wright, 2004). All of these laminae are interpreted as tempestites because (1) they contain coarser detrital sediment than the surrounding mudstone and (2) they are frequently laterally discontinuous, and therefore could not have been deposited by suspension settling. Likewise, the discontinuous laminae and thin beds of radiolaria-bearing mudstone also indicate that advective processes transported muddy sea floor sediment in this distal shelf environment. Additionally, clay clasts where they are present are generally larger within the intercalated laminae of siltstone and phosphate- and fossil-bearing mudstone than in the surrounding mudstone, further suggesting that these laminae represent higher energy events.

The very small size of the ichnofauna and the very low ichnodiversity within most of the upper Bakken member points to stressful environmental conditions on the sea floor during deposition of much of the succession (Buatois and Mangano, 2011, p. 105, 118). The occurrence of this diminutive ichnofauna in sediments that are relatively rich in organic matter argues for bottom conditions that were suboxic to moderately dysoxic (see Tyson and Pearson, 1991 for

definitions); however, short term seasonal fluctuations to anoxic or oxic conditions may have occurred (Oschmann 1994; Tyson and Pearson, 1991). It is difficult to determine the original depositional process of massive to faintly laminated mudstone (FA1) due to the thorough reworking by the organism producing the *Phycosiphon incertum* type B fecal strings. Nonetheless, the overall very low proportion of siliciclastic and carbonate grains larger than medium-silt size (Table 3) and the general absence of clay clasts argues for a depositional environment that was very calm and distal. This interpretation is supported by the overall lack of relict, high-energy laminae of siltstone and/or phosphate- and fossil-bearing mudstone. However, the sparse presence of these storm event laminae, the occurrence of rare clay clasts and discontinuous laminae and thin beds of radiolaria-bearing mudstone nonetheless indicates that bedload processes deposited at least some of the massive to faintly laminated mudstones (FA1). Well laminated mudstones (FA2a) and well laminated, clay clast-bearing mudstones (FA2b) are both interpreted to represent a higher energy setting than the massive to faintly laminated mudstones (FA1). This is because in comparison to facies association 1, well laminated mudstones (FA2a) and well laminated, clay clast-bearing mudstones (FA2b) both contain: (1) coarser grained detrital silt (Table 3), (2) more siltstone and phosphate- and fossil bearing laminae and (3) a greater abundance of mudstone ripple laminae. However, evidence of bedload transport within well laminated mudstone (FA2a) is not widespread because the finely laminated fabric was severely disrupted by the organism producing the *Phycosiphon incertum* type B fecal strings and most sedimentologic key textures were destroyed. In contrast, the abundance of clay clasts within well laminated, clay clast-bearing mudstones (FA2b) clearly indicates that sedimentation of this facies association was dominated by bedload transport processes. These clay clasts are interpreted to be water-rich mud fragments (Schieber et al., 2010) that were

eroded from the sea floor. Bottom water energy levels varied significantly during deposition of well laminated, clay clast-bearing mudstones (FA2b). This is indicated by the presence of intercalated event laminae of siltstone and clay clast-, phosphate- and fossil-bearing mudstone. The sparse laminae of dark brown, silt-poor, clay-dominated mudstone within well laminated mudstones (FA2a) and well laminated, clay clast-bearing mudstones (FA2b) are interpreted in this study, and by Egenhoff and Fishman (2013), to represent periods dominated by suspension sedimentation during very calm conditions. The paucity of these intercalated laminae within massive to faintly laminated mudstone (FA1) is probably due to the very thorough reworking of these sediments by the organism producing *Phycosiphon incertum* type B fecal strings. The clay-rich composition and absence of relict siltstone laminae or laminasets within burrow-mottled mudstone with shells (FA3) suggests that the depositional environment was probably distal from a source of detrital silt. The co-occurrence of numerous shells, relatively large indeterminate burrows and agglutinated foraminifera suggests that bottom waters were probably moderately dysoxic to occasionally oxic (Tyson and Pearson, 1991; Oschmann, 1994). Sedimentation of interlaminated siltstone and mudstone (FA4) was characterized by intermittent high-energy events that transported siliciclastic and carbonate silt with minor fine-grained sand by bedload processes depositing the intercalated siltstone laminae and laminasets. This is indicated by the presence of siltstone ripple laminae and erosion surfaces within these sediments (Fig. 12). The presence of *Phycosiphon incertum* fecal strings, as well as *Planolites* and *Teichichnus* burrows in places suggests that bottom waters that were at least moderately dysoxic to oxic at times (Tyson and Pearson, 1991).

Radiolaria are interpreted to have been deposited on the sea floor primarily during blooms which initially formed into laminae and thin beds of radiolarite. The intercalated laminae of radiolaria-

bearing mudstone are interpreted to represent radiolarite that was mixed with clay, silt and organic matter on the sea floor as a result of currents (Egenhoff and Fishman, 2013). This is supported by the presence of erosion surfaces at the base of some radiolaria-bearing mudstone laminae (Fig. 9F). Radiolarite occurs within massive to faintly laminated mudstone (FA1), well laminated mudstone (FA2a) and well laminated clay-clast-bearing mudstone (FA2b), indicating that conditions within these three depositional environments were often sufficiently calm for radiolaria bloom deposits to be preserved intact. In contrast, very thin discontinuous laminae (typically 2-5 tests thick) of radiolaria-bearing mudstone occur only within the higher energy well laminated mudstones (FA2a) and well laminated clay-clast-bearing mudstones (FA2b). These very thin laminae of radiolaria tests are therefore interpreted to represent radiolaria bloom deposits that have been thoroughly reworked and dispersed by currents.

5.0 FACIES ARCHITECTURE

5.1 Facies Distribution and Stacking Patterns

Three transects across the North Dakota portion of the Williston Basin including one well in eastern Montana illustrate a stratigraphic and areal distribution of facies associations. These facies associations are distributed regionally as well as on a smaller scale in coarsening-upward and fining-upward stacking patterns typically 0.2-0.5 m in thickness that are correlatable across distances of tens to hundreds of kilometers (Appendices 1-3). Individual stacking patterns are arranged into two higher order sediment packages within the upper Bakken member and these are interpreted to be parasequences-sets. These two parasequence-sets are represented by the stratigraphic units herein termed Interval 1 and Interval 2. Interval 1 represents the lowermost 0-3 m of the succession, which mostly ranges from 1.5-3.0 m in thickness, except in the Conoco Karsky 35 #2 well where it is almost 5 m thick. Interval 2 represents the upper 0-4 m of the succession except in the Conoco Karsky 35 #2 well where is it 7 m thick (Fig. 13, Appendices, 1-3). The boundary between Interval 1 and Interval 2 is conformable and regionally marks a distinct change in the predominant mudstone facies associations within these two units. These differences are described in detail below.

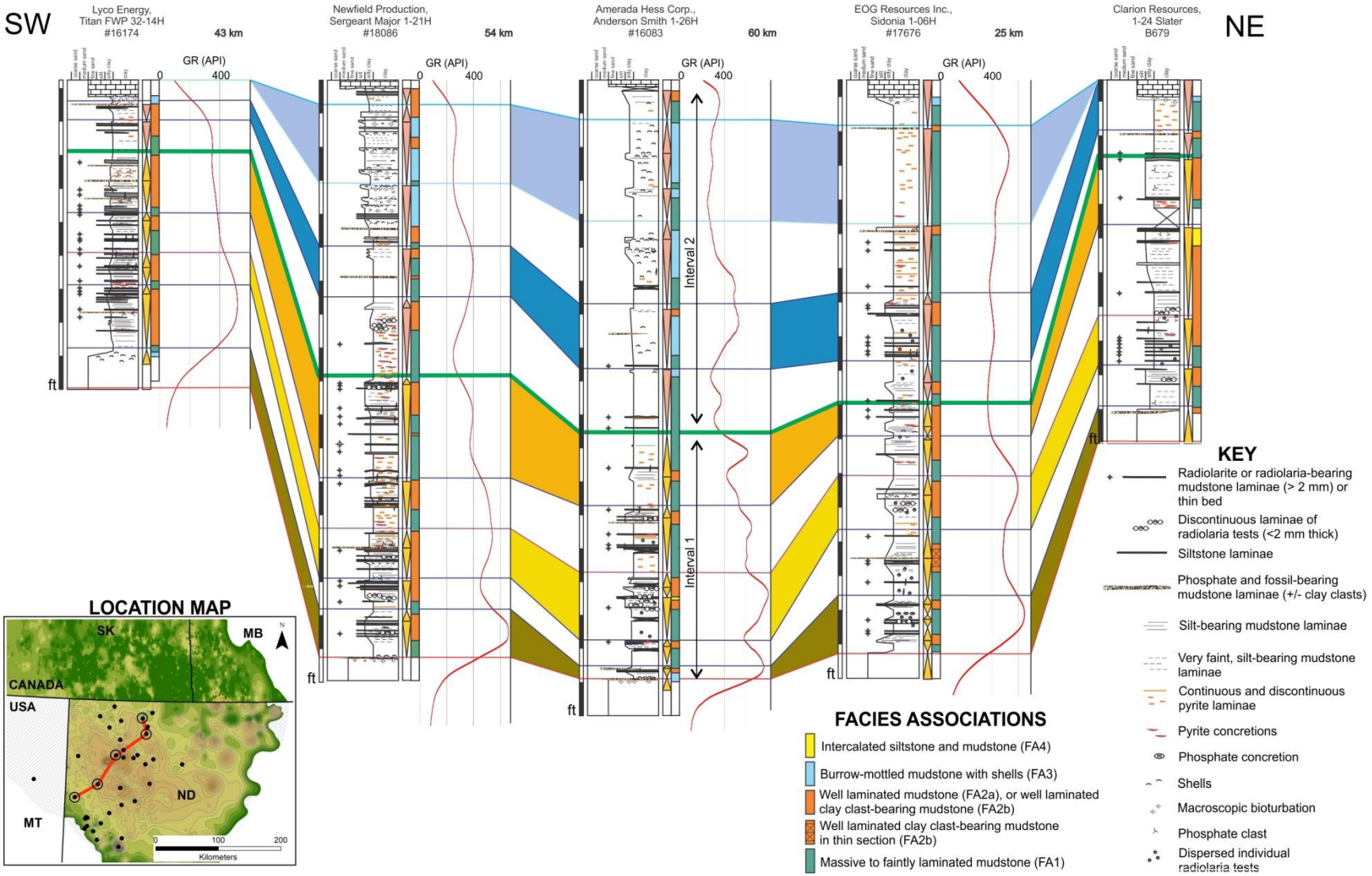

Figure 13. Transect consisting of five cores through the upper Bakken member showing detailed lithological core logs, gamma ray logs and correlation of stacking patterns.

5.1.1 Interval 1

The lower stratigraphic unit (Interval 1) occurs within all cores described in this project. It is readily distinguished from the overlying Interval 2 by the greater abundance of well laminated mudstones (FA2a) and well laminated, clay clast-bearing mudstones (FA2b). In general, this stratigraphic unit consists of three to five laterally correlatable coarsening-upward stacking patterns, each 150-400 mm in thickness. Fining-upward stacking patterns are also common and these are typically 10-100 mm thick (Fig. 13, Appendices 1-3). The lower parts of the coarsening-upward stacking patterns generally consist of massive to faintly laminated mudstone (FA1), which grades upward into slightly thicker-laminated and slightly coarser-grained, well laminated mudstones (FA2a) or well laminated, clay clast-bearing mudstones (FA2b). Near the basin margins, these stacking patterns consist predominantly of either well laminated mudstones (FA2a) or well laminated, clay clast-bearing mudstones (FA2b), whereas in the depocenter these cycles generally contain more massive to faintly laminated mudstone (FA1) (Fig. 14, Appendices 1-3). In some cores, one of the uppermost two stacking patterns in Interval 1 contains a 10-70 mm thick bed of ripple-laminated siltstone (e.g. Appendix 1: Amerada Hess Corp. Sara G Barstad 6-44H, 10,470.8 ft).

This distribution of thin sections containing either well laminated, clay clast-bearing mudstones (FA2b) or well laminated mudstones (FA2a) suggests that there is an areal distribution pattern of these two facies associations, indicated by the greater abundance of clay clasts in the northern, northeastern and eastern parts of the study area (Fig. 15). However, caution in interpreting this data is required given the irregular and less-than-ideal thin section coverage in mudstones with such small-scale facies heterogeneity. Despite this, Figure 15 illustrates that stacking patterns in the basin depocenter generally give way laterally toward the south and southwest to stacking

patterns containing well laminated mudstones (FA2a), whereas toward the north, northeast, and east, mudstones in the depocenter grade laterally into stacking patterns that generally frequently contain well laminated, clay clast-bearing mudstones (FA2b) (Fig. 15).

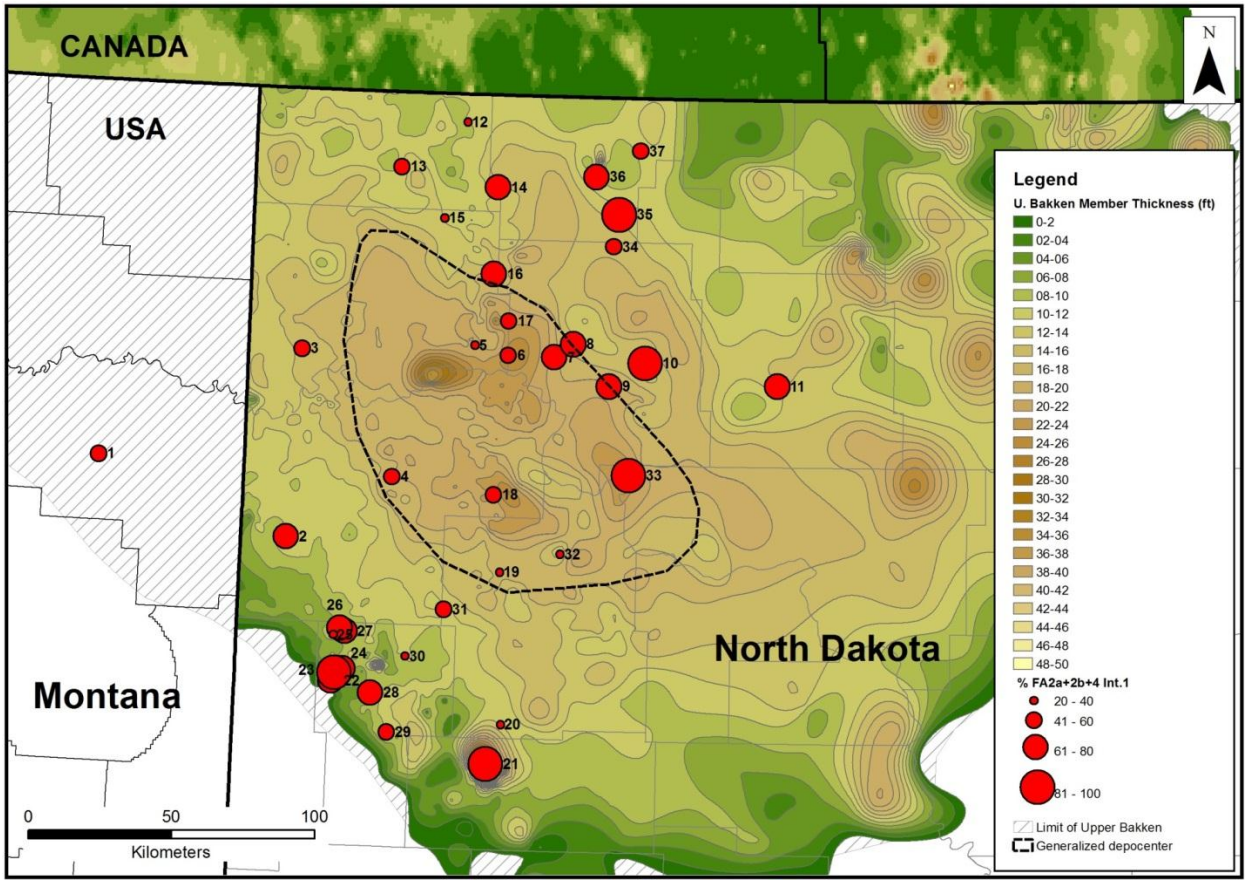

Figure 14. Isopach map of the upper Bakken member showing the percentage of rock in Interval 1 that consists of well laminated mudstone (FA2a), well laminated, clay clast-bearing mudstone (FA2b) and interlaminated siltstone and mudstone (FA4) combined for each well. Note the increased proportion of these three facies associations outside of the depocenter (dashed ellipse) relative to massive to faintly laminated mudstone (FA1). Number for each core refers to well name in Table 1.

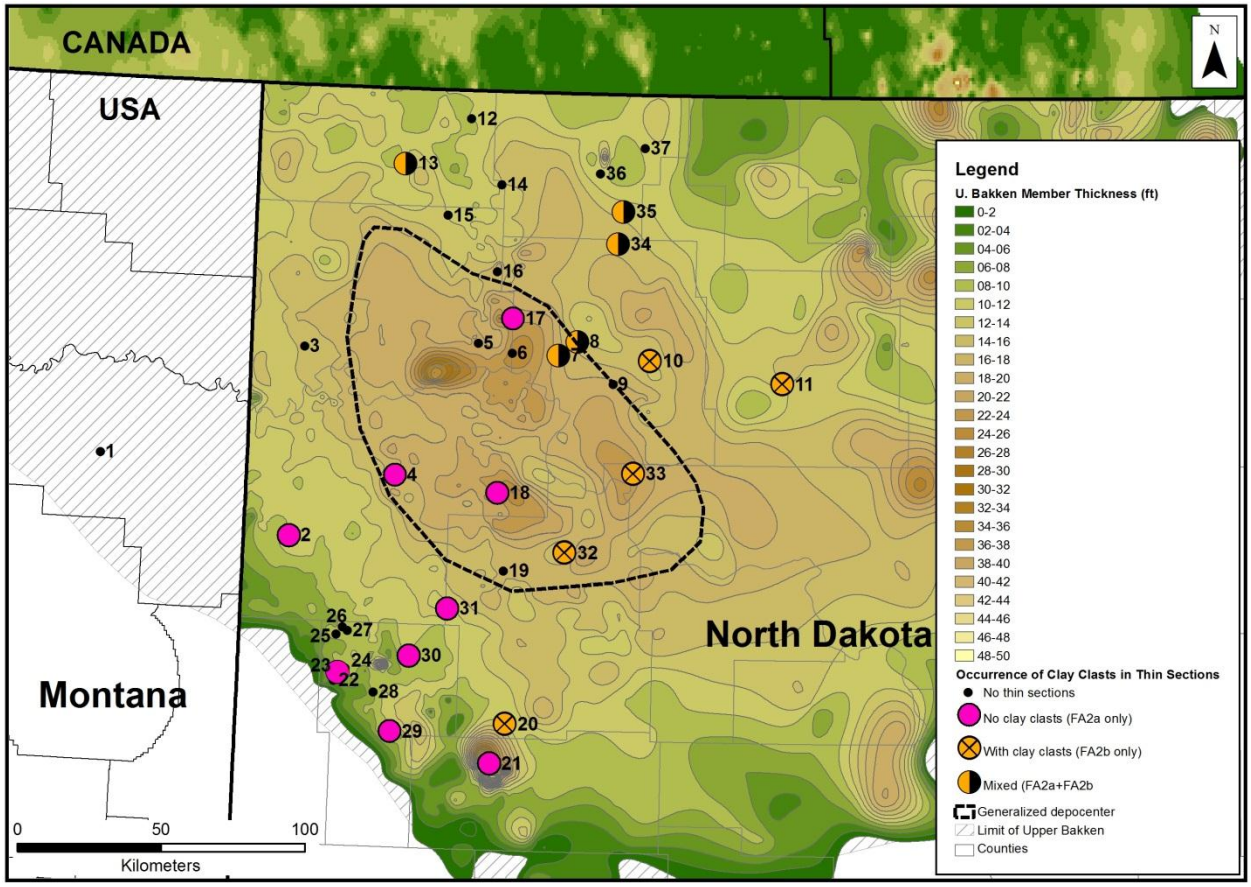

Figure. 15. Distribution of thin sections containing well laminated clay clast-bearing mudstone (FA2b) (i.e. > 5% clay clasts). Note the greater abundance of clay clasts in the northeastern part of the study area. See Appendices 1-3 for stratigraphic location and number of thin sections in each core. North Dakota isopach by Julie LeFever (pers. comm., 2013). Number for each core refers to well name in Table 1.

In most cores, intercalated laminae and thin beds of radiolaria-bearing mudstone and radiolarite are significantly more abundant within Interval 1. Laterally, however their abundance varies significantly from core to core. The transects illustrated in Appendices 1-3 show that laminae of radiolaria-bearing mudstone and radiolarite greater than 2 mm occur slightly more frequently within the massive to faintly laminated mudstones (FA1) at the base of individual parasequences than within the well-laminated mudstones (FA2a and FA2b). The abundance of laminae > 2 mm thick and thin beds of radiolarite and radiolaria-bearing mudstone also varies regionally. This is

shown by Figure 16, which illustrates that the average frequency of these radiolarite and radiolaria-bearing mudstone laminae per foot of Interval 1 mudstone is generally lowest for wells located in the depocenter. Moreover, wells with the greatest number of radiolarite and radiolaria-bearing mudstone laminae per foot of mudstone generally occur in wells located in a zone that lies roughly halfway between the depocenter and most proximal areas of upper Bakken member deposition (Fig. 16).

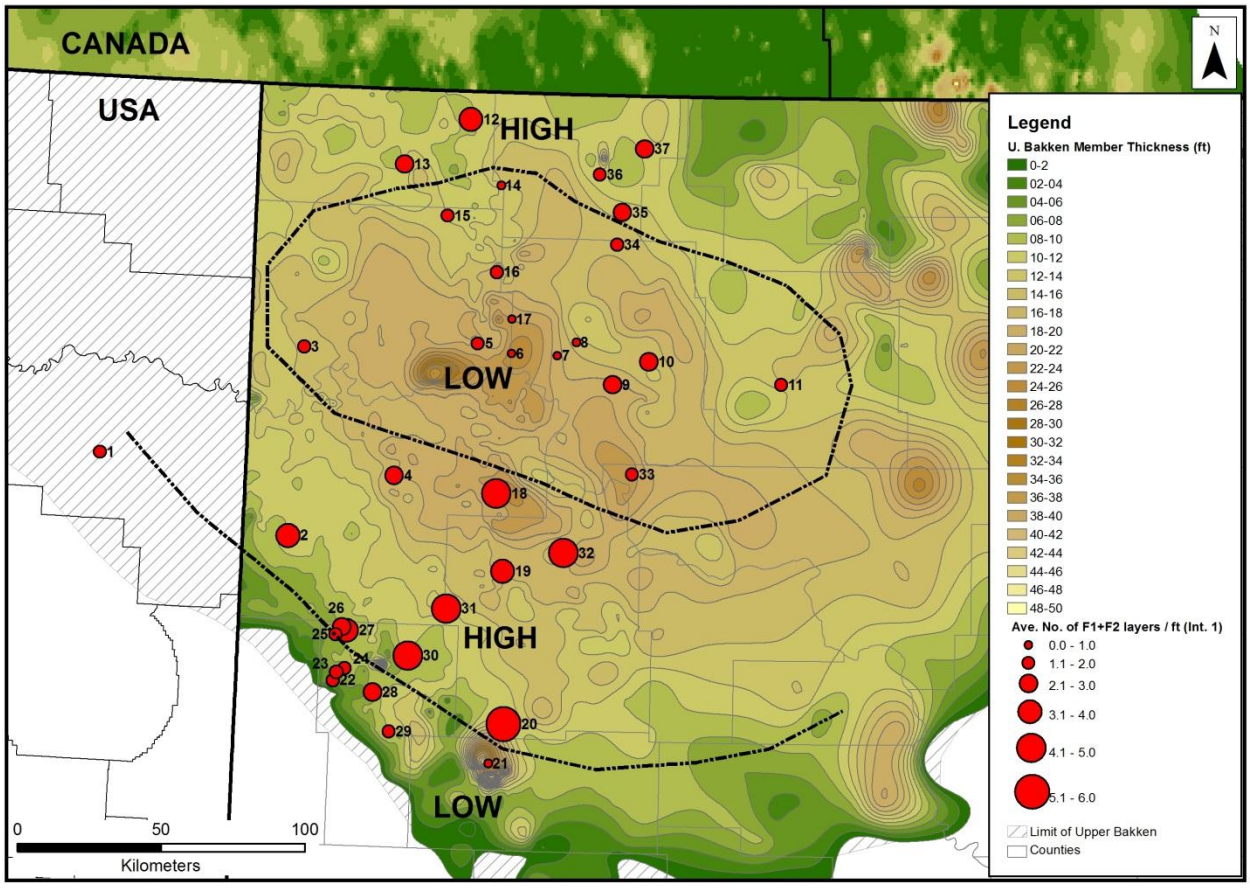

Figure 16. Map showing the average number of laminae > 2 mm thick of radiolaria-bearing mudstone and radiolarite per foot of mudstone within Interval 1. Isopach map by Julie LeFever (pers. comm., 2013). Layers of radiolarite and radiolaria-bearing mudstone are in general least abundant (LOW) in the depocenter and around the depositional edge, but more abundant (HIGH) between these two areas.

5.1.2 Interval 2

Interval 2 overlies Interval 1, is capped by the Lodgepole Formation, and contains five to seven small-scale coarsening-upward cycles predominantly 0.3-0.6 m in thickness. A few of these parasequences fine-upward and these are mainly 100-200 mm thick. This stratigraphic unit thins landward and was deposited within a slightly smaller area than Interval 1 (Appendices 1-3). In general, Interval 2 is thickest in the basin depocenter where it reaches 3-4 m in thickness. However, near the southern depositional edge there is small sub-basin where Interval 2 is 7n m thick in the Conoco Karsky 35 #2 core.

In the depocenter, the lower 2-3 m of Interval 2 consist of 60-95% massive to faintly laminated mudstone (FA1) intercalated with 20-100 mm thick horizons of well laminated mudstone (FA2a) or well laminated, clay clast-bearing mudstone (FA2b) (Fig. 13, Appendices 1-3). The thin horizons of well laminated mudstone (FA2a or FA2b), which may or may not contain clay-clasts, occasionally contain one or two laminae of phosphate- and fossil-bearing mudstone and siltstone, and form the tops of the coarsening-upward parasequences in this section. These cycles in the lower part of Interval 2 are in general very vaguely defined due to the subtle contrast in grain size, composition and laminae thickness between the top and base of these cycles. However, closer to the basin margins, parasequences within this lower part of Interval 2 are more distinct than those closer to the depocenter because they contain slightly more well laminated mudstone (FA2a or FA2b). Unlike within Interval 1, however, siltstone laminae are rare in Interval 2, even in core locations in proximal parts of the basin. Burrow-mottled mudstone with shells (FA3) occasionally occurs in this lower part of Interval 2 (e.g. Amerada Hess Corp Anderson Smith 1-26H, Fig. 13; Headington Oil Co. Nesson state 42X-36, Amarada Hess Corp. Sara G Barstad 6-44H, Appendix 2).

In the depocenter, the upper section of Interval 2 is composed of a 0.2-1.2 m thick stratigraphic zone dominated by burrow-mottled mudstone with shells (FA3). Laterally correlatable parasequences in this zone typically coarsen-upward from a horizon of massive to faintly laminated mudstone (FA1) at the base. The tops of these coarsening-upward cycles are commonly defined by a sharp surface which marks the fine-grained base of the overlying parasequence (Fig. 11A) (e.g. Helis Oil & Gas Linseth 4-8H, 10,777.5-10,781.0 ft (Appendix 2); Shell Oil Burbank BIA 23-8,10519.0-10524.0 ft, (Appendix 3)). In some cores, these laterally correlatable cycles contain smaller subordinate cycles <200 mm thick that represent an alternation of individual facies within burrow-mottled mudstone with shells (FA3) (e.g. Newfield Production Sergeant Major 1-21H, 11048.5 ft).

The Conoco Karsky 35 #2 core presents an exception to the general facies distribution pattern in Interval 2. This particular well represents a 20 km wide sub-basin located in the southern part of the study area near the depositional edge (Fig. 4). This core contains one of the thickest upper Bakken sections in the Williston Basin. Interval 2 in this core consists of a 7 m thick succession dominated by interlaminated siltstone and mudstone (FA4) with intercalated sections of well laminated mudstone (FA2a) that are 50-600 mm thick (Fig. 12, Appendix 2). Five small-scale, coarsening-upward cycles, each 1.2-1.5 m thick, occur within Interval 2 in this core, and these are defined by an increasing abundance of siltstone laminae and laminasets toward the top of each of the parasequences. The most silt-rich, coarsening-upward cycle, which is the second from the top in this core, is characterized by siltstone laminasets with abundant burrow-mottled siltstone (Fig. 5J).

6.0 GAMMA RAY LOGS AND TOTAL ORGANIC CARBON (TOC)

Total gamma ray (GR) logs for eighteen wells were used in this study. These were acquired from log ASCII files (LAS) and downloadable well files available on the NDGS website. Gamma ray logs were incorporated into this study to aid in stratigraphic correlations and to investigate how the abundance of radioactive constituents varies within the upper Bakken succession. Depths on gamma ray logs typically do not match the depths on the core, and have therefore been shifted to match the upper Bakken member contacts. Three cores drilled in the basin depocenter by Amerada Hess Corp. (i.e. Anderson Smith 1-26H, Sara G Barstad 6-44H, J. Horst 1-11H) are accompanied by high resolution spectral GR logs. These spectral logs provide insight into the small-scale variability and the source of gamma ray emissions.

The strongest gamma ray response within the upper Bakken member occurs consistently near the base of the succession where the log frequently reaches values of 800 API units (e.g. Fig. 13). The gamma ray response is typically lowest in two stratigraphic zones in the upper Bakken member, and these are: (1) a 0.6-1.2 m thick section at the base of Interval 2, which is dominated by massive to faintly laminated mudstone (FA1) and has GR values of 225-350 API units; and (2) the top 0.5-1.5 m of the succession in the basin depocenter where the rock is characterized by burrow-mottled mudstone with shells (FA3) and also GR values of 225-350 API units (e.g. Amerada Hess Corp Anderson Smith 1-26H (Fig. 13)). Outside of these two stratigraphic zones the GR log generally ranges between 350 and 600 API units. These two correlatable zones and the sections with distinctively elevated API units between them, particularly within Interval 1, aid with stratigraphic correlation of the lithologs on a regional scale. The small-scale variability shown in the spectral gamma ray logs does not correlate with the small-scale stacking of facies associations of the succession. Importantly however, the individual U, Th, and K spectra of these

logs follow each other very closely, indicating that the different sources of gamma ray emissions are coupled (Fig. 17).

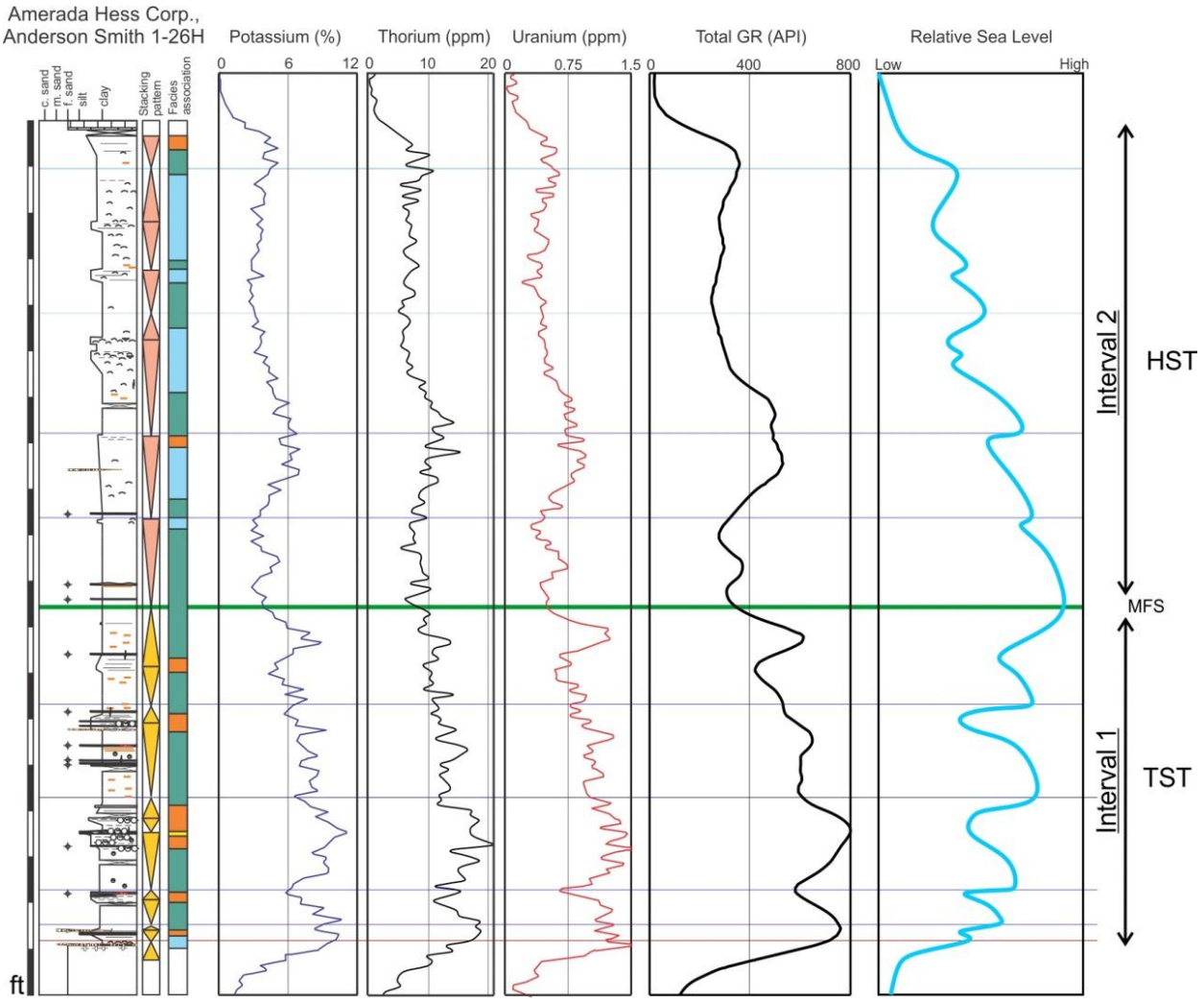

Figure 17. Lithology core log of Amerada Hess Corp. Anderson Smith 1-26H showing stacking patterns and spectral gamma ray logs. Interpretation of relative sea level curve with location of maximum flooding surface is also shown and is interpreted from stacking patterns. See Figure 13 for core log key.

The thorium/potassium crossplot (Quirein et al., 1982) for upper Bakken member mudstones indicates that Th and K spectra are derived primarily from illite and micas (Fig. 18).

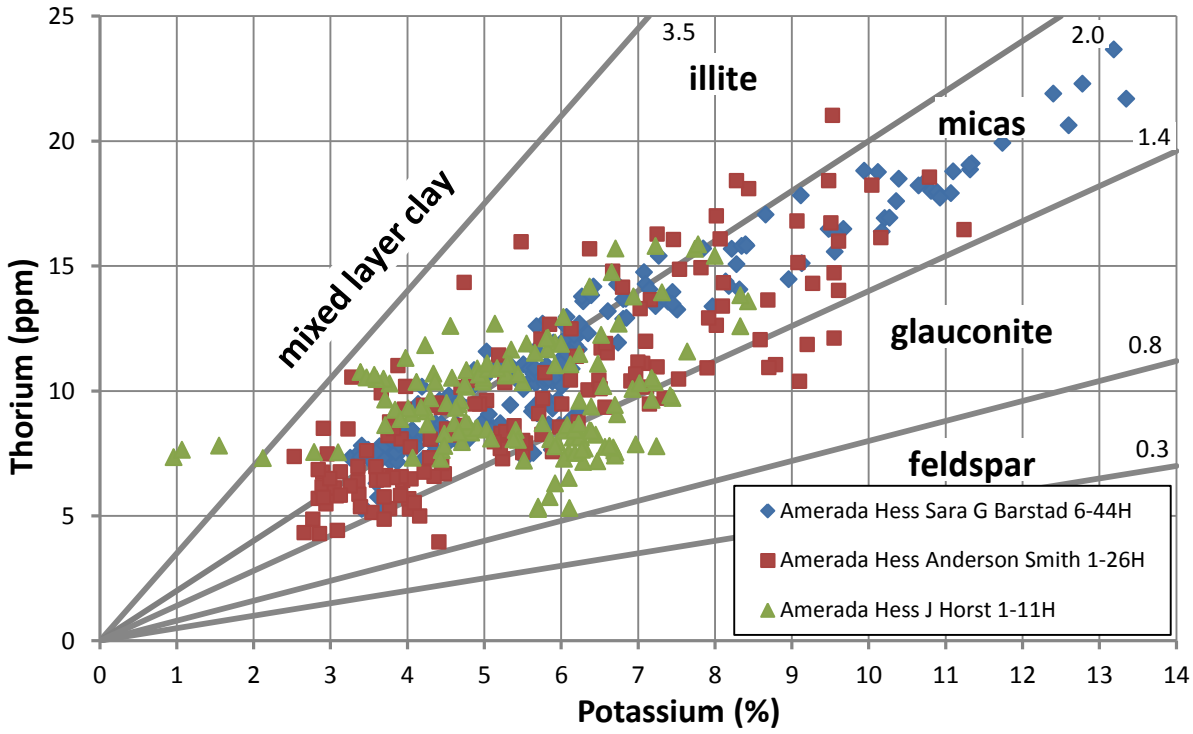

Fig. 18. Thorium/potassium crossplot of 497 data points from spectral gamma ray logs from three upper Bakken member cores. Crossplot modified after Quirein et al., (1982).

Twelve samples from the Helis Oil & Gas Linseth 4-8H core were analysed for TOC and values for these range from 3.09 to 11.45% (Fig. 19, 20). Whole rock vitrinite reflectance and Rock-Eval pyrolysis analyses performed on one sample of burrow-mottled mudstone with shells (FA3) from the Helis Oil & Gas Linseth 4-8H with 5.11% TOC indicate that the well sits in the oil window and has an Ro of 0.81 based on 17 measurements from material that appears to be vitrinite (Appendix 6). This sample has a Tmax of 446˚C and contains Type III kerogen (HI = 192 mg HC/g TOC, OI = 8 mg CO_2/g TOC) (Appendix 6). Research by Jin and Sonnenberg (2012) suggests that TOC within the upper Bakken member in thermally mature parts of the

Williston Basin decreased by 30-50% during catagenesis, which is a whole rock TOC reduction of 7-8%.

Seven of the twelve TOC samples consist of massive to faintly laminated mudstone (FA1) sampled from the lower part of coarsening-upward stacking patterns distributed at regular intervals over the entire thickness of the succession. The formation-scale TOC trend shown by these seven samples generally matches the GR log profile (Fig. 19), which is an overall decreasing TOC content from the base to the top of the succession. The highest TOC occurs in massive to well laminated mudstone (FA1) in the three samples from Interval 1, which have values between 10.6 and 11.5%, whereas the four samples of massive to well laminated mudstone (FA1) in Interval 2 have TOC values between 7.2% and 9.5%. The single sample of well laminated mudstone (FA2a) in Interval 2 contains 8.6% TOC, which is lower than all samples of massive to faintly laminated mudstone (FA1) except for two samples near the top of the succession. Two samples of burrow-mottled mudstone with shells (FA3) near the top of Interval 2 have two of the lowest TOC values within the succession, which are 5.1% and 7.4% (Fig. 19, 20). The data shown in Figure 18 also indicate that radiolaria-bearing mudstone contains significantly more TOC than (pyrite mineralized) radiolarite.

.

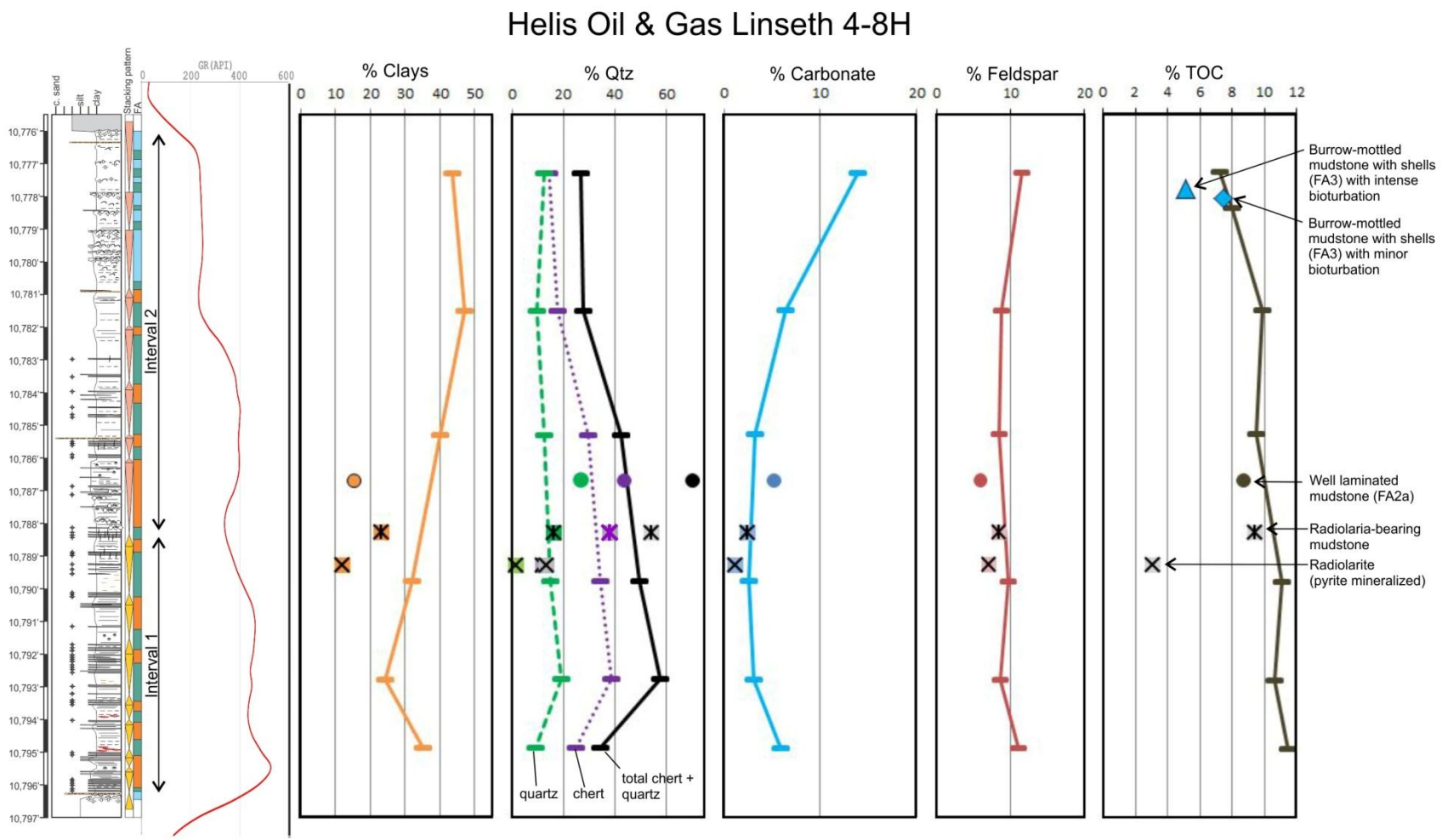

Figure 19. Lithology core log of Helis Oil & Gas Linseth 4-8H accompanied by gamma ray log, XRD and TOC data. Rectangular data points represent massive to faintly laminated mudstone (FA1) sampled from the lower part of coarsening-upward cycles. XRD data is not normalized with respect to TOC. Pyrite and gypsum content not shown. See Figure 13 for core log key and Appendix 5 for raw data.

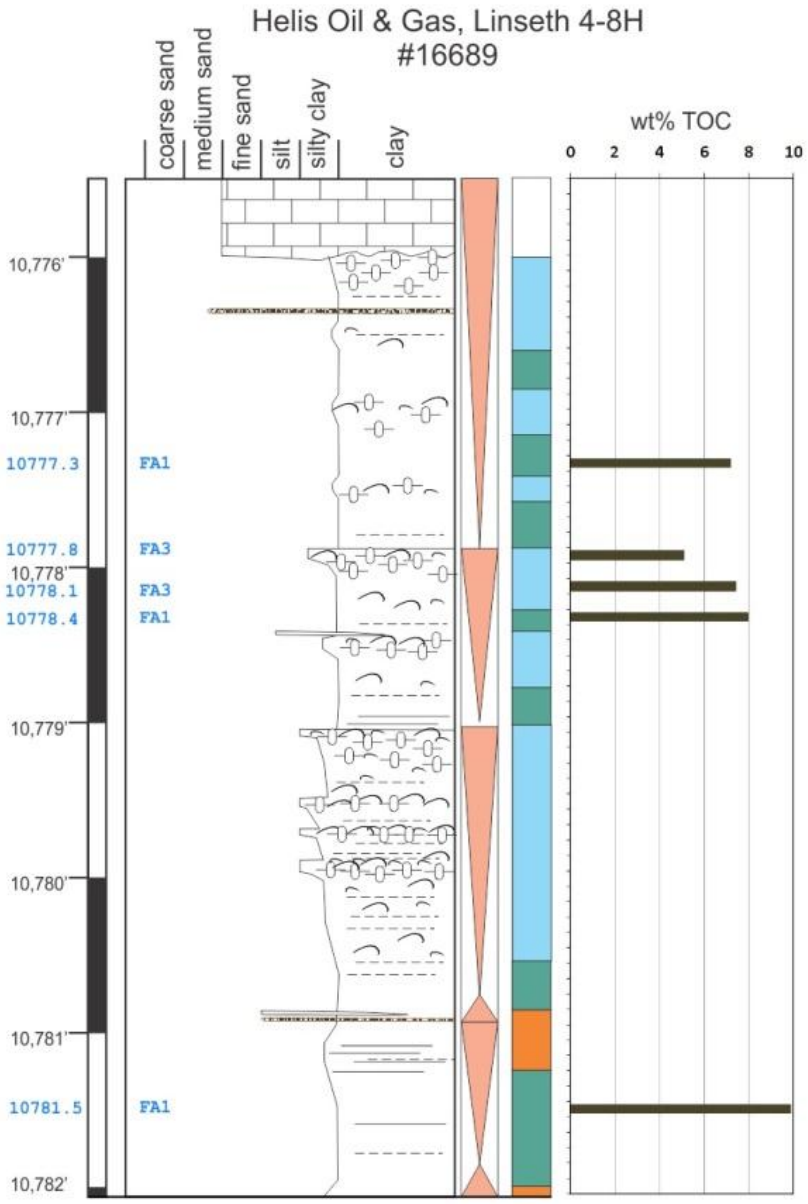

Figure 20. Detailed core log of the upper part of Helis Oil & Gas Linseth 4-8H shown in Figure 19 accompanied by TOC data showing small-scale TOC variability within a parasequence containing massive to faintly laminated mudstone (FA1 - green) and burrow-mottled mudstone with shells (FA3- blue). Note burrow-mottled mudstone with shells at 10777.8 ft is more intensely bioturbated than burrow-mottled mudstone with shells at 10778.1 ft and contains lower amounts of TOC. See Figure 13 for symbol key.

7.0 GEOCHEMISTRY (X-RAY DIFFRACTION DATA)

XRD analyses were performed on twenty-one samples from three cores (Helis Oil & Gas Linseth 4-8H, EOG Resources Sidonia 1-06H, and Samson Resources Nordstog 14-23-161-98H), which are located in different parts of the study area shown in Figure 21.

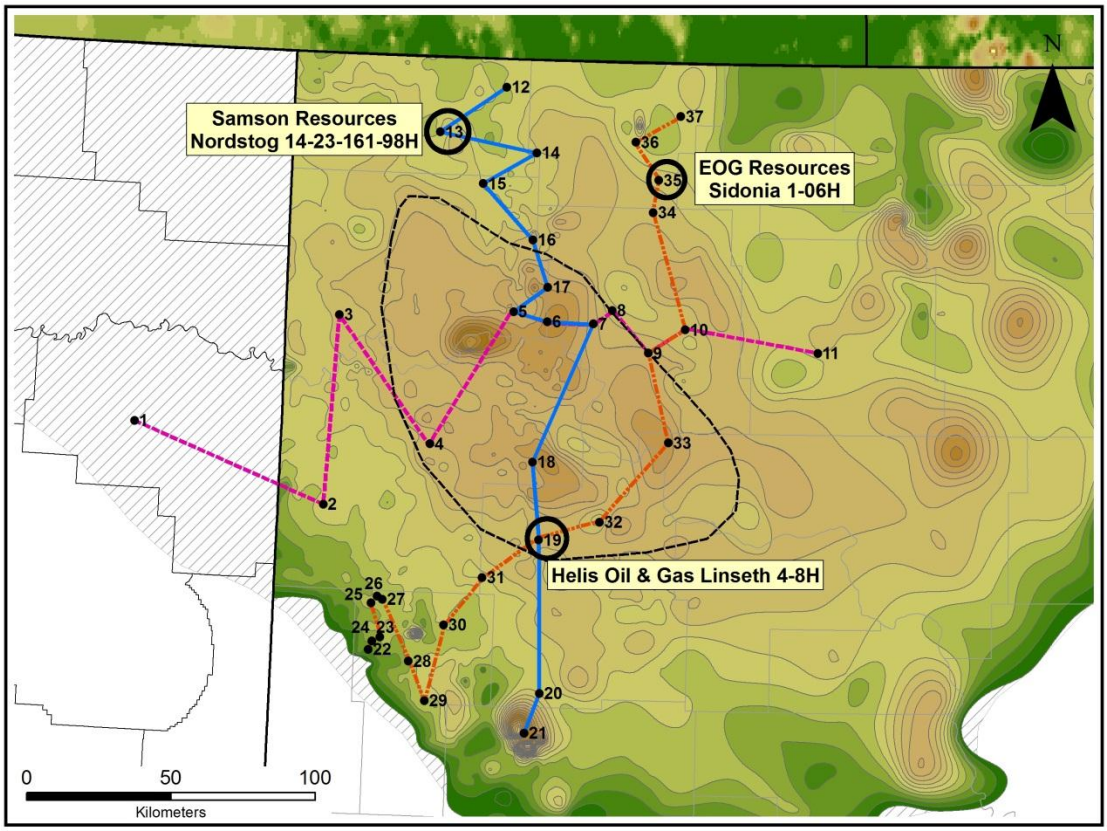

Figure 21. Isopach map of upper Bakken member showing location of three cores sampled for XRD analysis. Helis Oil & Gas Linseth 4-8H was also sampled for TOC. See Figure 4 for legend and Table 1 for additional well names.

Eight of the nine XRD samples from the Helis Oil & Gas Linseth 4-8H are paired with total organic carbon (TOC) analyses (Fig. 18), and five of these are paired with a polished thin section (see Appendix 2). Seventeen of the XRD samples consist of massive to faintly laminated mudstone (FA1) in the lower part of various small-scale coarsening-upward cycles distributed at

regular intervals over the entire thickness of the succession to test for changes in mineralogy in dthree different parts of the study area. Five additional XRD analyses were taken to determine the mineralogical composition of (pyrite mineralized) radiolarite, radiolaria-bearing mudstone, and burrow-mottled mudstone with shells (FA3) (Fig. 19).

The data show that stratigraphically, the biggest change in the mineralogical composition of massive to faintly laminated mudstone (FA1) occurs in the central part of Interval 2. Within all three cores this mineralogical change is represented by a sharp increase in the clay content, coupled with a large decrease in chert and a small to zero decrease in the amount of detrital quartz (Figs. 19, 22, 23). Within Helis Oil & Gas Linseth 4-8H, this vertical transition in XRD data to samples containing more clay (Fig. 19) also marks the lithological change between the lower section of Interval 2, which is dominated by massive to faintly laminated mudstone (FA1), and the upper section of Interval 2, which is dominated by burrow-mottled mudstone with shells (FA3). Within both the Helis Oil & Gas Linseth 4-8H and EOG Resources Sidonia 1-06H cores, carbonate is highest in samples closest to the upper and lower contacts (Fig. 19, 22). In contrast, the Samson Resources Nordstog 14-23-161-98H core shows a gradual increase in the carbonate content from the base of the succession toward the upper contact (Fig. 23).

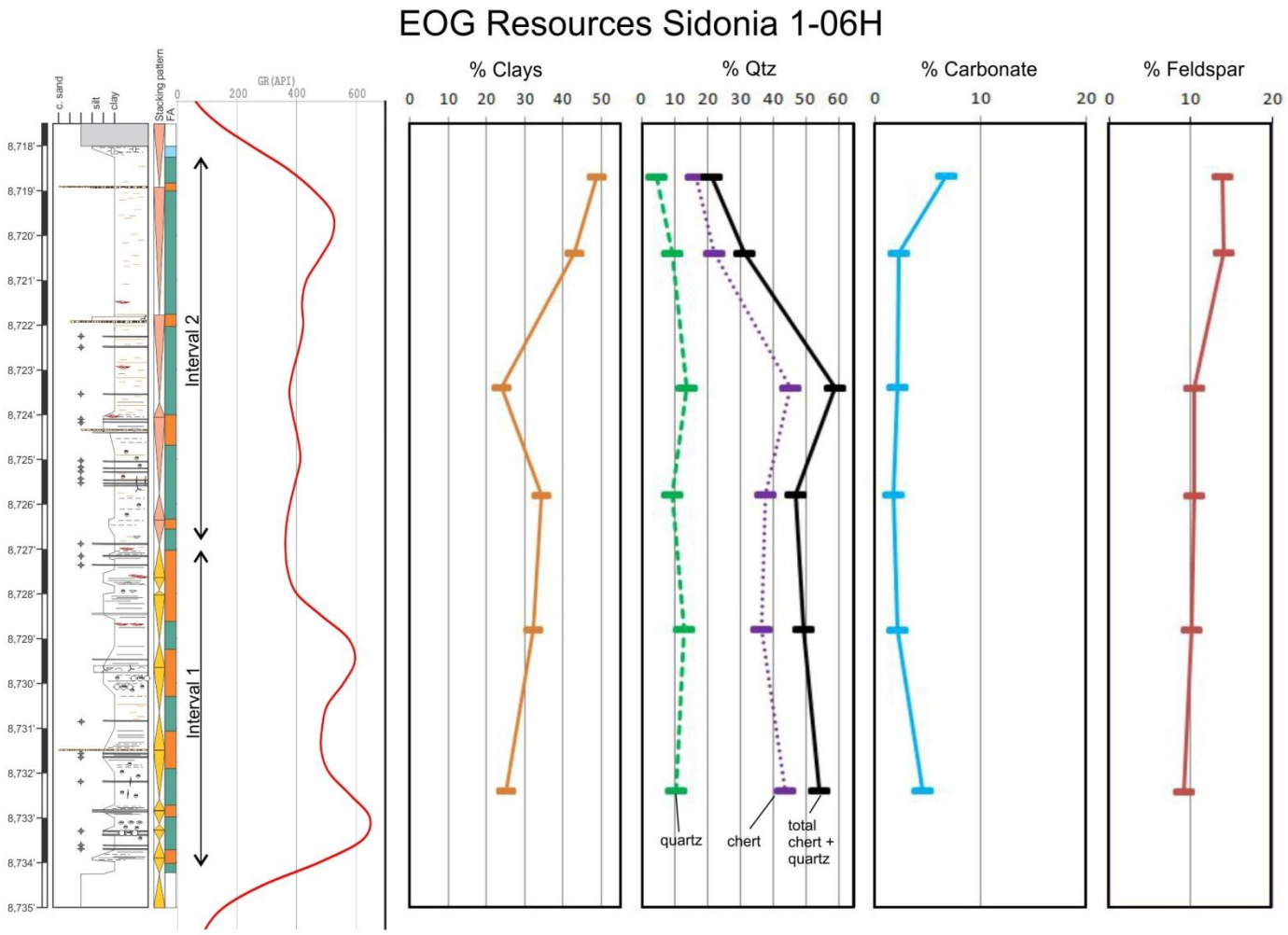

Figure 22. Lithology core log of EOG Resources Sidonia 1-06H accompanied by gamma ray log and XRD data. Rectangular data points represent massive to faintly laminated mudstone (FA1) sampled from the lower part of coarsening-upward cycles. XRD data is not normalized with TOC. Pyrite and gypsum content not shown. See Figure 13 for core log key.

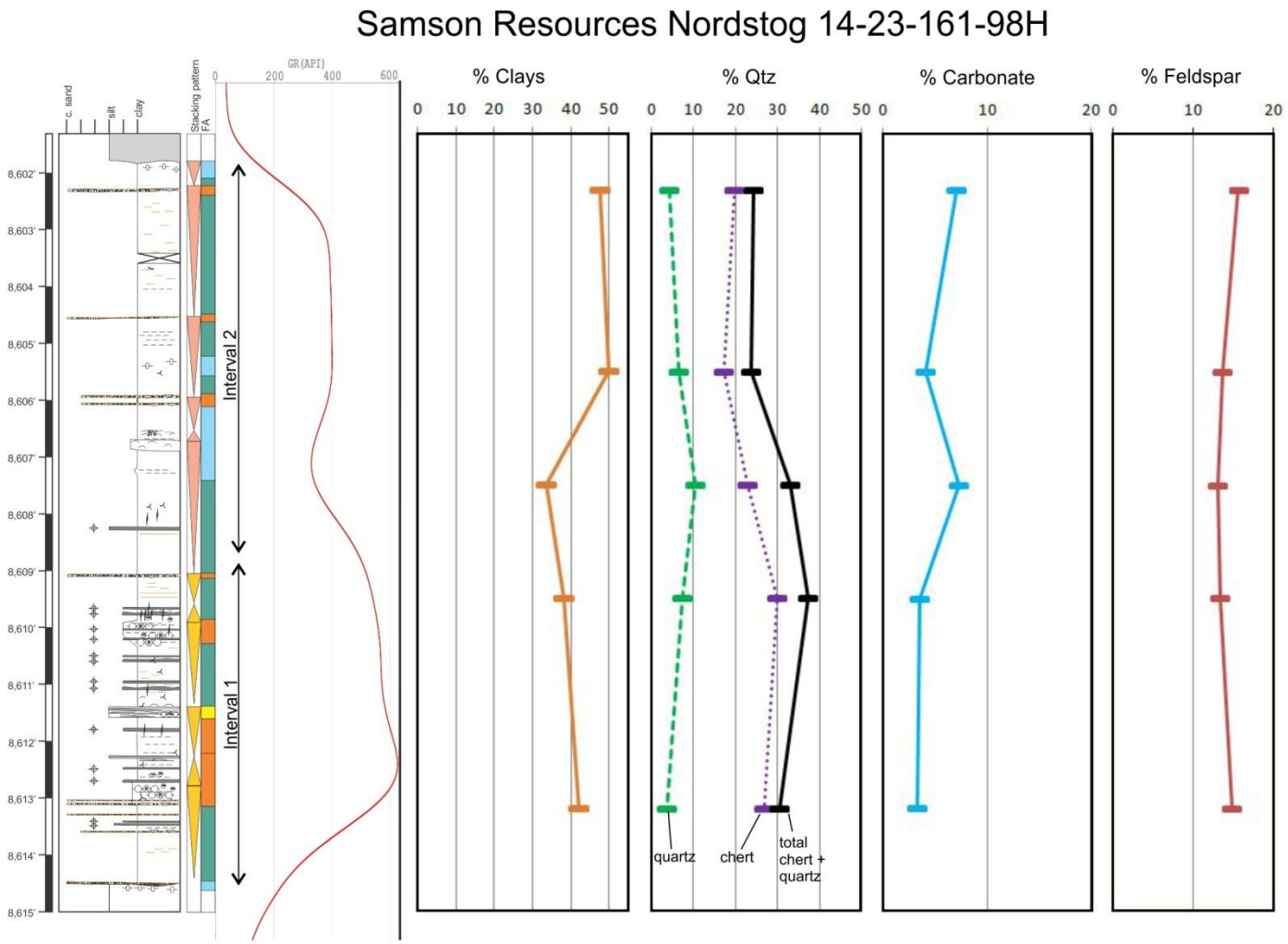

Figure 23. Lithology core log of Samson Resources Nordstog 14-23-161-98H accompanied by gamma ray log and XRD data. Rectangular data points represent massive to faintly laminated mudstone (FA1) sampled from the lower part of coarsening-upward cycles. XRD data is not normalized with TOC. Pyrite and gypsum content not shown. See Figure 13 for core log key.

Within the Helis Oil & Gas Linseth 4-8H core, the total-feldspar content increases gradually from the base to the top of the succession, whereas in the other two cores, total-feldspar is at a minimum in the central part of the succession. However, this variation in feldspar content is minor and close to the 5-10% margin of error (Adam Boehlke, pers. comm., 2013). Also, it should be noted that the Helis Oil & Gas Linseth 4-8H core is slightly different from most of the upper Bakken cores because the lower section of Interval 2 in this core contains more well laminated mudstone (FA2a) than is otherwise typical for this section (see Appendix 2).

8.0 INTERPRETATION

8.1. Depositional Model

The very fine overall grain sizes of the upper Bakken member sediments and the co-occurrence of siliciclastic and carbonate silt grains within this unit suggest that these were deposited offshore at the low energy end of a mixed carbonate-siliciclastic system (cf. Egenhoff et al., 2011b). Sedimentation of these fine grained sediments occurred in the offshore realm along a subtle energy gradient, which is herein subdivided into distal offshore and proximal offshore depositional environments (Fig. 24A, 24B, 25A, 25B).

Sediments representing the deepest offshore conditions have few event laminae because storms were rarely large enough to transport sediment at these depths. Pyrite laminae, discontinuous pyrite lenses and concretions formed preferentially within the distal offshore mudstones. The average grain size of silt in these distal offshore mudstones (FA1) is considerably finer than silt within the more proximal mudstones (i.e. FA2a, FA2b, FA3, FA4) because the environment was overall calmer and more of the detrital silt might have been derived from aerial fallout (cf. Egenhoff and Fishman, 2013). The very fine grain size of massive

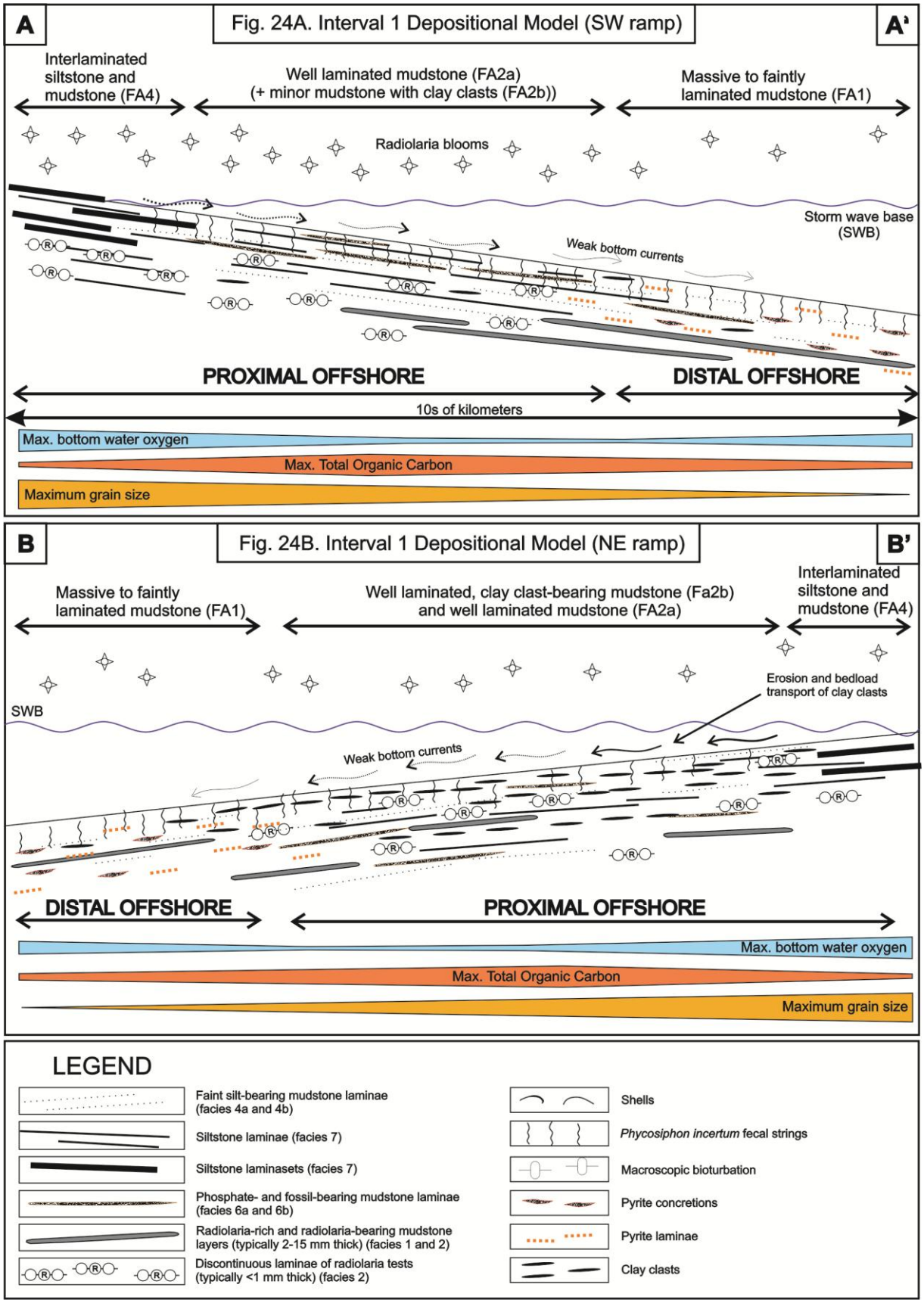
A
Fig. 24A. Interval 1 Depositional Model (SW ramp)
A'
Interlaminated siltstone and mudstone (FA4)
Well laminated mudstone (FA2a) (+ minor mudstone with clay clasts (FA2b))
Massive to faintly laminated mudstone (FA1)
Radiolaria blooms
Storm wave base (SWB)
Weak bottom currents
PROXIMAL OFFSHORE
DISTAL OFFSHORE
10s of kilometers
Max. bottom water oxygen
Max. Total Organic Carbon
Maximum grain size
B
Fig. 24B. Interval 1 Depositional Model (NE ramp)
B'
Massive to faintly laminated mudstone (FA1)
Well laminated, clay clast-bearing mudstone (Fa2b) and well laminated mudstone (FA2a)
Interlaminated siltstone and mudstone (FA4)
Erosion and bedload transport of clay clasts
SWB
Weak bottom currents
DISTAL OFFSHORE
PROXIMAL OFFSHORE
Max. bottom water oxygen
Max. Total Organic Carbon
Maximum grain size
LEGEND
Faint silt-bearing mudstone laminae (facies 4a and 4b)
Siltstone laminae (facies 7)
Siltstone laminasets (facies 7)
Phosphate- and fossil-bearing mudstone laminae (facies 6a and 6b)
Radiolaria-rich and radiolaria-bearing mudstone layers (typically 2-15 mm thick) (facies 1 and 2)
Discontinuous laminae of radiolaria tests (typically <1 mm thick) (facies 2)
Shells
Phycosiphon incertum fecal strings
Macroscopic bioturbation
Pyrite concretions
Pyrite laminae
Clay clasts

Figure 24 (previous page). Depositional models for Interval 1 in the SW part of the study area (Fig. 24A) and in the NE part of the study area (Fig. 24B) showing relative abundance of individual facies that occur along an energy gradient subdivided into distal offshore and proximal offshore depositional environments. The two transects, A-A' and B-B', are distinguished primarily by occurrence of clay clasts, which appear to be more abundant in the NE part of the study area and are also shown in Figure 26. The overall even thickness of the upper Bakken member in the northeast, indicated by the isopach map (see Figure. 4), suggests that the depositional slope was flatter in this part of the study area than in the SW. The bottom water oxygen level shown on the diagrams is interpreted from gamma ray logs, ichodiversity and qualitative estimates of overall burrow size and bioturbation intensity; see Sections 8.2 and 8.3.

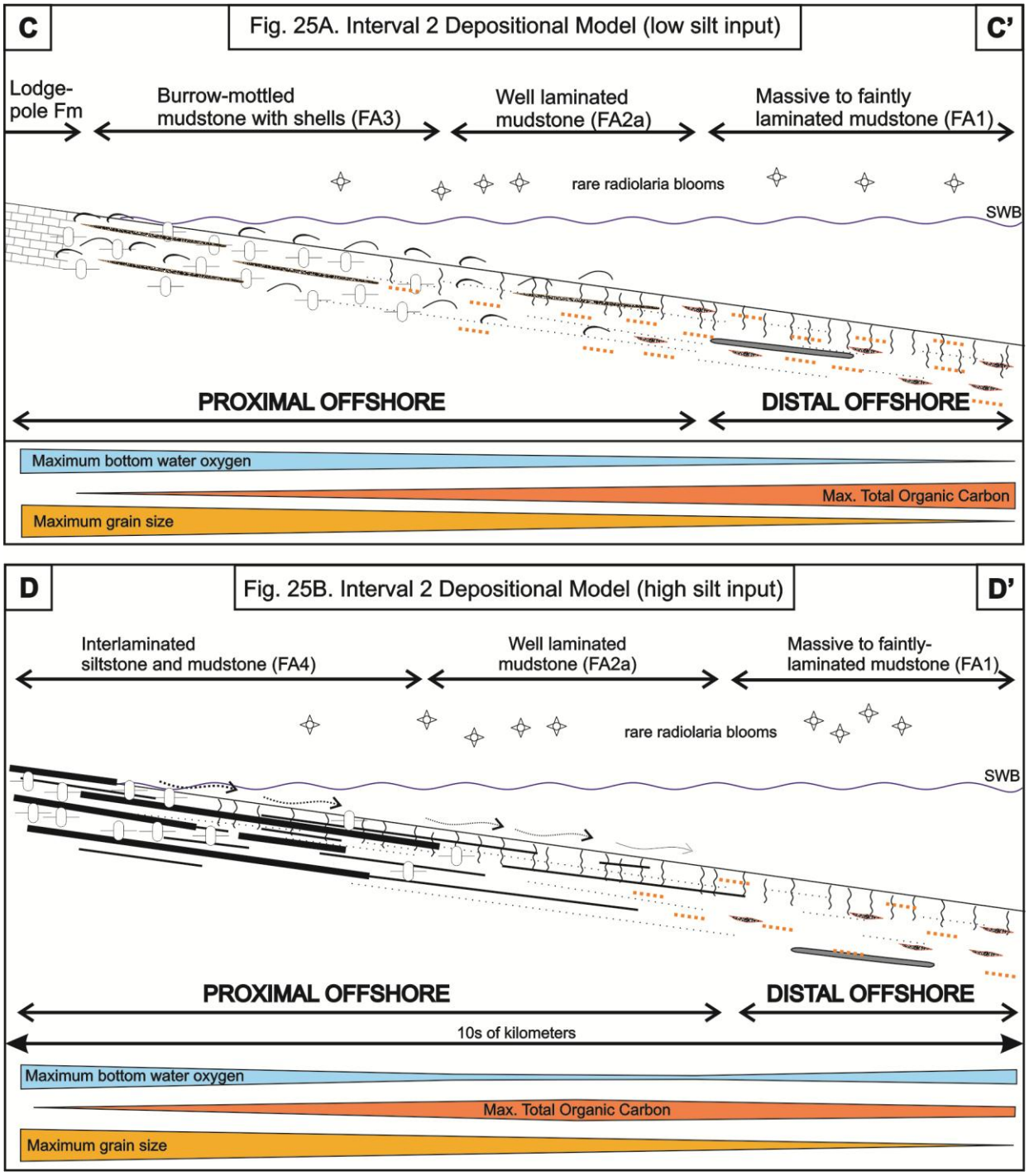

Figure 25. Depositional model for Interval 2 in areas with low input of silt-rich sediments (Fig. 25A) and in areas with high input of silt-rich sediment (Fig. 25B) showing subdivision into the distal offshore and proximal offshore depositional environment. C-C' is representative of sedimentation throughout most of the basin within Interval 2, whereas D-D' represents isolated locations with high silt input shown by the Conoco Karsky 35 #2 core, shown in Figure 27 also. See Figure 24 for symbol legend.

to faintly laminated mudstone (FA1), in comparison to the coarser grained, more proximal, well laminated mudstones (FA2a and FA2b) (Table 3), along with less frequent deposition of sediment by weak bottom currents, may have allowed the organism producing the *Phycosiphon incertum* type B fecal strings to more thoroughly destroy any laminated fabric in the distal offshore setting. Alternatively, (1) very slow sedimentation rates in the very distal offshore environment may have provided more time for the fine silt-bearing laminae to be homogenized; or (2) sediment in the very distal offshore environment was bioturbated faster than sediments in proximal offshore environment due to a larger population of organisms producing the *Phycosiphon incertum* fecal strings.

Sediments in the basinward part of the proximal offshore environment of Interval 1 were dominated by well laminated mudstones (FA2a) and well laminated clay clast-bearing mudstones (FA2b) (Fig. 24A, 24B, 26A, 26B). These contain numerous siltstone and phosphate- and fossil-bearing mudstone event laminae (mostly < 2mm), as well as of clay clasts in places, which were deposited by weak bottom currents probably during intermittent storms. The siltstone and phosphate- and fossil-bearing event laminae are equally abundant within well laminated mudstones (FA2a), and well laminated, clay clast-bearing mudstones (FA2b), and both of these mudstones also have a very similar average grain size of the silt fraction (Table 3). This suggests that both of these facies associations represent similar energy regimes and therefore were probably deposited below storm wave at a similar offshore depth. During deposition of Interval 2, however, within the basinward parts of the proximal offshore environment sediments consisting of burrow-mottled mudstone with shells (FA3) were more widespread than those composed of well laminated mudstones (FA2a and F2b) (Fig. 25A, 27). This is consistent with greater circulation in the shallower parts of the basin, and therefore higher bottom water oxygen

levels than in deeper water, which is reflected by the presence of large burrows and shells in burrow-mottled mudstone with shells (FA3) and their absence with

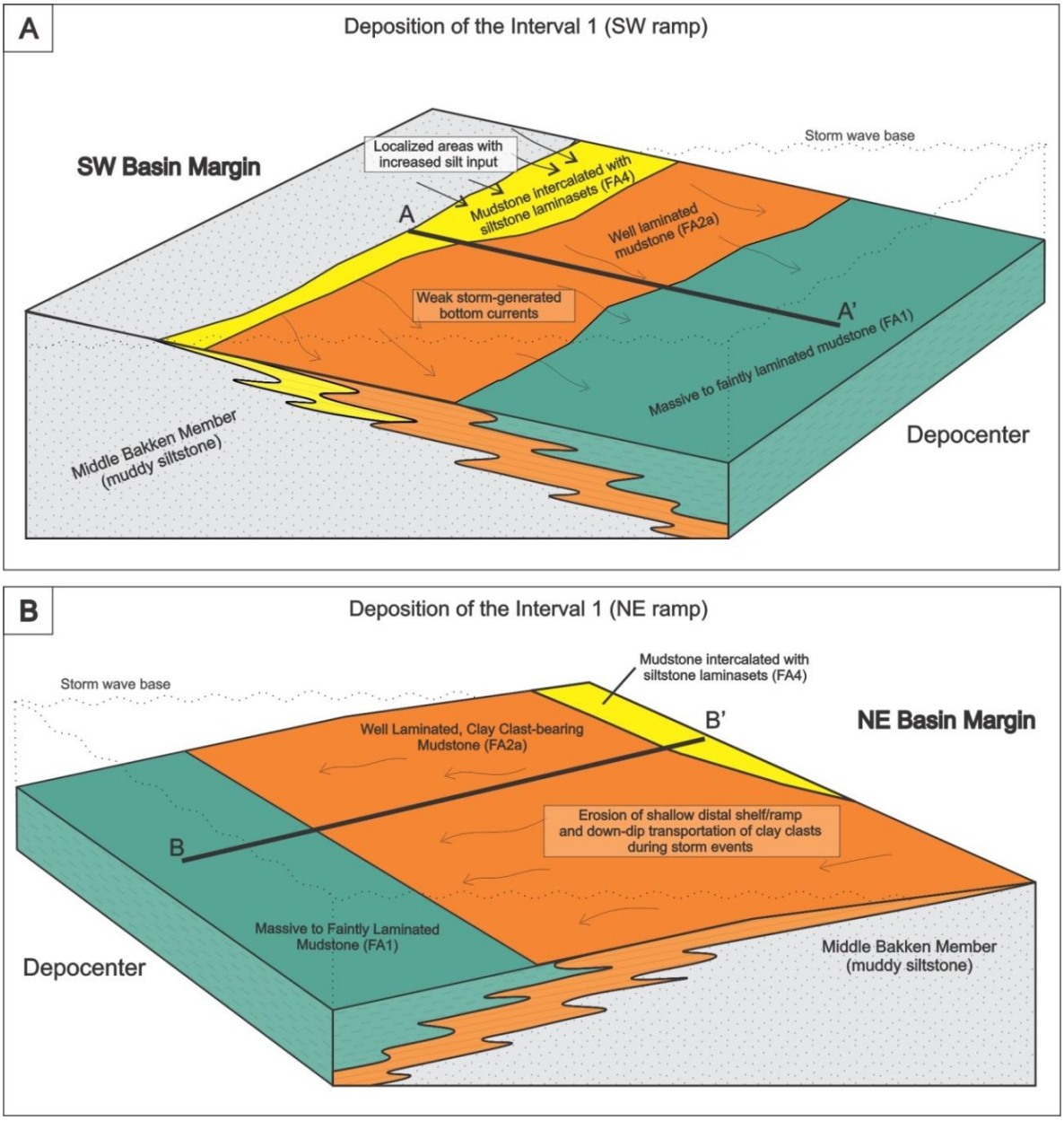

Figure 26. Schematic three-dimensional diagrams of the depositional models A-A' (Fig. 26A) and B-B' (Fig. 26B) shown in Figure 24. Both figures show the limited areal distribution of interlaminated siltstone and mudstone (FA4) and the overall transgressive architecture of Interval 1, which is discussed in Chapter 9 Sequence Stratigraphy.

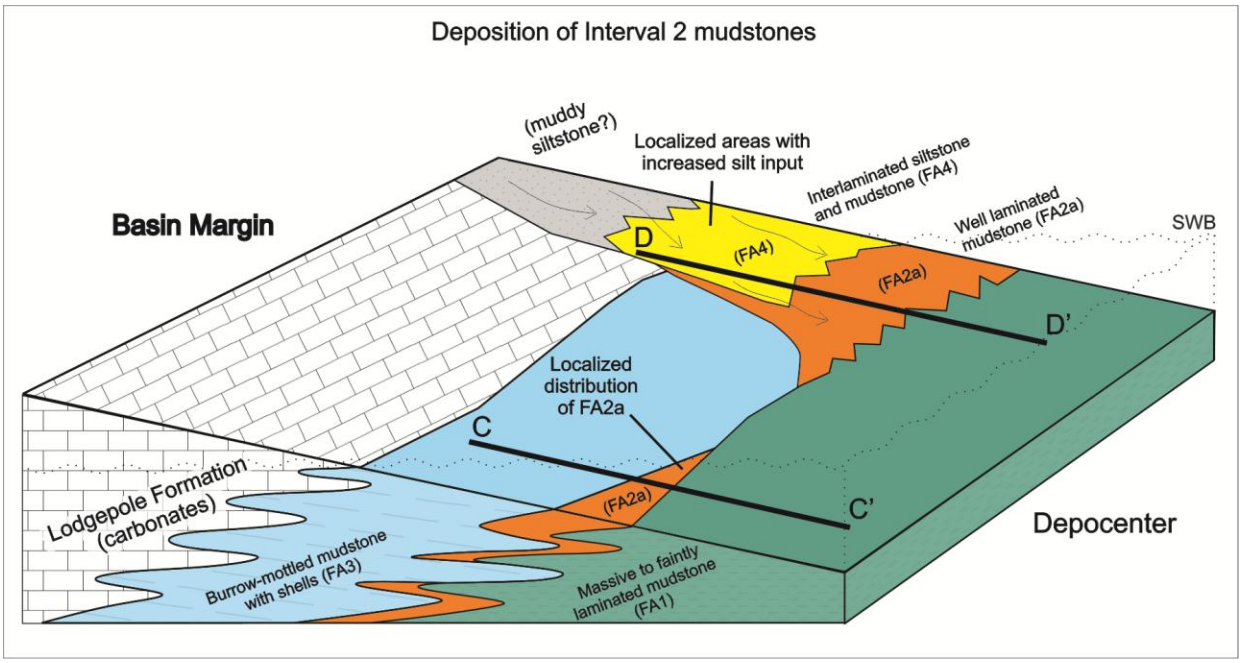

Figure 27. Schematic three-dimensional diagram of the depositional models C-C', and D-D' shown in Figure 25 and represented here by lines C-C', and D-D'. During deposition of Interval 2, burrow-mottled mudstone with shells (FA3) dominates the proximal offshore environment, except in localized areas where the input of silt from the nearshore environment is higher, which is indicated by the Conoco Kasky 35 #2 core and represented by the depositional model D-D' in Figure 25. The diagram also shows the regressive architecture of Interval 2 with the Lodgepole Formation prograding over the upper Bakken member, which is discussed in Chapter 9 Sequence Stratigraphy. Note the patchy areal distribution of well laminated mudstone (FA2a), which is indicated by the lithologs shown in the basin-wide transects in Appendices 1-3.

well laminated mudstones (FA2a and FA2b). Burrow-mottled mudstone with shells (FA3) generally lacks laminae, probably due to the intense infaunal reworking. Interval 2 parasequences in the Shell Oil Burbank BIA 23-8 core (Appendix 3) and in the Newfield Production Sergeant Major 1-21H (Appendix 1) core suggest that burrow-mottled mudstone with shells (FA3) were generally deposited in shallower water than the well laminated mudstones (FA2a and FA2b) (Fig. 27). In other cores, the distal offshore, massive to faintly-laminated mudstone (FA1) grades vertically into proximal offshore, burrow-mottled mudstone within shells

(FA3), indicating that during deposition of Interval 2, well-laminated mudstones (FA2a and FA2b) were deposited only locally (Fig. 27). The colonization of much of the Interval 2 proximal offshore environment by bivalves and by burrowing organisms that were much larger than those during deposition of Interval 1 argues for bottom waters that were more oxygenated than those during deposition of Interval 1.

Interlaminated siltstone and mudstone (FA4) was most likely deposited primarily in the shallowest parts of the proximal offshore environment (Fig. 25B), below, but possibly near to, storm base wave. This interpretation is supported by the abundance of clearly visible small erosion surfaces and the presence of numerous discontinuous siltstone laminasets that often display ripple laminae (Fig. 12). These silt-rich mudstones are abundant only locally, as shown by the Conoco Karsky 35 #2 core, and likely reflect lateral variation in the supply of terrigenous sediment (Fig. 27).

However, this relatively simple proximal-distal transect is complicated by the areal distribution of the different facies associations indicating that the upper Bakken member mudstones vary significantly in composition along the basin margin. This is shown in the proximal parts of this transect by both the areal distribution of clay clasts and the very local occurrence of interlaminated siltstone and mudstone (FA4) within the study area (Fig. 26, 27). Clay clasts are significantly more abundant within proximal offshore mudstones in the north, northeast, and eastern part of the study area (FA2b) (Fig. 15, 24B, 26B). Their presence indicates that there must have been an up-dip source of cohesive clay-rich sediment that was exposed to erosive currents. The occurrence of clay clasts primarily in the northern, northeastern and eastern part of the study area suggests that their presence reflects relatively shallow, very distal offshore conditions, such as a paleohigh, given that this location is in the geographic center of the basin

and 50-150 kilometers up-dip from the depocenter (Fig. 15). Similarly, interlaminated siltstone and mudstone (FA4), interpreted as being deposited primarily in the shallow parts of the proximal offshore environment (Fig. 25B), most likely represent sedimentation below but near to storm wave base. This interpretation is supported by the abundance of clearly visible small erosion surfaces as well as the presence of numerous discontinuous siltstone laminasets that often display ripple laminae (Fig. 12). These silt-rich mudstones are abundant only in a few areas, as shown by the Conoco Karsky 35 #2 core, and likely reflect lateral variation in the supply of terrigenous sediment (Fig. 27).

The offshore depositional environment was characterized by very wide facies belts. This is indicated by the fact that both distal offshore and proximal offshore facies associations are laterally correlatable across hundreds of kilometers within isochronous stacking patterns (parasequences) with only minor lateral variation in their relative abundance toward the shore. This implies that the basin had a very low inclination, which is typical of intracratonic basins (Einsele, 1985; see also Poppelreiter and Aigner, 2003).

Sediments bearing radiolarians or consisting mostly of these organisms occur in facies associations that represent the distal offshore and the proximal offshore depositional environments of the upper Bakken member. This indicates that the radiolarian blooms affected the entire deep shelf portion of the Williston basin during early Mississippian times. However, radiolarian abundances also show a distinct maximum about half way between the edge of upper Bakken member distribution and the deepest parts of the basin, and a decrease in radiolarian-bearing sediments both shore- and basinwards from this maximum (Fig. 16). This distribution pattern of radiolarian-rich sediments is most likely the effect of two different processes. These are (1) destruction and dispersal of many radiolaria deposited by blooms in the proximal offshore

environment by high-energy storm events, and (2) low radiolaria productivity in the depocenter, possibly due to reduced availability of nutrients. The former is indicated by the abundance of discontinuous very thin laminae of dispersed radiolaria tests within well laminated mudstones (FA2a and FA2b) (e.g. Conoco Karksy 35 #2, Appendix 2), and their corresponding absence within massive to faintly laminated mudstones (FA1). Nutrients may have been low in the basin depocenter, relative to shallower, more proximal areas because of (1) a limited supply of nutrients derived from storm reworking of the sea floor on the deep offshore shelf (e.g. Murphy et al., 2000), and (2) because of a lower supply of terrestrial-sourced nutrients in very distal locations because they are consumed first by plankton in more proximal locations (e.g. Noble et al., 2011).

8.2 Interpretation of gamma ray (GR) and total organic carbon (TOC) data

The very high total gamma ray values (typically 200-800 API units) recorded in logs of the upper Bakken member are typical for black shales with very high organic carbon (Luening and Kolonic, 2003) and primarily reflect the syngenetic uranium content (Rider, 1996, p. 76). The coupling of the U, Th and K gamma ray spectra (Fig. 17) suggests that preservation of organic matter is linked to the deposition of fine-grained detritus containing illite and mica, which provides the Th and K gamma radiation (Fig. 18). This relationship may indicate that (1) organic productivity was highest in proximal, nutrient-rich locations where input of clay-sized detritus was also high, or that (2) episodic deposition of clay-bearing event laminae helped preserve organic matter from exposure and degradation on the sea floor, or that (3) preservation of organic matter was aided due to the formation of organominerallic aggregates (marine snow) in the water column as described by Macquaker et al. (2010). It is likely that all of these factors influenced

preservation of TOC in the upper Bakken member to some degree. Point (1) is supported by the fact that radiolarite, radiolaria-bearing mudstone and dispersed radiolaria tests are least abundant in the depocenter, where nutrient levels were probably low. Preservation of organic matter by event laminae is indicated by the fact that Interval 1, which has higher TOC than Interval 2, also contains the greatest abundance of storm event laminae (i.e. laminae of phosphate- and fossil-bearing mudstone, siltstone and silt-bearing mudstone). In addition, episodic deposition of siliciclastic sediment has been associated with improved preservation of organic matter in other mudstone successions, such as the lower Bakken member (Smith and Bustin, 1998), the Mowry Shale (Bohacs et al., 2005), the Whitby Mudstone Formation (Ghadeer and Macquaker, 2012), and the Kimmeridge Clay Formation (Macquaker and Gawthorpe, 1993). Following these interpretations, the 0.6-1.2 m thick section of massive to faintly laminated mudstone (FA1) in the lower part of Interval 2 has a GR profile in many wells that is 100-400 API units lower than the rest of the succession because either: (1) bottom water oxygen levels were higher compared to during deposition of more organic-rich parts of the succession, thus enhancing organic matter degradation;(2) because burial and thus preservation of organic matter was low during this time because there were few storm events and siliciclastic sediment input was low; and/or (3) because organic productivity was lower during deposition of this lower part of Interval 2. All three of these possibilities are consistent with this part of the succession representing the maximum flooding of the shelf. Respectively, this is because (1) the bottom water layer would be more resistant to seasonal anoxia or dysoxia when the water is column is at its thickest due to its greater volume (Tyson and Pearson, 1991); (2) because during maximum flooding bottom waters during storms are likely to be at their calmest and detrital sediment input at its lowest; and (3) the source of terrestrial and nearshore recycled nutrients will be at their most distal during maximum

flooding. Furthermore, the Helis Oil & Gas Linseth 4-8H core that was sampled for TOC does not contain this correlatable zone of relatively low API values near the base of Interval 2 (Fig. 19, Appendix 2). Rather, this section in the Helis Oil & Gas Linseth 4-8 well is dominated by well laminated mudstone (FA2) with API values that are 150-200 API units higher than time-equivalent sections in adjacent cores. This is consistent with higher productivity and/or preservation occurring in the more energetic, proximal offshore environment that has higher detrital sediment input compared to the distal offshore environment.

The sections of burrow-mottled mudstone with shells (FA3) at the top of Interval 2 are interpreted to have gamma ray values up to 375 API units lower than many other parts of the succession primarily because of three factors. These are: (1) increased organic matter degradation during deposition of burrow-mottled mudstone with shells (FA3) relative to other facies associations due to higher bottom water oxygen levels as indicated by the presence of shells and large burrows; (2) greater consumption of organic matter by deposit feeders within burrow-mottled mudstone with shells (FA3) relative to other the facies associations; and (3) lateral variation in productivity, which is shown by the occurrence of radiolarite and radiolaria-bearing thin beds in Interval 2 within only several of the cores. These interpretations are supported by: (1) many sections of massive to faintly laminated mudstone (FA1), which have gamma ray values as much as 225 API units higher than time-equivalent sections of burrow-mottled mudstone with shells (FA3) (e.g. Helis Oil & Gas Linseth 4-8H versus Burlington Resources Oil & Gas Prairie Rose 24-3H (see Appendix 2)); and (2) TOC variability on a centimeter-scale, which shows that mudstone with intense bioturbation and many shells has lower TOC values than mudstone with minor bioturbation and fewer shells (Fig. 20).

Correlation of these GR logs, in conjunction with the lithologs, suggests that in proximal southwestern parts of the study area Interval 2 was either eroded or was not deposited (Fig. 13, Appendices 1, 3).

8.3 Interpretation of x-ray diffraction (XRD) data

The higher chert content of massive to partially laminated mudstones (FA1) within Interval 1 in comparison to the upper part of Interval 2, as determined by the XRD analyses and shown in Figures. 19, 22, 23, suggests that either (1) biological productivity of radiolaria or sponges was higher during deposition of Interval 1, or (2) that dilution of biologically derived chert by clay was higher during deposition of the upper part of Interval 2. The complete absence of radiolaria and the overall average thickness of individual parasequences in the upper part of Interval 2 suggest that dilution was not the primary cause of the low chert values. Instead, this trend is more likely to have been caused by much lower radiolaria productivity toward the top of Interval 2, relative to Interval 1. High radiolaria productivity during deposition of Interval 1 is consistent with the greater abundance of laminae and thin beds of radiolarite and radiolaria-bearing mudstone in Interval 1 than in Interval 2. Samples of massive to faintly laminated mudstone (FA1) selected for this XRD analysis do not include any radiolarite and radiolaria-bearing mudstone, or phosphate-and fossil-bearing lags that often contain sponge spicules. Therefore, these data suggest that a significant amount of authigenic silica was incorporated into the massive to partially laminated mudstones (FA1) that was deposited between radiolaria blooms. The higher clay, feldspar and carbonate content of massive to partially laminated mudstone (FA1) in the upper part of Interval 2, relative to the samples from the rest of the succession, is interpreted to be largely a function of the large decrease in chert content in the upper part of

Interval 2 (Fig. 19, 22, 23). Accordingly, the fact that the detrital quart content at the top of Interval 2 either remains steady, or decreases slightly in the three wells investigated, indicates that input of detrital siliciclastic sediment did not increase during the latter stages of upper Bakken member deposition. This is not too surprising given that the lower Lodgepole Formation carbonate system, whose muddy carbonate facies are largely free of siliciclastic detritus (Mackie, 2013), prograded over the top of the upper Bakken member supplying exclusively carbonate material into the Williston Basin.

8.4 Sequence stratigraphy

Vertical repetition of facies associations and the lateral correlation of stacking patterns, shown in the three regional-scale transects in Appendices 1-3, provide the basis for a sequence stratigraphic interpretation of the upper Bakken member. The cyclicity in the upper Bakken member reflects changes in the sediment caliber and variation in the overall bottom water energy regime. This is indicated within most parasequences by the coarsening-upward trend, the upward-increasing laminae thickness, and the increasing number of high-energy event laminae that occur toward the top of each of the well laminated coarsening-upward cycles. Following this interpretation, the bases of the coarsening-upward cycles represent minima in depositional energy and are therefore interpreted to be marine flooding surfaces (parasequences boundaries). These parasequences are interpreted to be one to two orders of magnitude thinner than typical nearshore parasequences due to much lower sedimentation rates. The very small-scale variation that occurs within some parasequences may represent local variation in the sediment supply, higher order cycles, or missing sections through erosion or non-deposition.

The upper section of the middle Bakken member shows a fining-upward trend that grades vertically into the overlying Interval 1 and records a marine transgression (Smith and Bustin, 2000; Egenhoff et al., 2011b). The upper Bakken member basal contact, which represents a transgressive surface (cf. Van Wagoner et al., 1988) varies from gradational over 100-300 mm, to knife-sharp, and in some places is marked by a thin (typically <20 mm) lag of phosphate- and fossil-bearing mudstone. Overall however, this transgressive surface is fairly conformable and does not appear to represent a significant regional hiatus or disconformity as is suggested by conodont data (Hayes, 1985). Furthermore, the absence of a distinct condensed section within any part of the upper Bakken member succession characterized by a phosphatic hardground (e.g. Bohacs et al., 2002), phosphatic nodules or carbonate concretions that might indicate regional breaks in sedimentation (Coleman, 1985; Curtis, 1980; Irwin et al., 1974; Macquaker and Gawthorpe, 1993) suggests that continuous sedimentation occurred throughout deposition of the upper Bakken member.

Interval 1 consists of three to five laterally correlatable coarsening-upward stacking patterns, each 150-400 mm in thickness, referred to as parasequences. The lowermost parasequence within the depocenter is interpreted to correlate laterally with the top of the middle Bakken member in more proximal positions, given that in general there are fewer parasequences within Interval 1 closer to the basin margin (e.g. Lyco Energy Titan FWP 32-14H, Fig. 13, Appendix 1; Whiting Oil & Gas Teddy 44-13TFH, Appendix 3). However, in wells located within only 20 km of the depositional edge (e.g. Meridian Oil Inc. MOI 44-27H, Appendix 3) it is not clear if the Interval 1 parasequences become amalgamated or if some of the lowermost Interval 1 parasequences grade laterally into the middle Bakken member through a facies change. Despite this, most

parasequences within Interval 1 are laterally correlatable through the more basinward portions of the succession with a reasonable degree of confidence for at least 300 km.

Although the upper Bakken member basal contact is a transgressive surface, Interval 1 in many wells exhibits a subtle progradational stacking of parasequences as indicated by the greater abundance of silt-bearing laminae and siltstone laminae in the upper one or two parasequences within this part of the succession (e.g. Whiting Oil & Gas Braaflat 11-11-H and Amerada Hess Corp. Sara G Barstad 6-44H, Appendix 1). In some wells however, the overall stacking pattern in Interval 1 is aggradational (e.g. EOG Resources Sidonia 1-06H, Appendix 3) or retrogradational (e.g. Newfield Production Sergeant Major 1-21H, Appendix 1), which probably reflect the presence of intrabasinal topography or local variation in sediment supply. The lower part of Interval 1 is therefore interpreted to record an initial marine transgression that was followed by a slight overall decrease in sea level during deposition of the top two parasequences within Interval 1 (Fig. 17). This subtle sea level fall was probably eustatic given that this subtle prograding pattern toward the top of Interval 1 is widespread in many wells throughout the study area. However, evidence of minor tectonism during Bakken deposition (Clement, 1987; Gibson, 1995) nonetheless indicates that this subtle progradational pattern could have been tectonic in origin rather than eustatic.

Interval 2 contains five to seven parasequences in the depocenter and pinches out basinward of the underlying Interval 1, where stacking patterns undergo a lateral facies change into the overlying carbonates of the Lodgepole Formation. Overall, facies associations in Interval 2 record a decreasing sea level and increasing bottom water oxygen levels. This is shown by the change from parasequences dominated by distal offshore, massive to faintly laminated mudstones (FA1) in the lower part of Interval 2, to parasequences dominated by proximal

offshore mudstones characterized by burrow-mottled mudstone with shells (FA3) in the top part of Interval 2. The predominance of massive to faintly laminated mudstone (FA1) in the lowermost one to two parasequences of Interval 2, and the paucity of high-energy event laminae or relict laminae within these mudstones suggest that this lower part of Interval 2 represent the deepest and calmest conditions during upper Bakken sedimentation. Therefore, this part of the succession interpreted to represent maximum flooding of the shelf. In addition, parasequences within Interval 2, overall, are generally thicker than those in Interval 1, which is consistent with an Interval 2 increase in sediment supply during sea level fall after maximum flooding (cf. Van Wagoner et al., 1988; Posamentier et al., 1988). Accordingly, Interval 2 represents the lower part of a highstand systems tract (HST), which continues into the overlying Lodgepole Formation, while the maximum flooding surface (MFS) sits at, or slightly above, the contact between Interval 1 and Interval 2 (Fig. 17). Following this interpretation, Interval 1 represents the distal expression of the transgressive systems tract (TST), in spite of a minor sea level fall recorded in the top one or two parasequences of Interval 1 in many wells (Fig. 17).

9.0. DISCUSSION

9.1 Stratigraphic changes in primary productivity and the distribution of radiolarite and radiolaria-bearing mudstone

Radiolarite and radiolaria-bearing mudstones are significantly more abundant in Interval 1 than in Interval 2. Importantly, the preservation of radiolaria tests can be influenced by changes in bottom water silica solubility (Boggs, 2009 p.285; Birnbaum and Wireman, 1985) and by changes in sedimentation rate and burial (De Wever and Baudin, 1996). However, in the upper Bakken member, the greater abundance of radiolaria within Interval 1 probably directly reflects increased primary productivity during this time. This interpretation is based primarily on nitrogen isotope data in Smith and Bustin (1998), which suggests that during the onset of upper Bakken deposition, surface waters were characterized by the highest nutrient concentrations and the highest rate of biological productivity, and from that point on primary productivity decreased throughout deposition of the upper Bakken member. The increased availability of nutrients, concomitant with increased radiolaria productivity during Interval 1 deposition, in comparison to deposition during Interval 2, may have been due to a wetter climate with increased runoff and terrestrial supply of nutrients (e.g. Noble et al., 2011). Furthermore, if the climate was indeed wetter during deposition of Interval 1, a change to a drier climate with less terrigenous input during deposition of Interval 2 in comparison to deposition during Interval 1, is consistent with the formation-scale change in the nearshore sedimentary system from the mixed siliciclastic-carbonate ramp of the middle Bakken member (Egenhoff et al, 2011b) to the carbonate ramp sediments of the overlying Lodgepole Formation. Alternatively, it is possible that primary productivity was higher during deposition of Interval 1 in comparison to Interval 2, because of improved recycling of nutrients (see Murphy et al., 2000), rather than due to increased nutrient

input from external sources. In this model by Murphy et al. (2000), oscillating benthic redox conditions (i.e. seasonal anoxia and seasonal water column mixing) during deposition of black shale can result in a positive feedback loop that enhances the recycling of biolimiting nutrients and therefore primary productivity.

The overall abundance of radiolarite and radiolaria-bearing mudstone can vary significantly from core to core. Patches within cores containing a greater abundance of radiolarite and radiolaria-bearing mudstone cannot be correlated laterally. This variation between cores is inferred to indicate that either radiolaria blooms were often localized, which may have been due to variations in surface water nutrient supply, or that erosion and reworking was not uniform. Despite this small-scale variability, the basin-wide areal distribution pattern of radiolarite and radiolaria-bearing mudstone (Fig.16) is interpreted to indicate that radiolaria productivity was highest in the proximal offshore environment, probably due to increased availability of nutrients nearer to shore than in the middle of the basin, but that these bloom deposits were more likely to be completely reworked and dispersed in shallower, more proximal locations. Therefore, this areal distribution pattern of radiolarite and radiolaria-bearing mudstone layers represents the intersection of processes affecting productivity and preservation.

Regardless of what caused the distinct reduction in radiolaria productivity that occurs near the base of Interval 2, its effect on the upper Bakken member sedimentology may have gone beyond the abundance of radiolaria bloom deposits: Burrow-mottled mudstone with shells (FA3) is absent in Interval 1, even though it is interpreted to have been deposited in a similar water depth to the well laminated mudstones (FA2a and FA2b), which are predominant in Interval 1. It is herein proposed that lower primary productivity during deposition of Interval 2 resulted in higher bottom water oxygen levels (than during deposition of Interval 1) because less reducing organic

matter was being delivered to the sea floor. As a result, bivalves and higher invertebrate organisms were able to colonize the Interval 2 proximal offshore environment. Whereas during the deposition of Interval 1 lower oxygen levels and/or frequent periods of anoxia prevented bivalves and higher invertebrate organisms from colonizing the proximal offshore environment. This is in agreement with (1) isotope data that are interpreted by Smith and Bustin (1998) to indicate that surface waters were characterized by the highest productivity during deposition of Interval 1, and (2) the fact that Interval 1 had greater radiolaria productivity than Interval 2, as indicated by the increased abundance of laminae and thin beds of radiolarite and radiolaria-bearing mudstone in Interval 1.

9.2 Stratigraphic position of the maximum flooding surface (MFS)

The MFS is interpreted to sit at or slightly above the contact between Interval 1 and 2 because of the predominance of massive to faintly laminated mudstones (FA1), which is interpreted to be deposited in the distal offshore environment, in the lower one to two parasequences of Interval 2. This sequence stratigraphic interpretation is favored given that massive to faintly laminated mudstone (FA1) repeatedly, and clearly, represents the deepest and calmest conditions at the fine-grained base of Interval 1 parasequences, as well as within numerous distinct parasequences within the upper part of Interval 2 throughout the study area. Furthermore, the stepwise decrease in the TOC toward the MFS in the distal TST (Interval 1), and then further TOC decrease in the HST in cores where burrow-mottled mudstone with shells (FA3) is present, is consistent with the systems tract TOC variation for a platform or ramp setting (Passey et al., 2010). This trend is shown clearly in the Amerada Hess Corp. Anderson Smith 1-26H and Helis Oil & Gas Linseth 4-8H wells (Fig. 17, 19).

However, it is possible that the predominance of massive to faintly laminated mudstone (FA1) in the lower part of Interval 2 compared to anywhere else in the succession, could represent a short term decrease in the amount of detrital silt being delivered to the basin due to a short term climate change, and not because of maximum flooding of the shelf. This is because another climate signal is possibly expressed within the upper Bakken succession, which is the proposition that Interval 2 was deposited during drier climatic conditions than Interval 1. These resulted in lower nutrient input into the basin, and consequently lower radiolaria productivity and production of organic matter. If the MFS is not located near the base of Interval 2, then this surface must therefore be either (1) somewhere in Interval 1, (2) in the upper part of Interval 2, or (3) close to the transgressive surface at the base of the upper Bakken member. The first two options, 1 and 2, are not good candidates for the MFS location because mudstones in these parts of the succession contain no laterally correlatable zone of condensation or detrital sediment starvation that might be expected during maximum flooding of the shelf, nor do they comprise a distinct correlatable zone representing very deep, calm conditions, relative to the rest of the succession, for an extended period of time. In fact, the upper part of Interval 2 in the Conoco Karsky 35 # 2 represents some of the most silt-rich and high energy facies documented within the upper Bakken member succession. Finally, if mudstones at or close to the transgressive surface at the base of the succession represent the MFS, then the entirety of the upper Bakken member falls into the HST. In this scenario, Interval 1 would represent, overall, some of the most distal mudstones within the entire succession. However, Interval 1 contains many times more radiolaria than Interval 2, and this is inconsistent with Interval 1 being the more distal part of the succession given that data from this study shows that radiolaria laminae and thin beds are in fact less common within the deepest, most farthest offshore parts of the basin (Fig. 16).

9.3 Significance of the geographic distribution of clay clasts

Clay clasts represent water-rich mud fragments eroded from the sea floor and transported by currents (Schieber et al., 2010). Proximal offshore mudstone samples containing abundant clay clasts (FA2b) are predominantly from cores located in the geographic center of the basin in wells 0-150 km up-dip from the basin depocenter in a northern, northeastern and eastern direction (Fig. 15). Most of these wells in the center of the basin are 100-200 km from the depositional edge. In contrast, samples of proximal offshore mudstones lacking clay clasts (FA2a) are from cores mostly within 100 km of the southwestern depositional edge. These facies associations (i.e. FA2a and FA2b) are interpreted to have been deposited at a similar water depth under similar energy regimes frequently influenced by storm currents. The distribution of clay clasts primarily in the geographic center of the basin (Fig. 15), therefore suggests that relatively shallow, but distal offshore environments with a very low sediment supply may be more prone to generating clay clasts and "lenticular laminated mudstones" (see Schieber et al., 2010) than more proximal offshore environments. This distinct contrast in clay clast abundance might be caused by subtle differences in sedimentation that affect the ability of sea floor mud to form cohesive fragments that can be transported long distances without being destroyed (see Schieber et al., 2010). Finally, it is likely that the prevailing transport directions also influenced the distribution of clay clasts.

9.4 Significance of pyrite laminae and concretions

Massive to faintly laminated mudstones (FA1), interpreted here to have been deposited in the deepest offshore environment, show a high abundance of pyrite laminae, pyrite lenses and pyrite concretions in comparison to other mudstones in the succession. In organic-rich sediment under

fully anoxic conditions, H_2S is produced in excess by anaerobic bacteria (Berner, 1984; Coleman, 1985). In these geochemical conditions reactive iron in the sediment is precipitated immediately to tiny pyrite grains (Raiswell, 1982; Schieber, 2003), therefore precluding the formation of localized pyrite lenses or concretions. However, if bottom waters are oxic or dysoxic, oxygen can diffuse downward into the top few millimeters to centimeters of sediment resulting in a non-sulfidic surface layer (Berner, 1984). In this thin surface layer, reactive iron becomes soluble and is able to migrate to localized microenvironments with reducing conditions where various kinds of pyrite accumulations may form (Brett and Baird, 1986). Therefore, the occurrence of pyrite lenses, laminae and pyrite concretions, which likely formed close to the sediment-water interface, further supports the interpretation that bottom waters were non-sulfidic and at least partially oxygenated (Brett and Baird, 1986). These findings suggest that during upper Bakken deposition, the deepest and most distal depositional environment within the Williston Basin was not characterized by a persistent non-circulating stagnant puddle of anoxic bottom water as proposed in the model by Smith and Bustin (1998).

9.5 Mudstone brittleness and porosity: implications for petroleum exploration

Brittleness, volume of clay and TOC are key parameters used in the oil industry for the evaluation of oil and gas shale plays (e.g. Buller, 2010; Buller et al., 2010, Quirein et al., 2012; Brooks and Montalvo, 2012); shale brittleness is closely related to the volume of clay relative to siliciclastic and carbonate constituents (Rickman et al., 2009; Passey et al., 2010). This is important because increased shale brittleness generally improves the productivity of shale reservoirs by increasing the complexity of induced fractures, the effective fracture length and height, and by achieving better proppant placement and reduced embedment (McKeon, 2011). In

contrast, shales with low brittleness (i.e. high ductility) generally make better reservoir seals (Ingram, 1997).

In the upper Bakken member, the volume of clay, siliciclastic and carbonate constituents varies significantly, primarily stratigraphically, as indicated by the lithology logs (Fig. 13, Appendices 1-3) and XRD data (Fig. 19, 22, 23). These show that the mudstones in Interval 1 have a much higher chert and detrital quartz content than in Interval 2, especially in comparison to the upper part of Interval 2. Furthermore, Interval 1 has a greater abundance of very thin siltstone laminae that Interval 2. Interval 1 also contains significantly more thin beds and laminae of fraccable radiolarite and radiolaria-bearing mudstone, and as a result is likely to have significantly higher brittleness than the overlying Interval 2. Furthermore, biogenic opaline silica (chert) has a tendency to form a recrystallized continuous framework of quartz (Jarvie et al., 2007), suggesting that the high abundance of radiolarite and radiolaria-bearing mudstone within Interval 1 may enhance the brittleness of this unit even more than if these layers consisted of detrital quartz silt. This is supported by the presence of small (typically 5-15 mm in length) mineralized fractures that commonly occur in laminae and thin beds of radiolarite and radiolaria-bearing mudstone (Fig. 6a, 10a). In addition, localized areas that are characterized by intercalated siltstone and mudstone (FA4) (e.g. see Conoco Karsky 35 #2) would also likely have higher brittleness than the well laminated (FA2a/2b) and massive to faintly laminated mudstones (FA1). The relatively thick and abundant siltstone laminae and thin beds in these mudstones would probably form an extensive network of fluid pathways if they were connected by hydraulic fractures.

In mudstones, the largest pores are carbonate dissolution pores (CD) and phyllosilicate framework pores (PF) (Schieber, 2010). Although in thermally mature mudstones organic matter

also contains pores, these are often an order of magnitude smaller than CD and PF pores (Schieber, 2010). CD porosity results from dissolution around the periphery of dolomite and calcite grains, and PF porosity is dependent largely on the presence of pressure shadows generated around the margins of hard mineral grains (Schieber 2010). However, in mudstones containing more than 7% TOC, porosity and permeability becomes reduced in comparison to mudstones with less organic matter because many of the CD and PF pores are filled with kerogen and bituminite (Schieber, 2010). Consequently, within the upper Bakken member, the greatest porosity and permeability is probably confined largely to individual laminae that have the lowest TOC and the highest concentration of silt. Therefore, as well as Interval 1 having higher brittleness than Interval 2 due to the abundance of radiolaria, Interval 1 would also be a better target for petroleum exploration than Interval 2 because CD and PF are likely concentrated within the more abundant siltstone laminae. However, the overall abundance of radiolarite and radiolaria-bearing mudstone within Interval 1 is generally greatest in a broad zone that lies between the depocenter and the depositional edge, whereas outside of localized depocenters siltstone laminae tend to be more abundant closer to the depositional edge. Furthermore, previous work suggests that natural fracturing is more abundant in locations closer to the depositional edge, although this fracturing could reflect the thin nature of the upper Bakken member in these areas rather than high brittleness of facies (Cramer, 1991; Druyff, 1991; Hansen and Long, 1991b).

On a carbonate-quartz-clay ternary diagram, the mineral composition of producing shale plays tends to lie below the 50% clay line (Passey et al., 2010). The ternary diagram in Figure 28 shows that six out of seven samples of massive to faintly laminated mudstone (FA1) (without radiolaria) from Interval 1 fall below the 50% line, despite the fact that these samples represent

the more distal sections in each of the parasequences. In contrast, six out of ten Interval 2 samples of massive to faintly laminated mudstone (FA1) and burrow mottled mudstone with shells (FA3) fall above the 50% clay line (Fig. 28). This diagram also shows that the most distal mudstones in the upper Bakken member are compositionally comparable to other shale plays in the U.S.A. If the bulk rock composition of Interval 1 was determined, thus accounting for the well laminated mudstones (FA2a and FA2b) and also the layers of radiolarite and radiolaria-bearing mudstone within this unit (Fig. 29), then it would likely plot much closer to the quartz-rich corner of the ternary diagram than some other shale plays in the U.S.A. In contrast, the higher clay content, the lack of radiolarite and radiolaria-bearing mudstone, and the widespread paucity of siltstone within Interval 2, suggests that this section might behave as a frac barrier (cf. Rickman et al., 2009).

Based on these findings, the proposed stratigraphic zones and areas with the highest exploration potential include: (1) Interval 1 of the upper Bakken member in thermally mature, proximal parts of the basin outside of the depocenter because of overall high brittleness and porosity where silt and radiolaria are abundant, and (2) localized silt-rich sub-basins in thermally mature areas. These upper Bakken shales may produce as well as, or better than, other economic shale plays shown Figure 28, such as the Barnett Siliceous Shale. Horizontal wells in the middle Bakken member may show improved productivity if propped hydraulic fractures extend vertically into Interval 1, while in more basinward areas, the ductile Interval 2 might act as a frac barrier.

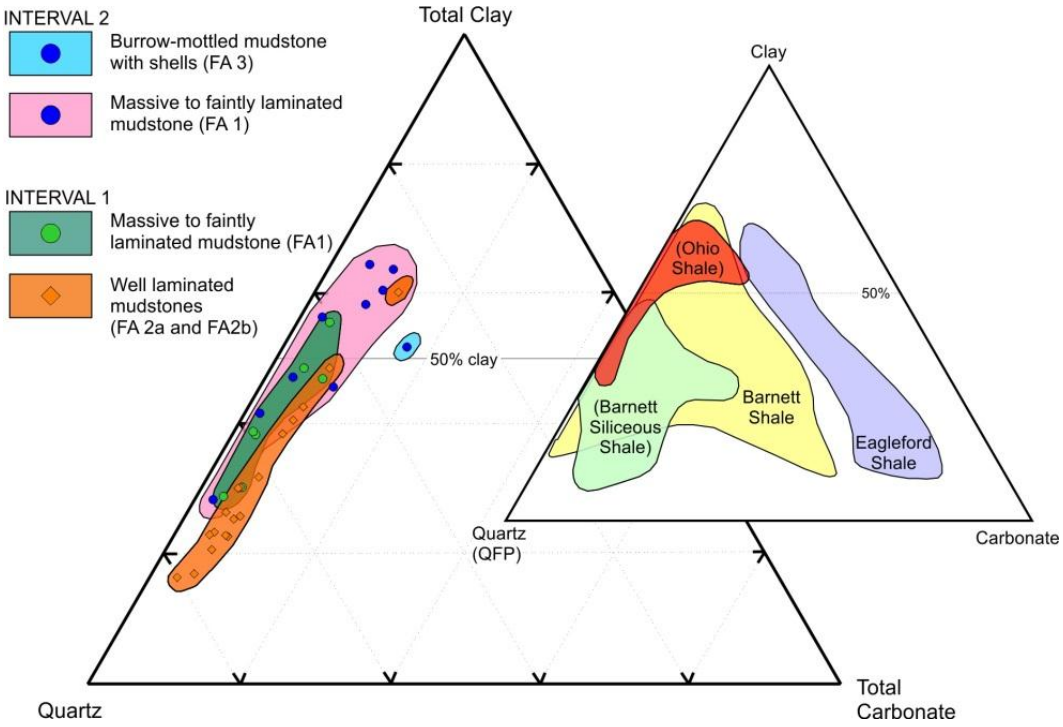

Figure 28. Ternary diagram showing mineral composition of facies associations within Interval 1 and Interval 2 using data from this study and from Sven Egenhoff and Neil Fishman (pers. comm., 2013). No data is available for FA4. Inset shows composition of mudstones from various USA shale plays (Li, X. J. et al., 2009; Passey et al., 2010). In the right diagram the quartz end member for the Ohio Shale and Barnett Siliceous Shale is measured as the sum of quartz, feldspar and pyrite contents (i.e. QFP) (Li, X. J. et al., 2009).

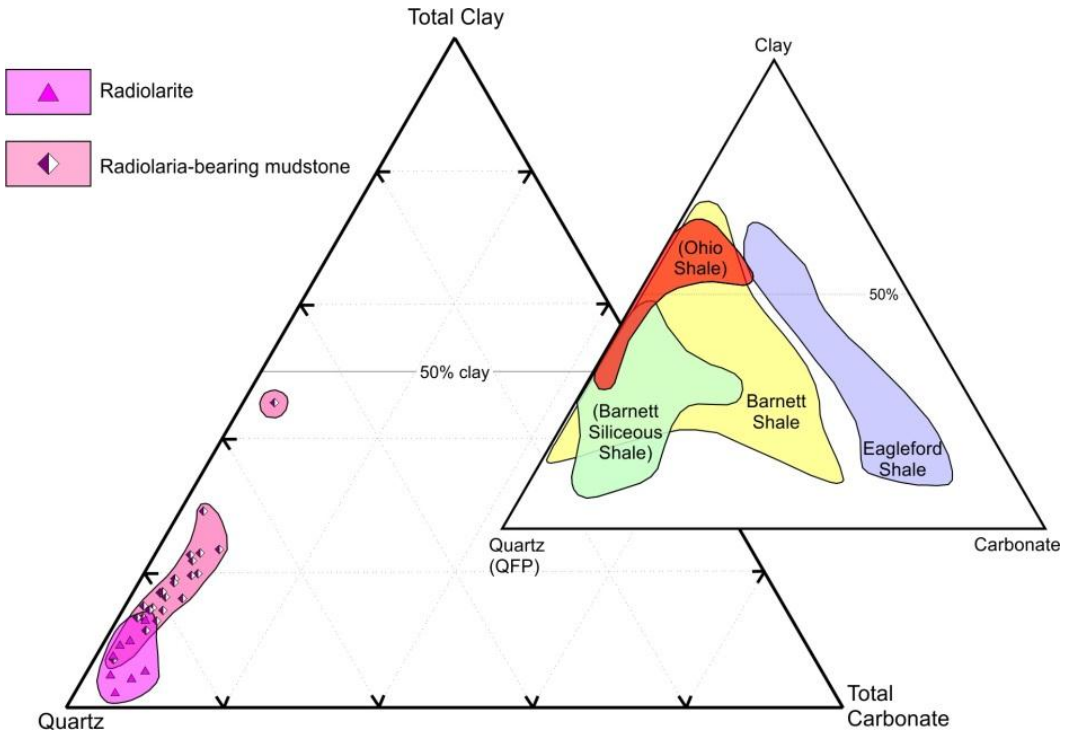

Figure 29. Ternary diagram showing mineral composition of individual laminae and thin beds consisting of radiolarite and radiolaria-bearing mudstone using data from this study and from Neil Fishman and Sven Egenhoff (pers. comm., 2013). Inset shows composition of mudstones from various USA shale plays (Li, X. J. et al., 2009; Passey et al., 2010). In the right diagram the quartz end member for the Ohio Shale and Barnett Siliceous Shale is measured as the sum of quartz, feldspar and pyrite contents (i.e. QFP) (Li, X. J. et al., 2009).

10.0 CONCLUSIONS

1. The upper Bakken member consists of twelve fine-grained facies that can be grouped into the following five mudstone facies associations: massive to faintly laminated mudstones (FA1), well laminated mudstones (FA2a), well laminated, clay clast-bearing mudstones (FA2b), burrow-mottled mudstone with shells (FA3) and interlaminated siltstone and mudstone (FA4).
2. The upper Bakken member mudstones were deposited offshore by both suspension settling and bedload transport processes during intermittent storm events on a low gradient distal ramp or shelf. The coarsest-grained sediments represent the proximal offshore environment and the finest-grained and typically more massive sediments represent the distal offshore environment. However, facies associations deposited in the proximal offshore environment vary laterally depending on bottom water oxygen levels during deposition, and on the abundance of siltstone laminae and clay clasts.
3. The upper Bakken member succession is dominated by two types of mostly coarsening-upward units composed of (1) massive to faintly laminated mudstones (FA1) and well laminated mudstones (FA2a) and/or, well laminated, clay clast-bearing mudstones (FA2b); and (2) massive to faintly laminated mudstones (FA1) and burrow-mottled mudstone with shells (FA3). Each of these coarsening-upward units defines one shallowing-upward, parasequence-scale cycle. The succession in the depocenter records ten of these cycles, whereas wells in the most proximal locations contain as few as one cycle due to lateral facies changes and possible erosion.
4. The upper Bakken member succession can be subdivided into two distinct stratigraphic zones, termed Intervals 1 and 2, which mark a regional facies change from mudstones

within Interval 1 that are overall siltier and contain more well-laminated mudstones (FA2a and FA2b) and thin beds and laminae of radiolarite and radiolaria-bearing mudstone than the overlying Interval 2. In contrast, Interval 2 is characterized by the occurrence of burrow-mottled mudstone with shells (FA3) and a greater amount of massive to faintly laminated mudstone (FA1) than Interval 1.

5. The coarsening-upward units represent parasequences that show a distinct sequence-scale fine-grained facies architecture, which can be correlated for up to 300 km through the study area. Interval 1 was deposited during overall transgression of the sedimentary system and Interval 2 was deposited during regression accompanied by basinward progradation of the overlying Lodgepole Formation carbonates. The maximum flooding surface (MFS) is located at the base of Interval 2.
6. Ubiquitous microscopic bioturbation in all facies associations, the presence of shells, centimeter-scale burrows in burrow-mottled mudstone with shells (FA3) and pyrite concretions indicates that the basin was not permanently stratified and anoxic as previously assumed, but was probably dysoxic with limited to moderate bottom water circulation.
7. Based on the findings is this research, areas of thermally mature shale with the highest exploration potential include: (1) local silt-rich sub-basins and (2) the Interval 1 stratigraphic unit. Interval 1 is likely to have higher brittleness than Interval 2 due to the greater abundance of thin siltstone laminae, and laminae and thin beds of radiolarite and radiolaria-bearing mudstone. Interval 1 may also have higher porosity and permeability than Interval 2 due to the greater abundance of siltstone laminae. Although siltstone laminae are more abundant closer to the basin margin, the laminae and thin beds of

radiolarite and radiolaria-bearing mudstone are more closely spaced within Interval 1 in areas located roughly halfway between the depocenter and the upper Bakken member depositional edge, indicating that the most marginal areas of the upper Bakken member may not be the most brittle.

11.0 REFERENCES

Baccelle, L., and Bosellini, A., 1965, Diagrammi per la stima visiva della composizione percentuale nelle rocce sedimentarie: Università degli studi di Ferrara, [Bologna].

Berner, R.A., 1984, Sedimentary pyrite formation; an update: Geochimica et Cosmochimica Acta, v. 48, no. 4, p. 605–615, doi: 10.1016/0016-7037(84)90089-9.

Berwick, B. R., and Hendricks, M., L., 2011, Depositional lithofacies of the Upper Devonian Three Forks Formation and the Grassy Butte Member of the Lower Bakken Shale in the Williston Basin, *in* Robinson, L., LeFever, J., and Gaswirth, S., eds., Bakken-Three Forks Petroleum System in the Williston Basin: RMAG guidebook, p. 159-172 (on CD).

Birnbaum, S.J., and Wireman, J.W., 1985, Sulfate-reducing bacteria and silica solubility: a possible mechanism for evaporite diagenesis and silica precipitation in banded iron formations: Canadian Journal of Earth Sciences, v. 22, no. 12, p. 1904–1909, doi: 10.1139/e85-206.

Boggs, S., 2009, Petrology of sedimentary rocks: Cambridge University Press Cambridge, England.

Bohacs, K.M., 1993, Source quality variations tied to sequence development in the Monterey and associated formations, southwestern California: AAPG Studies in Geology, v. 37, p. 177–204.

Bohacs, K.M., Grabowski Jr., G.J., Carroll, A.R., Mankiewicz, P.J., Miskell-Gerhardt, K.J., Schwalbach, J.R., Wegner, M.B., and Simo, J.A., 2005, Production, destruction, and dilution; the many paths to source-rock development: Special Publication - Society for Sedimentary Geology, v. 82, p. 61–101.

Bohacs, K.M., Neal, J.E., and Grabowski Jr., G.J., 2002, Sequence stratigraphy in fine-grained rocks; beyond the correlative conformity: Program and Abstracts - Society of Economic Paleontologists. Gulf Coast Section. Research Conference, v. 22, p. 321–347.

Bohacs, K.M., and Schwalbach, J.R., 1992, Sequence stratigraphy of fine-grained rocks with special reference to the Monterey Formation: Field Trip Guidebook - Pacific Section, Society of Economic Paleontologists and Mineralogists, v. 70, p. 7–19.

Brett, C.E., and Allison, P.A., 1998, Paleontological approaches to the environmental interpretation of marine mudrocks, *in* E. Schweizerbart'sche Verlagsbuchhandlung Naegele u. Obermiller : Stuttgart, Federal Republic of Germany, University of Rochester, Department of Earth and Environmental Sciences, Rochester, NY, United States; University of Texas at Arlington, Department of Geology, Arlington, TX, United States, p. 301–349.

Brett, C.E., and Baird, G.C., 1986, Comparative taphonomy; a key to paleoenvironmental interpretation based on fossil preservation: Palaios, v. 1, no. 3, p. 207–227.

Brooks, L., and Montalvo, R., 2012, The Integration of Key Petrophysical and Geomechanical Play Drivers into Geological Attribute Mapping- Getting Ahead of the Stampede: AAPG Search and Discovery Article #40948, 79p. http://www.searchanddiscovery.com/documents/2012/40948brooks/ndx_brooks.pdf

Brown, G., and Brindley, G.W., 1980, X-ray diffraction procedures for clay mineral identification: Crystal structures of clay minerals and their X-ray identification, Mineralogical Society Monography 5, p. 305-359.

Buatois, L.A., and Mángano, M.G., 2011, Ichnology: Organism-substrate interactions in space and time: Cambridge University Press.

Buller D., 2010, Haynesville Shale, Reservoir Evaluation and Stimulation Topics, Society of Petroleum Engineering luncheon presentation, Tulsa, Oklahoma, 11 March. 42p. http://spemc.org/resources/presentation_031110.pdf

Buller, D., Suparman, F.N.U., Kwong, S., Spain, D., and Miller, M., 2010, A Novel Approach to Shale-Gas Evaluation Using a Cased-Hole Pulsed Neutron Tool: Society of Petrophysicists and Well-Log Analysts Paper 87257. Presented at the SPWLA 51st Annual Logging Symposium, Perth, Australia, 19–23 June. 15p.

Burrus, J., Osadetz, K., Wolf, S., Doligez, B., Visser, K., and Dearborn, D., 1996, A two-dimensional regional basin model of Williston Basin hydrocarbon systems: AAPG Bulletin, v. 80, no. 2, p. 265–291, doi: 10.1306/64ED87AA-1724-11D7-8645000102C1865D.

Cecil, C.B., Dulong, F.T., Edgar, N.T., and Ahlbrandt, T.S., 1994, Carboniferous paleoclimates, sedimentation, and stratigraphy: U. S. Geological Survey : Reston, VA, United States, 27–28 p.

Chen, Z., Osadetz, K.G., Jiang, C., and Li, M., 2009, Spatial variation of Bakken or Lodgepole oils in the Canadian Williston Basin: AAPG Bulletin, v. 93, no. 6, p. 829–851, doi: 10.1306/03160908120.

Clement, J.H., 1985, Cedar Creek: a significant paleotectonic feature of the Williston Basin, *in* Longman, M.W., ed., Williston Basin: Anatomy of a cratonic oil province: Rocky Mountain Association of Geologists, p. 323–336.

Coleman, M.L., 1985, Geochemistry of diagenetic non-silicate minerals; kinetic considerations: Philosophical Transactions of the Royal Society of London, Series A: Mathematical and Physical Sciences, v. 315, no. 1531, p. 39–56.

Cramer, D.D., 1991, Stimulation treatments in the Bakken Formation; implications for horizontal completions, *in* W.B. Hansen, ed., 1991 Guidebook to Geology and Horizontal Drilling of the Bakken Formation: Montana Geological Society, Billings, Montana, p. 117-140.

Creaney, S., and Passey, Q.R., 1993, Recurring patterns of total organic carbon and source rock quality within a sequence stratigraphic framework: AAPG Bulletin, v. 77, no. 3, p. 386–401, doi: 10.1306/BDFF8C18-1718-11D7-8645000102C1865D.

Curtis, C.D., 1980, Diagenetic alteration in black shales: Journal of the Geological Society of London, v. 137, Part , p. 189–194.

Dalrymple, B., 2006, Where does the mud go? The dispersal of mud from rivers and the stratigraphic implications: Transactions - Gulf Coast Association of Geological Societies, v. 56, p. 155.

Dalrymple, R.W., and Cummings, D.I., 2005, The offshore transport of mud; why it doesn't happen and the stratigraphic implications: Abstracts with Programs - Geological Society of America, v. 37, no. 7, p. 403.

Drever, J.I., 1973, The Preparation of Oriented Clay Mineral Specimens for X-ray Diffraction Analysis by a Filter-Membrane Peel Technique: American Mineralogist, v. 58, no. 5-6, p. 553–554.

Druyff, L., 1991, Reservoir properties of the Bakken Shale, *in* W.B. Hansen, ed., 1991 Guidebook to Geology and Horizontal Drilling of the Bakken Formation: Montana Geological Society, Billings, Montana, p. 91.

Eberl, D.D., 2003, User's guide to RockJock, a program for determining quantitative mineralogy from powder X-ray diffraction data: US Geological Survey.

Egenhoff, S.O., and Fishman, N. S., 2013, Traces in the dark—Sedimentary processes and facies gradients in the upper shale member of the Upper Devonian–Lower Mississippian Bakken Formation, Williston Basin, North Dakota, U.S.A: Journal of Sedimentary Research, v. 83, p. 803-824.

Egenhoff, S., A. Jaffri, and P. Medlock, 2011a, Climate control on reservoir distribution in the Upper Devonian Three Forks Formation, North Dakota and Montana: AAPG Search and Discovery (Abstract) #90124. http://www.searchanddiscovery.com/abstracts/html/2011/annual/abstracts/Egenhoff2.html

Egenhoff, S.O., van Dolah, A., Jaffri, A. and Maletz, J., 2011b, Facies architecture and sequence stratigraphy of the Middle Bakken Member, Williston Basin, North Dakota, *in* Robinson, L., LeFever, J., and Gaswirth, S., eds., Bakken-Three Forks Petroleum System in the Williston Basin: RMAG guidebook, p. 27-47 (on CD).

Einsele, G., 1985, Response of sediments to sea-level changes in differing subsiding storm-dominated marginal and epeiric basins, *in* Sedimentary and evolutionary cycles, Springer, p. 67–97.

Einsele, G., 2000, Sedimentary basins: evolution, facies, and sediment budget. Springer-Verlag: Berlin, Heidelberg, Germany, New York.

Flannery, J., and Kraus, J., 2006, Integrated analysis of the Bakken petroleum system; U. S. Williston Basin: Abstracts: Annual Meeting - American Association of Petroleum Geologists, v. 15, p. 33–34.

Friedrichs, C.T., and Wright, L.D., 2004, Gravity driven sediment transport on the continental shelf: Implications for equilibrium profiles near river mouths: Coastal Engineering, v. 51, p. 795–811.

Gerhard, L.C., Anderson, S.B., and Fischer, D.W., 1990, Petroleum geology of the Williston Basin: AAPG Memoir, v. 51, p. 507–559.

Ghadeer, S.G., and Macquaker, J.H.S., 2011, Sediment transport processes in an ancient mud-dominated succession; a comparison of processes operating in marine offshore settings and anoxic basinal environments: Journal of the Geological Society of London, v. 168, no. 5, p. 1121–1132, doi: 10.1144/0016-76492010-016.

Ghadeer, S.G., and Macquaker, J.H.S., 2012, The role of event beds in the preservation of organic carbon in fine-grained sediments; analyses of the sedimentological processes operating during deposition of the Whitby Mudstone Formation (Toarcian, Lower Jurassic) preserved in northeast England: Marine and Petroleum Geology, v. 35, no. 1, p. 309–320, doi: 10.1016/j.marpetgeo.2012.01.001.

Gibson, R.I., 1995, Basement tectonics and hydrocarbon production in the Williston basin: An interpretive overview, *in* Hunter, L.D.V. and Schalla, R.A. eds., 7th International Williston Basin Symposium Guidebook, Montana Geological Society, North Dakota Geological Society, Saskatchewan Geological Society, and Fort Peck Tribes, p. 3–11.

Hansen, W.B., and Long, G.I.W., 1991a, Bakken production and potential in the U. S. and Canada; can the fairway be defined?, *in* W.B. Hansen, ed., 1991 Guidebook to Geology and Horizontal Drilling of the Bakken Formation: Montana Geological Society, Billings, Montana, p. 69–88.

Hansen, W.B., and Long, G.I.W., 1991b, Criteria for horizontal and vertical prospect generation in the Bakken Formation, Montana and North Dakota, *in* W.B. Hansen, ed., 1991 Guidebook to Geology and Horizontal Drilling of the Bakken Formation: Montana Geological Society, Billings, Montana, p. 151–163.

Hatch, J., 1988, Review of the geology of the Sioux uplift and Iowa shelf provinces as a basis for estimates of undiscovered hydrocarbon resources: U.S. Geological Survey Open-File Report 88- 450V, 20 p.

Hayes, M.D., 1985, Conodonts of the Bakken Formation (Devonian and Mississippian), Williston Basin, North Dakota: The Mountain Geologist, v. 22, no. 2.

Herbin, J.P., Fernandez-Martinez, J.L., Geyssant, J.R., Albani, A.E., Deconinck, J.F., Proust, J.N., Colbeaux, J.P., and Vidier, J.P., 1995, Sequence stratigraphy of source rocks applied to the study of the Kimmeridgian/Tithonian in the North-West European shelf (Dorset/UK, Yorkshire/UK and Boulonnais/France): Marine and Petroleum Geology, v. 12, no. 2, p. 177–194.

Holland Jr., F.D., Hayes, M.D., Thrasher, L.C., and Huber, T.P., 1987, Summary of the biostratigraphy of the Bakken Formation (Devonian and Mississippian) in the Williston

Basin, North Dakota: Special Publication - Saskatchewan Geological Society, v. 9, p. 68–76.

Ingram, G.M., Urai, J.L., and Naylor, M.A., 1997, Sealing processes and top seal assessment: Norwegian Petroleum Society Special Publications, v. 7, p. 165–174.

Irwin, H., Curtis, C., and Coleman, M., 1977, Isotopic evidence for source of diagenetic carbonates formed during burial of organic-rich sediments: Nature [London], v. 269, no. 5625, p. 209–213.

Jarvie, D.M., Hill, R.J., Ruble, T.E., and Pollastro, R.M., 2007, Unconventional shale-gas systems; the Mississippian Barnett Shale of North-Central Texas as one model for thermogenic shale-gas assessment: AAPG Bulletin, v. 91, no. 4, p. 475–499, doi: 10.1306/12190606068.

Jin, H., and Sonnenberg, S.A., 2012, Source Rock Potential of the Bakken Shales in the Williston Basin, North Dakota and Montana: AAPG Search and Discovery Article #20156 (poster). http://www.searchanddiscovery.com/documents/2012/20156jin/ndx_jin.pdf

Johnston, D.I., Henderson, C.M., and Schmidt, M.J., 2010, Upper Devonian to Lower Mississippian conodont biostratigraphy of uppermost Wabamun Group and Palliser Formation to lowermost Banff and Lodgepole Formations, southern Alberta and southeastern British Columbia, Canada; implications for correlations and sequence stratigraphy: Bulletin of Canadian Petroleum Geology, v. 58, no. 4, p. 295–341, doi: 10.2113/gscpgbull.58.4.295.

Kent, D.M., and Christopher, J.E., 1994, Geological history of the Williston Basin and the Sweetgrass Arch, *in* Geological Atlas of Western Canada. Mossop, G.D. and Shetson, I. (comps.). Canadian Society of Petroleum Geologists and Alberta Research Council, p. 421-430.

LeFever, J., and Helms, L., 2006, Bakken Formation reserve estimates: White paper, North Dakota Geological Survey, Bismarck, North Dakota , 6 p.

LeFever, J., 2005, Oil production from the Bakken Formation: A short history: North Dakota Geological Survey newsletter, v. 32, no. 1, p. 5–10.

Lefever, J.A., 1991, History of oil production from the Bakken Formation, North Dakota, *in* W.B. Hansen, ed., 1991 Guidebook to Geology and Horizontal Drilling of the Bakken Formation: Montana Geological Society, Billings, Montana,, p. 3–17.

Lefever, J.A., Martiniuk, C.D., Dancsok, E.F.R., and Mahnic, P.A., 1991, Petroleum potential of the middle member, Bakken Formation, Williston Basin, *in* W.B. Hansen, ed., 1991 Guidebook to Geology and Horizontal Drilling of the Bakken Formation: Montana Geological Society, Billings, Montana, p. 74–94.

Leventhal, J.S., 1998, Metal-rich black shales: Formation, economic geology and environmental considerations: *in* E. Schweizerbart'sche Verlagsbuchhandlung Naegele u. Obermiller : Stuttgart, Federal Republic of Germany, University of Texas at Arlington, Department of

Geology, Arlington, TX, United States; University of Texas at Arlington, Department of Geology, Arlington, TX, United States, p. 255-282.

Li, X., Lu, Z., Dong, D., and Cheng, K., 2009, Geologic controls on accumulation of shale gas in North America: Natural Gas Industry, v. 5, p. 6.

Link, T.A., 1958, The Williston basin is large and deep, *in* 2nd International Williston Basin Symposium Guidebook, North Dakota Geological Society, Saskatchewan Geological Society, p. 6.

Luening, S., and Kolonic, S., 2003, Uranium spectral gamma-ray response as a proxy for organic richness in black shales; applicability and limitations: Journal of Petroleum Geology, v. 26, no. 2, p. 153–174.

Mackie, J., 2013, Sedimentology and diagenesis of the lower Lodgepole Formation, Williston Basin, North Dakota, unpublished Master's thesis, Colorado State University, Fort Collins, CO, U.S.A.

Macquaker, J.H.S., and Taylor, K.G., 1996, A sequence-stratigraphic interpretation of a mudstone-dominated succession; the Lower Jurassic Cleveland Ironstone Formation, UK: Journal of the Geological Society of London, v. 153, Part , p. 759–770.

Macquaker, J.H.S., and Adams, A.E., 2003, Maximizing information from fine-grained sedimentary rocks; an inclusive nomenclature for mudstones: Journal of Sedimentary Research, v. 73, no. 5, p. 735–744.

Macquaker, J.H.S., Bentley, S.J., and Bohacs, K.M., 2010, Wave-enhanced sediment-gravity flows and mud dispersal across continental shelves; reappraising sediment transport processes operating in ancient mudstone successions: Geology [Boulder], v. 38, no. 10, p. 947–950.

Macquaker, J.H.S., and Gawthorpe, R.L., 1993, Mudstone lithofacies in the Kimmeridge Clay Formation, Wessex Basin, southern England: implications for the origin and controls of the distribution of mudstones: Journal of Sedimentary Research, v. 63, no. 6.

Macquaker, J.H.S., Gawthorpe, R.L., Taylor, K.G., and Oates, M.J., 1998, Heterogeneity, stacking patterns and sequence stratigraphic interpretation in distal mudstone successions; examples from the Kimmeridge Clay Formation, U.K., *in* E. Schweizerbart'sche Verlagsbuchhandlung Naegele u. Obermiller : Stuttgart, Federal Republic of Germany, University of Manchester, Department of Earth Sciences, Manchester, United Kingdom; University of Texas at Arlington, Department of Geology, Arlington, TX, United States, p. 163–186.

Macquaker, J.H.S., and Howell, J.K., 1999, Small-scale (<5.0 m) vertical heterogeneity in mudstones; implications for high-resolution stratigraphy in siliciclastic mudstone successions: Journal of the Geological Society of London, v. 156, p. 105–112.

Macquaker, J.H.S., Taylor, K.G., and Gawthorpe, R.L., 2007, High-resolution facies analyses of mudstones; implications for paleoenvironmental and sequence stratigraphic interpretations

of offshore ancient mud-dominated successions: Journal of Sedimentary Research, v. 77, no. 4, p. 324–339, doi: 10.2110/jsr.2007.029.

Mason, B.S., 2012, Oil Production Potential of the North Dakota Bakken: Oil & Gas Journal, v.110, no, 4.

Matthew, A.J., Woods, A.J., and Oliver, C., 1991, Spots before the eyes: new comparison charts for visual percentage estimation in archaeological material: Recent developments in ceramic petrology, British Museum Occasional Paper, no. 81, p. 211–263.

McKeon, M., 2011, Horizontal Fracturing in Shale Plays. Taking a Deeper Look at Shale: Geology and Potential of the Upper Ordovician Utica Shale in the Appalachian Basin, Petroleum Technology Transfer Council workshop presentation, New Philadelphia, Ohio, June 21. 28p. http://www.pttc.org/workshops/eastern_062111/eastern_062111_McKeon.pdf

Meissner, F.F., 1978, Petroleum geology of the Bakken Formation, Williston Basin, North Dakota and Montana, *in* D. Rehig, ed.: Williston Basin Symposium: Billings, Montana, Montana Geological Society 24th Annual Conference, p. 207-227.

Meissner, F.F., and Banks, R.B., 2000, Computer simulation of hydrocarbon generation, migration and accumulation under hydrodynamic conditions; examples from the Williston and San Juan basins, USA: AAPG Bulletin, v. 84, no. 9, p. 1464, doi: 10.1306/A9674A8A-1738-11D7-8645000102C1865D.

Mitchel, R., 2013, Sedimentology and reservoir properties of the Three Forks dolomite, Bakken petroleum system, Williston Basin, U.S.A: AAPG Search and Discovery Article #120079, 9p. http://www.searchanddiscovery.com/documents/2013/120079mitchell/ndx_mitchell.pdf

Monson, L.M., and Lund, D.F., 1991, Breaking into Bakken potential on the Fort Peck Reservation in northeastern Montana: *in* W.B. Hansen, ed., 1991 Guidebook to Geology and Horizontal Drilling of the Bakken Formation: Montana Geological Society, Billings, Montana, p. 95–102.

Moore, D.M., and Reynolds Jr., R.C., 1989, X-ray diffraction and the identification and analysis of clay minerals: Oxford University Press (OUP): New York, NY, United States, Illinois State Geological Survey, United States.

Murphy, A.E., Sageman, B.B., Hollander, D.J., Lyons, T.W., and Brett, C.E., 2000, Black shale deposition and faunal overturn in the Devonian Appalachian Basin: Clastic starvation, seasonal water-column mixing, and efficient biolimiting nutrient recycling: Paleoceanography, v. 15, no. 3, p. 280–291.

Noble, P.J., Naraoka, H., Poulson, S.R., Fukui, E., Jin, Y., and O'Connor, S., 2011, Paleohydrographic influences on Permian radiolarians in the Lamar Limestone, Guadalupe Mountains, West Texas, elucidated by organic biomarker and stable isotope geochemistry: Palaios, v. 26, no. 3, p. 180–186, doi: 10.2110/palo.2010.p10-059r.

Ormiston, A.R., 1993, The association of radiolarians with hydrocarbon source rocks: Radiolaria of giant and subgiant fields in Asia: Nazarov memorial volume. Micropaleontology Press, New York, p. 9–16.

Oschmann, W., 1994, Adaptive pathways of benthic organisms in marine oxygen-controlled environments.(With 14 figures in the text): Neues Jahrbuch fur Geologie und Palaontologie-Abhandlungen, v. 191, no. 3, p. 393–444.

Passey, Q.R., Bohacs, K.M., Esch, W.L., Klimentidis, R., and Sinha, S., 2010, From Oil-Prone Source Rock to Gas-Producing Shale Reservoir - Geologic and Petrophysical Characterization of Unconventional Shale-Gas Reservoirs, *in* Chinese Petroleum Society/Society of Petroleum Engineers International Oil and Gas Conference and Exhibition, Beijing, China, Society of Petroleum Engineers, Exxon Production Research Company, Houston, TX, United States; Ohio University, Department of Geological Sciences, Athens, OH, United States.

Pollastro, R.M., 1982, A recommended procedure for the preparation of oriented clay-mineral specimens for X-ray diffraction analysis; modifications to Drever's filter-membrane peel technique: U. S. Geological Survey: Reston, VA, United States.

Posamentier, H.W., Jervey, M.T., and Vail, P.R., 1988, Eustatic controls on clastic deposition; I, Conceptual framework: Special Publication - Society of Economic Paleontologists and Mineralogists, v. 42, p. 109–124.

Posamentier, H.W., and Vail, P.R., 1988, Eustatic controls on clastic deposition; II, Sequence and systems tract models: Special Publication - Society of Economic Paleontologists and Mineralogists, v. 42, p. 125–154.

Potter, P.E., Maynard, J.B., and Depetris, P.J., 2005, Mud and mudstones; introduction and overview: Springer-Verlag: Berlin, Federal Republic of Germany, University of Cincinnati, Department of Geology, Cincinnati, OH, United States.

Pöppelreiter, M., and Aigner, T., 2003, Unconventional pattern of reservoir facies distribution in epeiric successions: Lessons from an outcrop analog (Lower Keuper, Germany): AAPG bulletin, v. 87, no. 1, p. 39–70

Quirein, J., D. Buller, J. Witkowsky, and J. Truax, 2012, Integrating core data and wireline data for formation evaluation and characterization of shale gas reservoirs: AAPG Search and Discovery Article #41073, 22p. http://www.searchanddiscovery.com/documents/2012/41073quirein/ndx_quirein.pdf

Quirein, J., Gardner, J., and Watson, J., 1982, Combined natural gamma ray spectral/litho-density measurements applied to complex lithologies, *in* SPE 1982 Annual Technical Conference and Exhibition.

Raiswell, R., 1982, Pyrite texture, isotopic composition and the availability of iron: American Journal of Science, v. 282, no. 8, p. 1244–1263.

Raiswell, R., and Berner, R.A., 1985, Pyrite formation in euxinic and semi-euxinic sediments: American Journal of Science, v. 285, no. 8, p. 710–724.

Richards, B.C., 1989, Upper Kaskaskia Sequence; Uppermost Devonian and Lower Carboniferous, *in* Can. Soc. Pet. Geol. : Calgary, AB, Canada, Geol. Surv. Can., Inst. Sediment. and Pet. Geol., Calgary, AB, Canada; Geol. Surv. Can., Inst. Sediment. and Pet. Geol., Calgary, AB, Canada, p. 165–201.

Rickman, R., Mullen, M., Petre, E., Grieser, B., and Kundert, D., 2009, Petrophysics Key In Stimulating Shales: American Oil and Gas Reporter, March 2009, p. 121–127.

Rider, H., 1996, The Geological Interpretation of Well Logs, 2nd edition, Whittles Publishing Services, Glasgow, U.K.

Robinson, J.W., Gaswirth, S.B., and LeFever, J.A. Bakken-Three Forks Petroleum System in the Williston Basin :.

Sarg, J.F., 1988, Carbonate sequence stratigraphy: Special Publication - Society of Economic Paleontologists and Mineralogists, v. 42, p. 155–181.

Schieber, J., 2010, Common themes in the formation and preservation of intrinsic porosity in shales and mudstones-illustrated with examples across the Phanerozoic, *in* SPE 2010 Unconventional Gas Conference.

Schieber, J., 1999, Distribution and deposition of mudstone facies in the Upper Devonian Sonyea Group of New York: Journal of Sedimentary Research, v. 69, no. 4, p. 909–925, doi: 10.1306/D4268AB8-2B26-11D7-8648000102C1865D.

Schieber, J., 1996, Early diagenetic silica deposition in algal cysts and spores; a source of sand in black shales?: Journal of Sedimentary Research, v. 66, no. 1, p. 175–183, doi: 10.1306/D42682ED-2B26-11D7-8648000102C1865D.

Schieber, J., 1998, Sedimentary features indicating erosion, condensation, and hiatuses in the Chattanooga Shale of central Tennessee; relevance for sedimentary and stratigraphic evolution, *in* E. Schweizerbart'sche Verlagsbuchhandlung Naegele u. Obermiller : Stuttgart, Federal Republic of Germany, Department of Geology, University of Texas at Arlington, Arlington, TX, United States; p. 187–215.

Schieber, J., 2003, Simple gifts and buried treasures—implications of finding bioturbation and erosion surfaces in black shales: The Sedimentary Record, v. 1, no. 2, p. 4–8.

Schieber, J., and Baird, G., 2001, On the origin and significance of pyrite spheres in Devonian black shales of North America: Journal of Sedimentary Research, v. 71, no. 1, p. 155–166.

Schieber, J., Krinsley, D., and Riciputi, L., 2000, Diagenetic origin of quartz silt in mudstones and implications for silica cycling: Nature, v. 406, no. 6799, p. 981–985.

Schieber, J., Southard, J.B., and Schimmelmann, A., 2010, Lenticular shale fabrics resulting from intermittent erosion of water-rich muds; interpreting the rock record in the light of recent flume experiments: Journal of Sedimentary Research, v. 80, no. 1, p. 119–128.

Schieber, J., Southard, J., and Thaisen, K., 2007, Accretion of mudstone beds from migrating floccule ripples: Science, v. 318, no. 5857, p. 1760–1763, doi: 10.1126/science.1147001.

Scotese, C.R., 1994, Carboniferous paleocontinental reconstructions: U. S. Geological Survey Bulletin 2110, p. 3–6.

Smith, M.G., and Bustin, R.M., 2000, Late Devonian and Early Mississippian Bakken and Exshaw black shale source rocks, Western Canada sedimentary basin; a sequence stratigraphic interpretation: AAPG Bulletin, v. 84, no. 7, p. 940–960, doi: 10.1306/A9673B76-1738-11D7-8645000102C1865D.

Smith, M.G., and Bustin, R.M., 1998, Production and preservation of organic matter during deposition of the Bakken Formation (Late Devonian and Early Mississippian), Williston Basin: Palaeogeography, Palaeoclimatology, Palaeoecology, v. 142, no. 3-4, p. 185–200.

Sonnenberg, S.A., and Pramudito, A., 2009, Petroleum geology of the giant Elm Coulee Field, Williston Basin: AAPG Bulletin, v. 93, no. 9, p. 1127–1153, doi: 10.1306/05280909006.

Soukup, A.D., Drees, R.L., and Lynn, C. W., 2008, Sampling soils for mineralogical analyses: Methods of Soil Analysis Part 5—Mineralogical Methods, p. 1–11.

Stasiuk, L.D., and Fowler, M.G., 2004, Organic facies in Devonian and Mississippian strata of Western Canada Sedimentary Basin: relation to kerogen type, paleoenvironment, and paleogeography: Bulletin of Canadian Petroleum Geology, v. 52, no. 3, p. 234–255.

Tyson, R.V., and Pearson, T.H., 1991, Modern and ancient continental shelf anoxia: an overview: Geological Society, London, Special Publications, v. 58, no. 1, p. 1–24.

Vail, P.R., Mitchum Jr., R.M., and Thompson III, S., 1977, Seismic stratigraphy and global changes of sea level; Part 3, Relative changes of sea level from coastal onlap: Memoir - American Association of Petroleum Geologists, , no. 26, p. 63–81.

Van Wagoner, J.C., Mitchum, R.M., Campion, K.M., and Rahmanian, V.D., 1990, Siliciclastic sequence stratigraphy in well logs, cores, and outcrops; concepts for high-resolution correlation of time and facies: Methods in Exploration Series, v. 7.

Van Wagoner, J.C., Posamentier, H.W., Mitchum, R.M.J., Vail, P.R., Sarg, J.F., Loutit, T.S., and Hardenbol, J., 1988, An overview of the fundamentals of sequence stratigraphy and key definitions. Sea-Level Changes: An Integrated Approach: SEPM, Special Publication, 42, 39-45.

Webster, R.L., 1984, Petroleum source rocks and stratigraphy of Bakken Formation in North Dakota: AAPG Bulletin, v. 68, no. 7, p. 593.

De Wever, O., and Baudin, F., 1996, Palaeogeography of radiolarite and organic-rich deposits in Mesozoic Tethys: Geologische Rundschau, v. 85, no. 2, p. 310–326.

Wignall, P.B., and Newton, R., 2001, Black shales on the basin margin; a model based on examples from the Upper Jurassic of the Boulonnais, northern France: Sedimentary Geology, v. 144, no. 3-4, p. 335–356.

Wright, L.D., and Friedrichs, C.T., 2006, Gravity-driven sediment transport on continental shelves; a status report: Continental Shelf Research, v. 26, no. 17-18, p. 2092–2107, doi: 10.1016/j.csr.2006.07.008.

12.0 APPENDICES

Appendix 1: West-East transect from eastern Montana to central North Dakota through the upper Bakken member of the Bakken Formation, Williston Basin

Appendix 2: North-South transect through the North Dakota portion of the upper Bakken member, Bakken Formation, Williston Basin

Appendix 3: Southwest-Northeast transect through the North Dakota portion of the upper Bakken member, Bakken Formation, Williston Basin

Folded transects (Appendices 1-3) are located in the back pocket.

Appendix 4: Thin section index

Original Operator	Original Well Name	Well File No.	Thin Section No. (Depth (ft))	Facies Association	Facies	Silt Min. (%)		Total Silt	Dominant Grain-size (Normalized to 100%)			
						Detrital Qtz	Carbo-nate		Fine silt	Medium silt	Coarse silt	Clay Clasts
								(%)	(%)	(%)	(%)	(%)
Amerada Hess Corp.	J. Horst 1-11H	15986	10515.9	1	4a	15	4	19	60	38	2	0
Amerada Hess Corp.	J. Horst 1-11H	15986	10520.5 (upper)	1	4a	17	3	20	55	40	5	0
Amerada Hess Corp.	J. Horst 1-11H	15986	10520.5 (lower)	1	4a	8	4	12	55	44	1	0
Amerada Hess Corp.	J. Horst 1-11H	15986	10524.1A	1	4	THIN SECTION TOO THICK			-	-	-	-
Amerada Hess Corp.	J. Horst 1-11H	15986	10524.1B	1	4b	20	1	21	70	30	0	10
Amerada Hess Corp.	J. Horst 1-11H	15986	10525.1	2a	4a	20	2	22	70	30	0	5
Amerada Hess Corp.	J. Horst 1-11H	15986	10527.0 (lower)	2b	4b	18	3	21	30	30	40	15
Amerada Hess Corp.	J. Horst 1-11H	15986	10527.0 (upper)	2b	4b	18	1	19	40	50	10	10
Ansbro Petroleum Co.	Loucks	15722	7626.0	1	4a	30	4	34	60	38	2	0
Ansbro Petroleum Co.	Loucks	15722	7629.2	2a	4a	17	1	18	70	28	2	0
Brigham Oil & Gas	Olson 10-15 1H	17513	10610.3 (upper)	2a	4a	23	7	30	45	45	10	0
Brigham Oil & Gas	Olson 10-15 1H	17513	10610.3 (lower)	2a	4a	18	5	23	35	30	35	0
Brigham Oil & Gas	Olson 10-15 1H	17513	10610.5 (upper)	2a	4a	22	3	25	30	55	20	3
Brigham Oil & Gas	Olson 10-15 1H	17513	10610.5 (lower)	2a	4a	17	5	22	50	45	5	0
Brigham Oil & Gas	Olson 10-15 1H	17513	10612.0 (upper)	2a	4a	12	3	15	35	55	10	0
Brigham Oil & Gas	Olson 10-15 1H	17513	10612.0 (lower)	2a	4a	12	3	15	20	30	50	0
Brigham Oil & Gas	Olson 10-15 1H	17513	10613.3X	1	4a	10	6	16	42	50	8	0
Brigham Oil & Gas	Olson 10-15 1H	17513	10613.5 (upper)	2a	4a	22	5	27	45	50	15	0
Brigham Oil & Gas	Olson 10-15 1H	17513	10613.5 (lower)	2a	4a	25	2	27	50	45	5	0
Brigham Oil & Gas	Olson 10-15 1H	17513	10615A	2	4	THIN SECTION TOO THICK			-	-	-	-
Brigham Oil & Gas	Olson 10-15 1H	17513	10615.0	2a	4a	22	6	28	40	55	5	0
Cirque Resources	Trippell 32-16H	17699	8327.8	1	4b	10	2	12	25	50	25	20
Cirque Resources	Trippell 32-16H	17699	8328.9	2a	4a	13	4	17	40	50	10	2
Cirque Resources	Trippell 32-16H	17699	8332.1 (i)	2a	4a	15	5	20	5	15	80	5
Cirque Resources	Trippell 32-16H	17699	8332.2 (ii)	2a	4a	15	5	20	10	35	55	3
Cirque Resources	Trippell 32-16H	17699	8332.4 (iii)	2b	4b	15	5	20	10	40	50	10
Cirque Resources	Trippell 32-16H	17699	8332.5 (iv)	2a	4a	10	5	15	15	25	60	5
Cirque Resources	Trippell 32-16H	17699	8332.7 (v)	2a	4a	8	2	10	20	30	50	1
Cirque Resources	Trippell 32-16H	17699	8332.8 (vi) upper	2a	4a	6	2	8	20	30	50	2
Cirque Resources	Trippell 32-16H	17699	8332.8 (vi) lower	2a	4a	20	10	30	20	60	20	2
Cirque Resources	Trippell 32-16H	17699	8332.9 (vii)	2a	4a	25	7	32	15	60	25	2
Conoco	Karsky 35 #2	13789	10117.6	2a	4a	30	5	35	25	50	25	0
Conoco	Karsky 35 #2	13789	10128.6	2a	4a	30	10	40	20	50	30	0
Conoco	Karsky 35 #2	13789	10145.8	1	4a	12	7	19	30	60	10	0

Original Operator	Original Well Name	Well File No.	Thin Section No. (Depth (ft))	Facies Association	Facies	Silt Min. (%)		Total Silt	Dominant Grain-size (Normalized to 100%)			
						Detrital Qtz	Carbo-nate		Fine silt	Medium silt	Coarse silt	Clay Clasts
								(%)	(%)	(%)	(%)	(%)
EOG Resources Inc.	Sidonia 1-06H	17676	8720.4	1	4a	9	1	10	60	40	0	3
EOG Resources Inc.	Sidonia 1-06H	17676	8725.8	1	4b	10	2	12	85	15	0	8
EOG Resources Inc.	Sidonia 1-06H	17676	8726.4	2a	4a	3	2	5	90	10	0	2
EOG Resources Inc.	Sidonia 1-06H	17676	8729.7	2a	4a	3	2	5	50	50	0	2
EOG Resources Inc.	Sidonia 1-06H	17676	8731.4	2b	4b	14	4	18	5	50	45	20
EOG Resources Inc.	Sidonia 1-06H	17676	8732.4	1	4b	10	5	15	15	70	15	10
Florida Exploation Co.	Federal 34-1	10803	10495.5	2a	4a	22	10	32	35	50	15	0
Gulf Oil Corp.	Martin Weber 1-18-C	6082	10969.3	3	4a	17	11	28	50	40	10	0
Gulf Oil Corp.	Martin Weber 1-18-C	6082	10977.0	2a	4a	15	8	23	43	50	7	0
Headingston Oil Co.	Nesson State 42X-36	17015	10296.4 (upper)	3	4a	15	10	25	70	30	0	0
Headingston Oil Co.	Nesson State 42X-36	17015	10296.4 (lower)	3	10	10	8	18	25	75	0	0
Headingston Oil Co.	Nesson State 42X-36	17015	10299.8	2a	4a	15	12	27	55	40	5	0
Headingston Oil Co.	Nesson State 42X-36	17015	10302.3	3	4a	15	15	30	75	20	5	0
Headingston Oil Co.	Nesson State 42X-36	17015	10303.7	1	4a	11	9	20	40	50	10	0
Headingston Oil Co.	Nesson State 42X-36	17015	10311.8	2a	4a	12	8	20	20	55	25	0
Helis Oil & Gas	Linseth 4-8H	16690	10777.3	1	4a	15	5	20	60	39	1	0
Helis Oil & Gas	Linseth 4-8H	16690	10777.8	3	9, 10	15	20	35	15	55	30	0
Helis Oil & Gas	Linseth 4-8H	16690	10778.1	3	10	13	7	20	40	55	5	0
Helis Oil & Gas	Linseth 4-8H	16690	10778.4	1	4a	10	8	18	30	60	10	0
Helis Oil & Gas	Linseth 4-8H	16690	10779.8	3	10	13	7	20	10	75	15	0
Helis Oil & Gas	Linseth 4-8H	16690	10781.5	1	4a	13	5	18	45	50	5	0
Helis Oil & Gas	Linseth 4-8H	16690	10786.7	2a	4a	7	1	8	50	50	0	0
Helis Oil & Gas	Linseth 4-8H	16690	10789.3	1	4a	5	3	8	20	80	0	0
Helis Oil & Gas	Linseth 4-8H	16690	10795.9	2a	4a	15	18	33	5	40	55	0
Lyco Energy	Titan F-WP 32-14H	16174	10676.5	2a	4a	10	8	18	28	70	2	0
Lyco Energy	Titan F-WP 32-14H	16174	10680.7	2b	4b	12	5	17	20	30	50	4
Marathon	Jensen #12-44	8069	9158.2	1	4a	17	4	21	65	30	5	0
Marathon	Jensen #12-44	8069	9160.0	1	4b	5	2	7	40	58	2	20
Marathon	Jensen #12-44	8069	9162.0	1	4a	20	5	25	58	40	2	3
Marathon	Jensen #12-44	8069	9163.5	2b	4b	15	10	25	25	50	25	15
Marathon	Jensen #12-44	8069	9164.2	2b	4b	10	4	14	55	40	5	20
Marathon	Jensen #12-44	8069	9165.2	1	4a	13	4	17	20	40	40	12
Marathon	Jensen #12-44	8069	9169.0	2b	4b	16	3	19	25	20	55	15
Marathon	Jensen #12-44	8069	9165.0	2b	4b	10	2	12	20	50	30	25
Marathon	Jensen #12-44	8069	9166.2	2b	4b	8	2	10	24	75	1	50
Meridian Oil	MOI #44-27H	12331	10224.4	2a	4a	15	20	35	35	50	15	0
Meridian Oil	MOI #44-27H	12331	10225.9 (upper)	2a	4a	10	5	15	80	20	0	0
Meridian Oil	MOI #44-27H	12331	10225.9 (lower)	2a	6a	100	0	30% silt + sand		5% silt	95% fine sand	0

Original Operator	Original Well Name	Well File No.	Thin Section No. (Depth (ft))	Facies Association	Facies	Silt Min. (%)		Total Silt (%)	Dominant Grain-size (Normalized to 100%)			
						Detrital Qtz	Carbo-nate		Fine silt (%)	Medium silt (%)	Coarse silt (%)	Clay Clasts (%)
Newfield Production	Sergeant Major 1-21-H	18086	11048.6	3	10	18	12	30	5	25	70	0
Newfield Production	Sergeant Major 1-21-H	18086	11053.8	1	4a	12	6	18	35	60	5	0
Newfield Production	Sergeant Major 1-21-H	18086	11060.0	2a	4a	9	6	15	15	80	5	2
Northern Plains Energy	Comford 9-12H	19060	9639.8	1	4a	2	4	6	50	50	0	0
Questar Exploration	MHA 1-18H	17434	9736.9	2b	4b	11	8	19	25	50	25	20
Questar Exploration	MHA 1-18H	17434	9737.5	2b	4b	11	7	18	35	50	15	15
Questar Exploration	MHA 1-18H	17434	9737.8	1	4a	13	6	19	30	40	30	3
Oxy USA Inc.	Sadowsky 24-14H	17808	10459.5	1	4a	20	8	28	40	50	10	0
Oxy USA Inc.	Sadowsky 24-14H	17808	10464.5	1	2	2	3	5	50	50	0	radiolaria
Oxy USA Inc.	Sadowsky 24-14H	17808	10466.3	2b	4b	9	6	15	10	60	30	20
Oxy USA Inc.	Sadowsky 24-14H	17808	10468.0	2b	4b	8	4	12	30	45	25	35
Samson Resources	Nordstog 14-23-161-98H	16069	8602.3	1	4a	10	4	14	40	59	1	0
Samson Resources	Nordstog 14-23-161-98H	16069	8605.5	3	4a	10	5	15	40	57	3	0
Samson Resources	Nordstog 14-23-161-98H	16069	8607.5	1	4a	9	3	12	40	50	10	2
Samson Resources	Nordstog 14-23-161-98H	16069	8609.5	1	4a	10	3	13	60	40	0	0
Samson Resources	Nordstog 14-23-161-98H	16069	8611.6 (upper)	4	4b	7	4	11	30	65	5	6
Samson Resources	Nordstog 14-23-161-98H	16069	8611.6 (lower)	4	7	10	90	100	15	75	10	0
Samson Resources	Nordstog 14-23-161-98H	16069	8613.1	2a	4a	10	2	12	90	10	0	2
Shell Oil	Burbank BIA 23-8	8709	10538.0	1	COMPLETE DIAGENETIC OVER PRINT				-	-	-	-
Shell Oil	Burbank BIA 23-8	8709	10540.0	2b	4b	10	13	23	20	55	25	12
Stanolind Oil & Gas	W & I Waswick 1	105	7567.9	2b	4b	10	2	12	50	48	2	35
Stanolind Oil & Gas	W & I Waswick 1	105	7570.1	2b	4b	7	2	9	48	50	2	12
Stanolind Oil & Gas	W & I Waswick 1	105	7570.7	2b	4b	5	3	8	25	40	35	50
Stanolind Oil & Gas	W & I Waswick 1	105	7571.4	2b	4b	21	9	30	20	30	50	15
Texaco Inc.	Thompson Unit #5-1	12748	11049C	2a	4a	21	4	25	72	25	3	0
Texaco Inc.	Thompson Unit #5-1	12748	11049E	2a	4a	?	2		40	50	10	0
Texaco Inc.	Thompson Unit #5-1	12748	11048E	2a	4a	22	8	30	50	35	15	0
Texaco Inc.	Thompson Unit #5-1	12748	11048 B	2a	4a	20	7	27	40	40	20	0
Texaco Inc.	Thompson Unit #5-1	12748	11048 A1	2a	4a	24	6	30	40	50	10	0
Texaco Inc.	Thompson Unit #5-1	12748	11048 C2	2a	4a	30	3	33	40	45	15	0
Texaco Inc.	Thompson Unit #5-1	12748	11048 D	2a	4a	22	8	30	30	45	25	0
Texaco Inc.	Thompson Unit #5-1	12748	11048 A3	2a	4a	30	10	40	25	45	30	0
Texaco Inc.	Thompson Unit #5-1	12748	11048 A2	2a	4a	24	4	28	20	45	35	0
Texaco Inc.	Thompson Unit #5-1	12748	11048 C1	2a	4a	20	12	32	20	30	50	0
Texaco Inc.	Thompson Unit #5-1	12748	11049 B	2a	4a	20	10	30	15	30	55	0
Texaco Inc.	Thompson Unit #5-1	12748	11049 A2	2a	4a	27	10	37	20	20	60	0
Texaco Inc.	Thompson Unit #5-1	12748	11049 (7)	2a	4a	30	5	35	20	20	60	0
Texaco Inc.	Thompson Unit #5-1	12748	11048 F	2a	4a	27	8	35	60	25	15	0
Texaco Inc.	Thompson Unit #5-1	12748	11049 D	2a	4a	17	4	21	20	60	20	0
Corp.	Braaflat 11-11H	17023	9869.3	2a	4a	17	9	26	20	50	30	0
Corp.	Braaflat 11-11H	17023	9871.3	2b	4b	10	3	13	70	30	0	6
Corp.	Braaflat 11-11H	17023	9872.9	2b	4b	14	8	22	30	60	10	10

Appendix 5: X-ray diffraction data

#16089 Samson Resources Nordstog 14-23-161-98H

Sample name:	Depth	Facies Association or Facies	NON-CLAYS	Quartz	Chert (13.1 nm)	**Total Quartz**	Kspar (intermediate microcline)	Kspar (sanidine)	Plagioclase (albite, var. cleavelandite)	**Total Feldspar**	Calcite	Dolomite	Ankerite	**Total Carbonate**	Pyrite	Gypsum	**Total non-clays**	CLAYS	Kaolinite (disordered)	Illite (1Md)	Illite (2M1; SG4)	Chlorite (Fe-rich; Tusc)	**Total clays**		TOTAL
16089-8602.3	8602.3	FA1		4.39	19.82	24.21	8.68	4.94	2.06	15.68	1.82	2.26	2.98	7.06	4.13	1.42	52.52		1.26	32.72	9.30	4.20	47.48		100.00
16089-8605.5	8605.5	FA1		6.53	17.17	23.69	7.25	4.67	1.76	13.68	0.10	1.60	2.36	4.06	7.05	1.57	50.08		1.76	33.13	9.41	5.62	49.92		100.00
16089-8607.5	8607.5	FA1		10.37	22.76	33.13	5.93	4.93	2.29	13.15	1.81	2.68	2.74	7.23	11.35	1.53	66.42		1.22	22.48	5.14	4.74	33.58		100.00
16089-8609.5	8609.5	FA1		7.51	29.82	37.34	6.68	4.55	2.22	13.46	0.00	1.15	2.33	3.48	6.13	1.41	61.84		1.16	24.67	6.31	6.02	38.16		100.00
16089-8613.1	8613.2	FA1		3.81	26.80	30.61	7.55	5.58	1.73	14.86	0.00	1.53	1.76	3.29	7.33	1.84	57.95		1.91	29.40	4.57	6.17	42.05		100.00

#16689 Helis Oil & Gas Linseth 4-8H

Sample name:			NON-CLAYS	Quartz	Chert (13.1 nm)	**Total Quartz**	Kspar (intermediate microcline)	Kspar (sanidine)	Plagioclase (albite, var. cleavelandite)	**Total Feldspar**	Calcite	Dolomite	Ankerite	**Total Carbonate**	Pyrite	Gypsum	**Total non-clays**	CLAYS	Kaolinite (disordered)	Illite (1Md)	Illite (2M1; SG4)	Chlorite (Fe-rich; Tusc)	**Total clays**		TOTAL
16689-10777.3	10777.3	FA1		12.57	14.30	26.87	6.66	2.91	1.92	11.49	4.46	5.10	4.39	13.95	2.87	1.39	56.57		0.82	28.16	8.59	5.87	43.43		100.00
16689-10781.5	10781.5	FA1		9.85	17.87	27.72	5.14	1.61	1.96	8.72	0.73	3.03	2.55	6.31	8.62	1.41	52.78		0.71	27.45	11.96	7.09	47.22		100.00
16689-10785.3	10785.3	FA1		12.71	29.58	42.29	3.74	2.67	2.12	8.52	0.00	1.38	1.74	3.12	4.78	1.13	59.87		2.04	26.85	7.62	3.62	40.13		100.00
16689-10789.8	10789.8	FA1		15.14	34.60	49.73	4.87	2.90	1.95	9.72	0.00	1.28	1.32	2.60	4.52	1.26	67.84		1.71	21.60	4.65	4.20	32.16		100.00
16689-10792.8	10792.8	FA1		19.07	38.88	57.95	4.06	3.13	1.43	8.62	0.00	2.22	0.80	3.02	5.06	0.98	75.64		1.10	16.20	4.21	2.86	24.36		100.00
16689-10794.9	10794.9	FA1		9.27	25.05	34.31	5.38	3.90	1.73	11.02	1.02	2.70	2.10	5.82	12.26	1.44	64.86		0.87	20.94	7.88	5.45	35.14		100.00
16689-10786.7	10786.7	FA2a		26.69	43.41	70.10	3.62	1.17	1.00	5.78	0.95	1.39	2.70	5.04	3.44	0.63	85.01		1.25	11.67	1.08	0.99	14.99		100.00
16689-10788.3	10788.3	Facies 2		16.12	38.43	54.55	4.93	1.87	1.67	8.47	0.25	1.08	1.03	2.36	10.20	1.14	76.73		1.26	14.70	5.25	2.06	23.27		100.00
16689-10789.3	10789.3	Facies 1		11.84	1.79	13.63	5.44	0.56	1.11	7.12	0.09	0.67	0.32	1.08	63.94	2.06	87.85		2.03	6.70	0.00	3.42	12.15		100.00

#17676 EOG Sidonia 1-06H

Sample name:			NON-CLAYS	Quartz	Chert (13.1 nm)	**Total Quartz**	Kspar (intermediate microcline)	Kspar (sanidine)	Plagioclase (albite, var. cleavelandite)	**Total Feldspar**	Calcite	Dolomite	Ankerite	**Total Carbonate**	Pyrite	Gypsum	**Total non-clays**	CLAYS	Kaolinite (disordered)	Illite (1Md)	Illite (2M1; SG4)	Chlorite (Fe-rich; Tusc)	**Total clays**		TOTAL
17676-8718.7	8718.7	FA1		4.64	16.59	21.23	6.44	4.84	2.54	13.83	1.81	1.45	3.45	6.71	7.12	2.44	51.35		2.72	34.06	6.32	5.55	48.65		100.00
17676-8720.4	8720.4	FA1		9.15	22.04	31.19	6.69	5.01	2.27	13.97	0.01	0.67	1.56	2.24	7.58	2.15	57.15		2.39	30.82	4.60	5.04	42.85		100.00
17676-8723.4	8723.4	FA1		13.58	45.50	59.08	4.07	4.93	1.45	10.45	0.37	0.63	1.03	2.04	3.61	0.97	76.16		1.27	17.46	3.35	1.76	23.84		100.00
17676-8725.8	8725.8	FA1		9.21	37.86	47.06	5.07	3.37	1.96	10.41	0.21	0.92	0.53	1.66	4.15	2.31	65.62		2.12	24.14	2.76	5.35	34.38		100.00
17676-8728.8	8728.8	FA1		12.76	36.41	49.17	4.53	3.68	1.92	10.12	0.07	0.81	1.21	2.09	5.03	1.41	67.84		1.59	21.23	5.85	3.49	32.16		100.00
17676-8732.4	8732.4	FA1		10.56	43.63	54.19	4.33	2.94	1.81	9.08	0.86	2.25	1.33	4.44	5.06	2.13	74.93		2.03	20.25	0.00	2.79	25.07		100.00
17676-8777.7	dup (8718.7)			4.63	17.34	21.98	6.86	4.22	2.41	13.49	1.57	1.86	2.73	6.16	6.90	2.20	50.75		2.54	33.71	6.56	6.45	49.25		100.00
17676-8731.4	8731.4	FA2b		9.50	44.97	54.47	5.15	3.87	1.64	10.66	0.00	2.44	1.62	4.05	4.61	1.29	75.11		1.51	16.82	4.12	2.44	24.89		100.00

XRD data from Neil Fishman and Sven Egenhoff (pers. comm., 2013):

X-ray diffraction analyses for samples from the upper shale member of the Bakken Formation. Quant., quantitative; wt %, weight percent; Qtz, quartz; XRD, X-ray diffraction; Det, detrital; Auth, authigenic; Dol, dolomite; Fe, iron; t, trace. Detrital quartz and carbonate determined by visual estimations from petrographic analysis.

Well file # / Sample #	Approx. depth	Facies Assoc.	Quartz (wt %)	K-Feldspar (wt %)	Albite (wt %)	Calcite (wt %)	Dolomite (wt %)	Total Carb	Siderite (wt %)	Pyrite (wt %)	Sphalerite (wt %)	1M Illite R>3 (wt %)	Fe-Chlorite (wt %)	2M1 Illite / Muscovite (wt %)	Total (wt %)
E349 11048B-1	11048.2	FA2a	60	10	2	1	6	6	0	3	0	8	3	8	100
E349 11048B-6	11048.27	FA2a	55	15	2	1	5	5	0	2	0	14	0	6	100
E349 11048B-7	11048.3	FA2a	62	10	2	0	4	4	0	3	0	10	2	7	100
E349 11048(C) 1 #1	11048.35	FA2a	62	11	2	0	4	4	0	2	0	10	1	9	100
E349 11048C(1)-2	11048.5	FA2a	51	13	2	0	6	6	0	3	1	16	1	10	100
E349 11048C(1)-3	11048.52	FA2a	57	12	2	0	6	6	0	1	1	12	1	9	100
E349 11048D #1	11048.6	FA2a	59	10	1	1	4	4	0	3	0	12	1	9	100
E349 11048D #8	11048.77	FA2a	64	9	1	0	5	5	0	2	0	9	0	8	100
E349 11049B-2	11049.4	FA2a	73	6	1	0	3	3	0	2	0	10	3	2	100
E349 11049C-1	11049.5	FA2a	39	15	1	1	5	6	0	6	0	16	4	12	100
E349 11049C-2	11049.55	FA2a	47	5	1	1	3	4	0	22	0	11	2	8	100
E349 11049C-5	11049.7	FA2a	41	14	1	1	4	5	0	7	0	16	3	12	100
E349 11049C-6	11049.8	FA2a	35	14	2	1	5	6	0	4	0	21	6	11	100
E349 11049E-1	11049.9	FA2a	46	13	1	1	4	5	0	3	0	17	5	9	100
B832 10352A #1	uncertain	FA2a	22	14	2	0	9	9	1	5	0	21	13	12	100
B832 10354E(1) #2	uncertain	FA2a	52	9	0	1	4	5	0	2	16	11	4	2	100
E349 11048B-2	11048.2	RBM	63	7	1	2	4	6	0	10	0	8	1	4	100
E349 11048B-5	11048.24	RBM	62	11	2	1	4	4	0	3	1	12	0	6	100
E349 11048(C) 2 #1	11048.4	RBM	61	9	1	2	3	6	0	6	1	8	2	6	100
E349 11048(C) 3	11048.42	RBM	62	6	2	1	3	3	0	4	10	8	0	5	100
E349 11048C-5	11048.46	RBM	70	12	2	0	3	3	0	0	1	11	1	0	100
E349 11048C-6	11048.48	RBM	73	7	1	1	4	4	0	2	1	7	0	4	100
E349 11048C(2)-1	11048.54	RBM	54	12	1	3	3	6	0	5	3	11	1	6	100
E349 11048C(2)-3	11048.56	RBM	58	8	1	1	4	5	0	0	9	11	3	5	100
E349 11048C(2)-6	11048.58	RBM	75	8	1	2	2	4	0	0	2	8	0	2	100
E349 11048D #2	11048.62	RBM	67	8	1	1	3	4	0	7	2	8	0	4	100
E349 11048D #7	11048.74	RBM	71	6	1	0	3	3	0	5	1	8	0	5	100
E349 11048E-1	11048.8	RBM	63	10	2	1	3	4	0	0	1	14	0	5	100
E349 11048E-2	11048.81	RBM	76	7	1	0	2	3	0	0	1	10	0	2	100
E349 11048E-5	11048.85	RBM	63	11	2	2	3	5	0	0	3	10	2	4	100
E349 11048E-6	11048.87	RBM	66	11	2	0	3	4	0	1	1	11	0	5	100
E349 11048E-7	11048.9	RBM	75	7	1	0	2	2	0	2	0	6	1	6	100
E349 11049B-3	11049.45	RBM	70	5	1	0	4	4	0	3	0	10	4	2	100
E349 11049C-3	11049.6	RBM	62	4	0	0	2	3	0	18	0	8	0	5	100
E349 11049C-4	11049.65	RBM	61	7	0	1	2	3	0	15	0	8	0	5	100
B832 10352D #1	uncertain	RBM	76	4	1	0	2	2	0	2	10	6	0	0	100
B832 10352D #2	uncertain	RBM	75	5	0	0	2	2	0	1	4	8	4	0	100

Well file # / Sample #	Approx. depth	Facies Assoc.	Quartz (wt %)	K-Feldspar (wt %)	Albite (wt %)	Calcite (wt %)	Dolomite (wt %)	Total Carb	Siderite (wt %)	Pyrite (wt %)	Sphalerite (wt %)	1M Illite R>3 (wt %)	Fe-Chlorite (wt %)	2M1 Illite / Muscovite (wt %)	Total (wt %)
E349 11048B-3	11048.3	RAD	77	4	1	0	3	3	0	2	0	7	0	4	100
E349 11048B-4	11048.22	RAD	81	4	1	0	3	3	0	2	0	6	0	3	100
E349 11048C-4	11048.44	RAD	76	6	1	5	2	6	0	1	6	3	0	1	100
E349 11048D #3	11048.64	RAD	88	3	1	2	1	3	0	1	0	3	0	1	100
E349 11048D #4	11048.66	RAD	84	6	1	5	1	6	0	0	0	4	0	0	100
E349 11048D #5	11048.68	RAD	90	2	0	4	1	5	0	1	0	1	0	0	100
E349 11048D #6	11048.7	RAD	84	6	1	0	1	2	0	0	1	7	0	0	100
E349 11048E-4	11048.83	RAD	83	3	1	0	2	2	0	1	2	5	0	3	100

RAD = radiolarite (facies 1)
RBM = radiolarian-bearing mudstone (facies 2)
FA2a = well laminated mudstone

Appendix 6: Total organic carbon, Rock-Eval pyrolysis and whole rock vitrinite reflectance analyses

Well Name: Helis Oil & Gas Linseth 4-8H. Well file: Number: 16689. Analysis by Weatherford Laboratories, Shenandoah Texas

Depth	Facies Association	TOC (wt %)	S1	S2	S3	Tmax	Measured % R0	HI	OI	S2/S3	S1/TOC *100	PI
10777.3	1	7.21										
10777.8	3	5.11	5.63	9.80	0.41	446.00	0.81	191.67	8.02	23.90	110.11	0.36
10778.1	3	7.44										
10778.4	1	7.99										
10785.3	1	9.52										
10781.5	1	9.90										
10788.3	RBM	9.44										
10786.7	2a	8.64										
10789.3	RAD	3.09										
10789.8	1	11.10										
10792.8	1	10.60										
10794.9	1	11.45										
10799.9	duplicate of 10785.3	9.51										

RAD : Radiolarite (facies 1)

RBM : Radiolaria-bearing mudstone (facies 2)

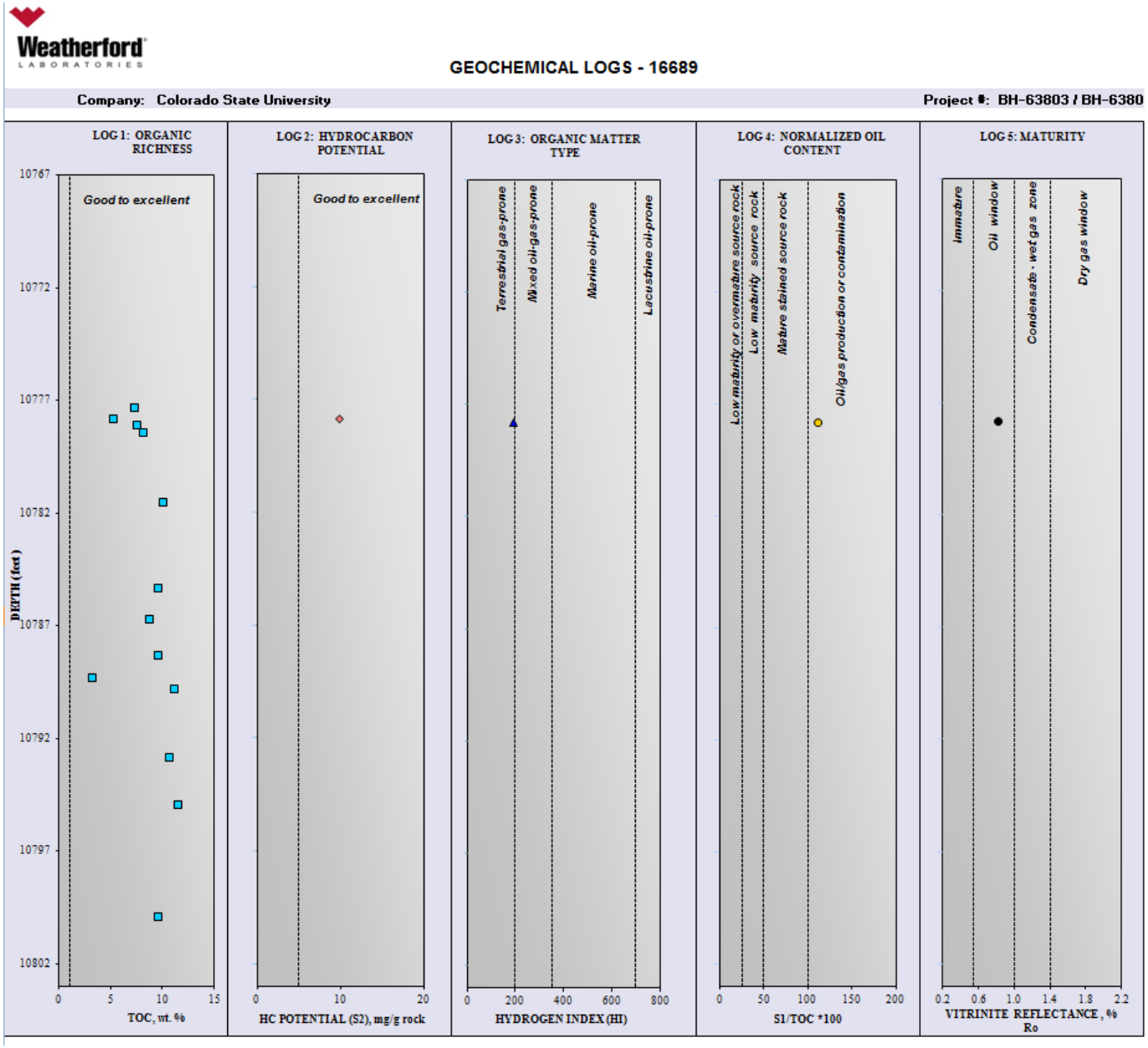
Weatherford
LABORATORIES
GEOCHEMICAL LOGS - 16689
Company: Colorado State University
Project #: BH-63803 / BH-6380
LOG 1: ORGANIC RICHNESS
LOG 2: HYDROCARBON POTENTIAL
LOG 3: ORGANIC MATTER TYPE
LOG 4: NORMALIZED OIL CONTENT
LOG 5: MATURITY
DEPTH (feet)
10767
10772
10777
10782
10787
10792
10797
10802
Good to excellent
Terrestrial gas-prone
Mixed oil-gas-prone
Marine oil-prone
Lacustrine oil-prone
Low maturity or overmature source rock
Low maturity source rock
Mature stained source rock
Oil/gas production or contamination
Immature
Oil window
Condensate - wet gas zone
Dry gas window
0 5 10 15
TOC, wt. %
0 10 20
HC POTENTIAL (S2), mg/g rock
0 200 400 600 800
HYDROGEN INDEX (HI)
0 50 100 150 200
S1/TOC *100
0.2 0.6 1.0 1.4 1.8 2.2
VITRINITE REFLECTANCE, % Ro

Weatherford LABORATORIES

Project BH-63803

Vitrinite Reflectance and MOA

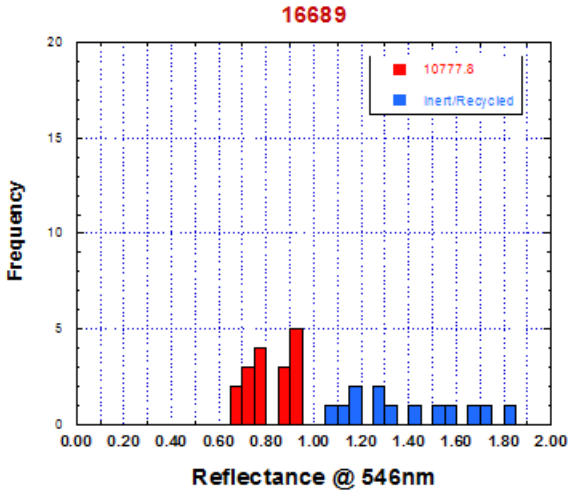

1	10777.80
Minimum	0.68
Maximum	0.94
Points	17
Std Deviation	0.09
Mean	**0.81**

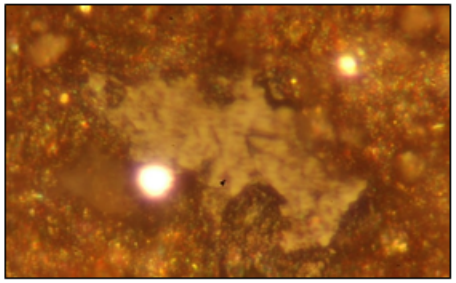

Comments: Sample preparation consists of whole rock material (i.e., not a kerogen isolate) from core chip mounted in an epoxy plug and polished. **Terrestrially derived (Type III) organic matter is moderately abundant on the reflectance plug, although the organic matter tends to be degraded.** Based on 17 measured values of the better polished, lower reflecting material that appears to be vitrinite, the average Ro is 0.81%. Values ranging from 0.68% to 0.94% are interpreted to be the indigenous population, and the mean %Ro is calculated based on this population. Although somewhat arbitrary, values greater than 1.00% are considered to be inert macerals or recycled vitrinite (blue). Based on the 17 measured values of reflectance for the indigenous vitrinite population, OM in this sample has reached the peak stage of thermal maturity for oil generation from oil-prone OM. Photomicrograph shows a vitrinite particle (Ro=0.89%) in the whole rock mount (reflected white light).

Ordered Ro Values *(Reflectance Standard = 0.51% Ro)*

0.68	0.69	0.71	0.72	0.73	0.76	0.77	0.78	0.79	0.86	0.88	0.89
0.90	0.91	0.92	0.92	0.94	1.08	1.11	1.18	1.19	1.25	1.28	1.33
1.44	1.52	1.55	1.65	1.73	1.84						